Alma Mater Studiorum – Università di Bologna

Dottorato di Ricerca in

Ingegneria Civile, Chimica, Ambientale e dei Materiali

Ciclo XXIX

Settore Concorsuale: Area 09/D2

Settore scientifico disciplinare: ING/IND-24

SYNTHESIS AND CHARACTERIZATION OF NOVEL FACILITATED TRANSPORT MEMBRANES FOR CO$_2$ SEPARATION

Presentata da: Davide Venturi

Coord. scuola di dottorato:
Prof. Luca Vittuari

Relatore:
Prof. Marco Giacinti Baschetti

Correlatrice:
Prof. Maria Grazia De Angelis

Esame finale anno 2017

Table of content

Abstract

As a response to the growing concern linked to the anthropogenic contribution to global climate change due to carbon emission, a large amount of research is now focused to develop new technologies for its capture prior to the release in the atmosphere. Amongst the various methodologies, gas separation membranes occupy an ever-growing share of the separation technologies. In particular, facilitated transport membranes (FTMs) are gaining an exponentially large interest in the research community. These films rely on a reversible reaction between a target component in the gas feed and functionalized groups embedded in the membrane matrix. Throughout this work different kinds of FTMs have been synthesized and tested, in order to gain insight on their permeation properties. A first part of the work was dedicated to the study of Polyvinyl alcohol based membrane, which were functionalized in two different ways: by the grafting of amine functionalized molecule to the polymeric chain and by the addition of nanoparticles provided with amine moieties. Subsequently, the main study presented in this thesis concerned the synthesis of selective films, resulted by the blending of polyvinylamine (for the functionality) and nanocellulose (for the structural support). Various ratios of the two components where explored at different degrees of humidity and good results were achieved, maxing the CO_2/N_2 selectivity at 211 the CO_2/CH_4 one at 122 at 35 °C. When swelling at high humidity was observed, several polymer modification were employed to tackle the issue, ranging from chemical cross-linking, thermal treatment and polymer purification. This allowed to increase the CO_2/CH_4 selectivity up to 410 at 35 °C and minimize swelling. Overall, it was possible to synthesize performing amine based fixed site facilitated transport membranes for the separation of carbon dioxide and find new methods for the improvements of their characteristics.

Introduction

From the industrial revolution to our present day, the anthropogenic impact on the environment has been increasing at an alarming and exponential rate. Amongst the various effect, that human activities have had on their surroundings, climate change due to greenhouse gases appears to be one of the most dire issues of our time [1]. This well known phenomenon is caused by the accumulation of gases in the atmosphere, which can create a so called *greenhouse effect*, increasing its average temperature and causing global scale negative effect on a number of ecosystems. The most widely emitted greenhouse gas is carbon dioxide, whose concentration has increased from 315 ppm in the first half of the last century, up to more than 400 ppm in the present day [2]. Hence, the reduction of the emission of this gas represents one of the priorities and challenges of our society. A long term solution is of course represented by the substitution of carbon emitting activities with more sustainable ones. However, while in the waiting for new, efficient and carbon neutral technologies to spread worldwide, an interesting and more immediate solution can be found in the process of *carbon capture and storage* [3]. This methodology consist in the separation of CO_2 prior to its emission in the atmosphere and its storage in underground cavities.

The implementation of similar actions, indeed, would allow to maintain the current energy production trend, at a fraction of the environmental cost, while better long-term solutions are developed. Several technologies are being investigated for this purpose, ranging from chemical or physical absorption, adsorption on porous supports and gas separation membranes [4]. Between the different options, gas separation membranes do offer a series of interesting advantages, ranging

from the simplified operability, small volume occupation, energy efficiency and lack of solvents [5,6]. Usually, a membrane is capable of separating gases via a *solution-diffusion* mechanism, which rely on differences in solubility or diffusivity between different chemical species [7]. This technology proved itself to be quite efficient and flexible, with its applications constantly growing since a few decades [8]. On the other side, though, this specific transport mechanism tends to suffer from a trade-off between the permeability of the film (the total flow separated), and its selectivity towards a specific pair of gases (the ability to allow one to permeate, while rejecting another) [9], meaning that, if one property is to be increased, the other will most likely diminish.

To overcome this issue, a different kind of membranes has started to gain interest in recent years, even though the first studies were developed in the late 60s [10]. These films rely on the fact that within their matrix a series of functional groups, called *carriers* can chemically interact with a specific group of molecules in a mixture, which share a common chemical behavior. Once the chosen molecule is absorbed into the membrane, it can react reversibly with these moieties, which *facilitate* its transport through the thickness of the film [11]. Since this mechanism is only available for one chemical species (or more, that have a similar chemical nature), only the permeability of this single component will be enhanced. This results in an increment of both permeability *and* selectivity at the same time.

The first films were mainly based on a so called Supported Liquid Membrane (SLM) [12], which relied on ion dispersed in a liquid-like film. These guaranteed good performances, but suffered from a severe lack of long-term stability, since nothing prevented both the liquid and the carriers from passing to the vapor phase. For this reason more and more research has been lately dedicated to improving the stability of these films, limiting carrier leakage. One of the solution to this issue is represented by the use of Fixed Site Carriers (FSC); in other words, this consist in the use of carriers, which are covalently bonded to the structural components of the films, such as the backbone of the polymeric chain [13,14]. This determines a restricted mobility for the carriers, but a much higher stability and much lower probability of a leakage of the moieties.

When the separation of an acidic gas, such as carbon dioxide, is tackled, it appears quite natural to shift the attention towards alkaline functional groups as carriers. In particular, the use of aminated polymeric membranes have been increasingly studied in the past years [15,16]. Amine moieties are capable of reacting with the dissolved CO_2 in presence of water and facilitate its transport from one site to another and they are considered to be one of the most efficient options for the separation of carbon dioxide.

Introduction

The investigation of amine based facilitated transport membranes, is the main scopus of the present activity, which also aims at the development of a new type of facilitated transport membranes able to overcome the current limitation of this type of systems.

In particular, during the work, this goals have been pursued by developing two main approaches. The first one, which represents the first part of the activity, involves the use of a non functionalized hydrophilic matrix (here polyvinyl alcohol, PVA), to which amine functionalities are then added via chemical reaction [16] or by the incorporation of functionalized nanoparticles. The second approach, on the other hand, was focused on the development of polyvinylamine (PVAm)-Nanocellulose based films.

In particular while the first approach was somewhat introductory to start understanding the realm of transport facilitation, by applying already known relationships and components, the second one represent the main focus of and the real innovative part of the present research activity which for the first time try to couple PVAm and Nanocellulose to obtain facilitated transport membranes.

Nowadays, PVAm is a relatively common polymer for this kind of applications [17–19], thanks to its high density of amine moieties and hydrophilicity. Unfortunately, this material tends to have poor mechanical properties, which compromise its stability at high humidity. For this reason most of the work done here has been focused on introducing a secondary, nano dispersed phase into the membrane film, that could guarantee better stability also at high humidity and when subjected to a pressure differential.

The material chosen for this purpose is, as said above, Nanocellulose or more precisely Nano Fibrillated Cellulose (NFC), also known as Microfibrillated Cellulose (MFC) or Cellulose Nano Fibers (CNF). This is a name used to indicate a type of hierarchical aggregation of cellulosic chains found in many vegetable structures [20]. In particular, several polysaccharide chains (few nanometers) can reorder themselves in elementary fibrils, which on their own can create a higher order structure (tens of nanometers). These last fibers represent our material of choice, thanks to their great mechanical properties and hydrophilicity. In fact, a single nanocellulosic fiber can reach an elastic modulus of up to 100 GPa [21] paired with a density of the crystalline material around 1.5-1.6 g/cm^3. This determines that microfibrillated cellulose possesses a mechanical strength per unit of mass higher than the one of steel (E = 210 GPa, Density = 8 g/cm^3 [22]). Moreover, the addition of these fibrils to an adequate matrix has been reported to drastically improve its mechanical properties [23,24]. This is usually due to a phenomenon called *percolation* [25], a term that indicating the connection of the cellulose nanoparticles with one another to form a three-dimensional continuous hydrogen-bonded pathway through the nanocomposite network of the film.

4

These nanofibrils can be obtained by almost any kind of vegetable pulp via a number of methodologies, which all rely in some way to the degradation of the walls of the plant cells. Mechanical treatments are the most straightforward and involve a process called homogenization, which is based on the application of extremely high pressures (up to 2000 bar) and high velocities on the pulp [23] Other treatments hinge around a chemical or enzymatic degradation of the cells and can be applied in combination with a mechanical treatment. During these treatments, the fibrils can also be functionalized by grafting specific moieties to the exposed hydroxyl groups on their surface [20].

Due to all these properties and for its inherent environmental sustainability, nanocellulose has been deemed quite interesting for several applications, ranging from electronic sensor [26] to packaging material [27]. In our case, it was chosen, not only as an enhancement of the mechanical properties of the polymer, thanks to its high affinity with it, since both are highly hydrophilic, but also to investigate possible synergic interactions with the polymeric chains, as a way to obtain an even better facilitation effect within the selective layer.

This work will be structured into two main section, with the first one dedicated to the introduction of gas separation membranes and their functioning in general terms and the mechanism, which regulates the transport facilitation of carbon dioxide. Within the same section, the materials (reagents and experimental setups) used for testing the films will be described along with the procedures followed to prepare all the various films and their modifications. The second section, instead will present all the experimental results of the work, divided by type of film tested, starting from the polyvinyl alcohol films, followed by the PVAm-Nanocellulose blends and concluding with the various modification implemented on these last ones. Each presentation of the results will be accompanied by a discussion aimed at interpreting and analyzing them.

Section 1: Backgrounds and Methodology

.

Chapter 1. *Membranes for gas separation*

Here, an overview regarding gas separation membranes and facilitated transport will be given. Firstly, the basic functioning of a gas separation membrane will be explored, in particular, the solution-diffusion mechanism will be presented as the typical phenomenon exploited to obtain a separation between different gases. Subsequently, the chapter will go in deep to explore the mechanisms related to the facilitated transport of gases and the development of this technology throughout the years. Specifically, the different theories regarding the reactions involved will be presented and how the transport is affected. Moreover, a brief explanation on some of the main transport equations used during the work will be given along with an introduction of the principal units of measure typical of the gas separation field.

1.1 Gas separation membranes

A membrane can be defined as a selective barrier, which is capable of allowing the permeation of different chemical species at a different rate. This results in the fact that the composition of the flow, which is fed to a membrane module will vary from the two, which depart from it. A property like this one can be exploited to enrich a stream of a specific compound or to purify it, by removing a pollutant. Membranes can work on both a liquid or gaseous flow, depending on their structure and composition. In general, membranes for liquid separation show a measurable porosity, through which the liquid or the solutes can pass, while gas separation membranes are dense films, where molecular diffusion happens. Even though particular materials such as metals and ceramics are sometimes used to synthesize these films, the vast majority of membranes are made of polymers, which can also include secondary phases to improve their performances.
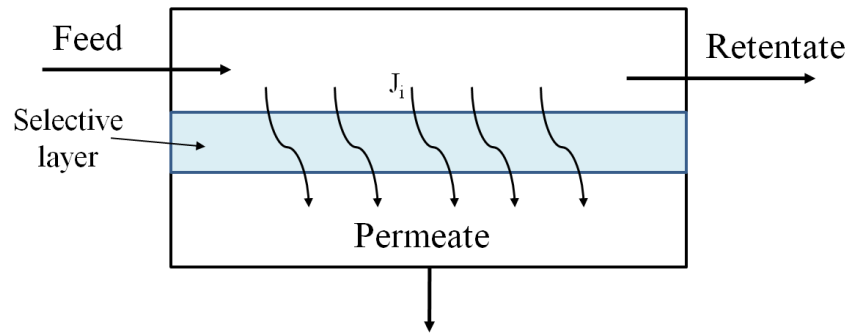
Figure 1.1: generic layout of a membrane module, with the main gas flows outlined

Figure 1.1 shows the typical layout of a membrane module and the presence of three main streams: the *feed* is the flow of gas to be treated, which reaches the membrane on the upstream side, while the *retentate* represents the same upstream flow once the separation took place. Here, with J_i is indicated the molar flow of the species *i*, which permeates through the selective layer of the membrane and eventually becomes what is usually named as the *permeate*.

In general, a membrane for gas separation relies on a chemical potential differential between the two sides, upstream and downstream, and is capable of separating different chemical species thanks to its structural and/or thermodynamics properties.

Several parameters can be measured to experimentally evaluate the performances of a membrane, but the two most important one are the *gas permeability* and the gas *selectivity*.

The first parameter is generally defined as the amount of gas passing through the membrane film per unit of time and area scaled down respect to the film thickness and the partial pressure drop of the same gas. Referring to the system outlined in Figure 1.2, the permeability of the generic species *i* is then defined by Eq. 1.1.

$$Permeability_i = \frac{Moles_i}{Area \cdot Time} \cdot \frac{Thickness}{Driving\ Force} = \frac{J_i \cdot \delta}{p_i^{Up} - p_i^{Down}} \tag{1.1}$$

As it can be seen, the first terms represents the molar flux of *i* through the film, as the total number of moles, that pass through a given area of the film in a certain amount of time. This term is usually expressed as *J*, while the second one multiply it by the thickness of the film and divide by the driving force. By multiplying the thickness (δ), the permeability becomes independent by this parameter, making it an intrinsic parameter of the material itself. Finally, the driving force, in the cases that we are going to analyze, is expressed as the difference of partial pressure of the gas between the upstream (p_i^{Up}) and the downstream (p_i^{Down}) side.
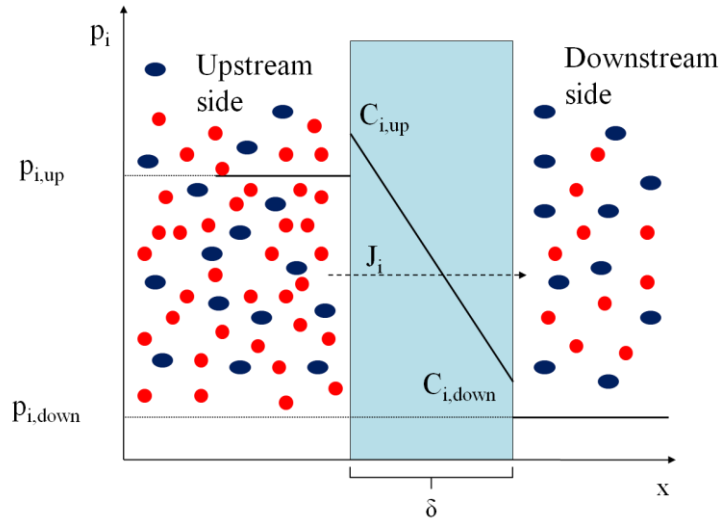
Figure 1.2: schematization of the diffusion process between the two sides of a membrane of the generic species i.

Several units of measure can be employed, in order to express the permeability of a given gas; the most commonly used is the Barrer (named after chemist Richard Barrer), which is defined as in Eq. 1.2 along its conversion into SI units.

$$1 \, Barrer = 10^{-10} \frac{cm^3(STP) \cdot cm}{cm^2 \cdot cmHg \cdot s} = 3.364 \cdot 10^{-16} \frac{mol}{m \cdot Pa \cdot s} \tag{1.2}$$

As previously mentioned, permeability does not depend on the geometry of the film (namely its thickness). In a more applicative view, when comparison with other separation technologies is required, a slightly different quantity, *permeance*, is employed. This one is defined as the gas flow through the film divided by the area and the partial pressure difference (Eq. 1.3).

$$Permeance_i = \frac{J_i}{p_i^{UP} - p_i^{DOWN}} \tag{1.3}$$

In this case, the amount measured will depend on the thickness of the film, since a thinner membrane will have a higher permeance than a thicker one of the same material. It is commonly expressed in Gas Permeation Units (GPUs), which are defined in Eq. 1.4, along with other commonly used unit of measure.

$$1 \, GPU = 10^{-6} \frac{cm^3(STP)}{cm^2 \cdot cmHg \cdot s} = 3.3 \cdot 10^{-1} \frac{mol}{m^2 \cdot Pa \cdot s} = 2.76 \cdot 10^{-3} \frac{m^3(STP)}{m^2 \cdot bar \cdot h} \tag{1.4}$$

A series of theoretical frameworks have been developed, in order to describe the diffusion mechanism of a molecule in a dense polymeric layer. Amongst these, one of the most commonly accepted and widespread nowadays is the Free Volume Theory (FVT) [28]. This one sees the

molecules within the polymeric matrix as moving via a jumping mechanism, which relies on the free volume (V_f) of the polymer, as well as the available energy, which is needed to overcome the interaction forces between two polymeric segments. Following this view, low molecular weight species can permeate thanks to a temperature activated process, which involves the motion of chain segments, that move in such a way to temporary create an opening, through which the molecule can jump, passing from a volume element to another. In view of these considerations, the permeability will increment along with the *fractional free volume* (FFV = $V_f/\hat{V}$, with $\hat{V}$ being the specific volume of the polymer) with a relation such as (Eq. 1.5):

$$P_i = A_i \cdot exp\left(-\frac{B_i}{FFV}\right)$$
(1.5)

Here, A_i and B_i represent constant parameters characteristics for the considered pair polymer-penetrant. Within the free volume theory, temperature plays a major role in the permeation process, usually enhancing the film performance and its influence can me modeled via an Arrhenius-like behavior [29](Eq. 1.6).

$$P_i = P_{i,0} \cdot exp\left(-\frac{E_{p,i}}{RT}\right)$$
(1.6)

Where $P_{i,0}$ is a pre-exponential factor, $E_{p,i}$ represents the activation energy of the permeation, R is the ideal gas constant and T the absolute temperature. In a more detailed way, the permeation of molecules through a dense selective layer can be described via the solution-diffusion mechanism. This can be broken down into three main steps: firstly the penetrant is solubilized into the film on the upstream side at the gas-membrane interface; subsequently it diffuses through the thickness of the selective layer and finally it is desorbed into the downstream side returning into the gas phase. If the steps of sorption and desorption at the gas-membrane interface are considered to occur in an equilibrium state and the diffusion coefficient is expressed through Fick's law, the expression for the penetrant flux at stationary conditions will be then be written as (Eq. 1.7):

$$J_i = D_i \cdot S_i \cdot \frac{\Delta p_i}{\delta}$$
(1.7)

Here, Δp_i represents the difference in partial pressure of the component *i* across the selective layer of thickness δ, D_i and S_i are respectively the diffusivity and solubility coefficients. This last one can be expressed by the ratio $\Delta C_i/\Delta p_i$, where the numerator represents the drop in concentration within the two gas-membrane interfaces of the film. Hence remembering the definition of permeability given by Eq. 1.1, it can be written:

$$P_i = D_i \cdot S_i \tag{1.8}$$

This expression relates the permeability of a given molecule as the product of its solubility and diffusivity in the polymeric matrix. Solubility is an expression of the partition coefficient between the gas and the matrix phase and it is mainly depending on temperature and penetrant condensability. Diffusivity, instead, relates more to the kinetic properties of the pair polymer-penetrant, also a function of temperature, to the geometrical properties of the diffusing molecule and available volume in the matrix. As mentioned, both parameters are function of temperature and this dependency is usually expressed via an exponential equation similar to the one seen for permeability (Eq.1.6).

$$D_i = D_{i,0} \cdot exp\left(-\frac{E_{D,i}}{RT}\right) \tag{1.9}$$

$$S_i = S_{i,0} \cdot exp\left(-\frac{\Delta H_{S,i}}{RT}\right) \tag{1.10}$$

As before, $D_{i,0}$ and $S_{i,0}$ are pre-exponential factors, non dependent on the temperature of the system, while $E_{D,i}$ is the energy characteristic of the diffusion process and $\Delta H_{S,i}$ the heat of sorption. Overall, the permeation energy $E_{p,i}$ can be interpreted as the sum of the contributions of the energy needed for the solubilization of the penetrant and the one required for it to jump from one volume available for diffusion to the other.

Beyond permeability, another important parameter required to properly evaluate the performances of a membrane is the separation factor or selectivity. This is a measure of how much a gas is enriched or depleted respect to another from the upstream to the downstream and can be defined by the expression:

$$\alpha_{i,j} = \frac{y_i^d / y_j^d}{y_i^u / y_j^u} \tag{1.11}$$

With *y* is indicated the molar fraction of the components *i* and *j* for both the upstream (*u*) and downstream (*d*) side of the film. In general, this factor is dependent on the specific process considered and it is not an intrinsic property of the film, but when the pressure in the downstream side tends to zero, the selectivity can be seen as characteristic of the polymer and the two gases which are competing for the diffusion. In mathematical terms, remembering the definition of permeability given in Eq. 1.1, the flow of each gas in the permeate side can be written as:

$$Q_P \cdot y_i^d = \frac{P_i \cdot A_m}{\delta} \left(p_i^u - p_i^d\right) \tag{1.12}$$

$$Q_P \cdot y_j^d = \frac{P_j \cdot A_m}{\delta} \left(p_j^u - p_j^d\right) \tag{1.13}$$

Where Q_p represents the total permeate flow, A_m the membrane area and p the partial pressure of the two components i and j in the upstream and downstream side. Grouping all the common elements from the two equations the system becomes:

$$\frac{P_i}{y_i^d}\left(p_i^u - p_i^d\right) = \frac{P_j}{y_j^d}\left(p_j^u - p_j^d\right) \tag{1.14}$$

Collecting the ratio of the two molar fraction downstream, will be obtained the relation:

$$\frac{y_i^d}{y_j^d} = \frac{P_i\left(p_i^u - p_i^d\right)}{P_j\left(p_j^u - p_j^d\right)} = \frac{P_i\left(P^u y_i^u - P^d y_i^d\right)}{P_j\left(P^u y_j^u - P^d y_j^d\right)} \tag{1.15}$$

Where P represents the total pressure of the downstream and upstream side. In the case of $P^d \to 0$ the equation will eventually results to be:

$$\frac{y_i^d}{y_j^d} \simeq \frac{P_i}{P_j}\frac{P^u y_i^u}{P^u y_j^u} \tag{1.16}$$

And eventually:

$$\frac{P_i}{P_j} \simeq \frac{y_i^d/y_j^d}{y_i^u/y_j^u} = \alpha_{i,j} \tag{1.17}$$

When the separation factor is calculated directly in this way, using pure gas permeability, the resulting value is called *ideal selectivity* (Eq. 1.18), meaning it represents an estimation of the actual value, since it does not consider the unpredictable effects given by the interactions of two or more molecules permeating at the same time. Moreover considering also Eq. 1.8, ideal selectivity can be expressed via the diffusion and solubility coefficients of the two penetrants.

$$\alpha_{i,j} = \frac{P_i}{P_j} = \frac{D_i}{D_j} \cdot \frac{S_i}{S_j} = \alpha_D \cdot \alpha_S \tag{1.18}$$

The separation factor, then, can be seen as the product of two contributions: α_D, the diffusion contribution to selectivity, which depends on kinetic parameters, and α_S, the solubility contribution, which, instead, will be function of thermodynamic parameters.

The combination of permeability and selectivity for a given film, can then allow to assess its performances respect to other membranes, even if of a different nature. Amongst the first ones to perform this kind of comparison, Robeson observed in 1991 [30] the presence of an upper bound in terms of permselectivity of the best performing membranes for a given pair of gases. This way, the now well-known Robeson Plot was born (Fig. 1.3). Since then, the upper bound has been updated in 2008, considering the technological advancement made during the time [9]. The importance of this chart is represented in the possibility of a quick and easy determination of the performances of a certain film respect to a common and recognized reference.
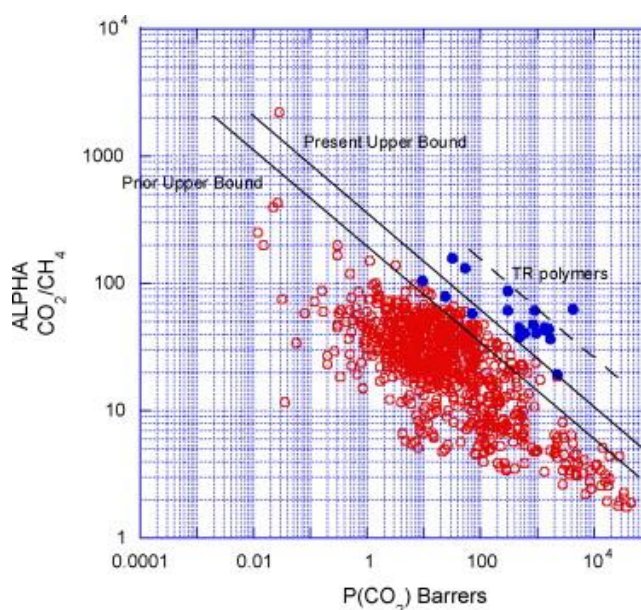

Figure 1.3: Robeson Plot for the separation CO_2/CH_4. The chart presents both the 1991 and 2008 upper bounds [9].

Once all collected together, the permeability and selectivity of a large number of film, showed the clear presence of a trade-off between these two parameter. More in detail, this means that an increment in selectivity is usually accompanied by a decrease in permeability and vice versa. The ideal direction, which is mainly pursued within the membrane development research is the one that points at increasing both parameters at the same time, moving the upper bound to the top right corner of the chart.

For regular glassy and rubbery membranes this improvement can be particularly challenging. In fact, the mechanism though which these film separate gas can rely on two different principles, each based on one of the two contributions to selectivity seen in Eq. 1.18. In terms of separation by diffusion, it has been observed that the diffusion coefficient scales quite accurately with the kinetic diameter of the penetrant, while the solubility is mainly controlled by the condensability of a gas, a parameter related to its critical temperature. For example, for a generic separation of two gases A/B, if the kinetic diameter of B is smaller, it will diffuse faster than A, resulting in $\alpha_D < 1$. Instead, if

the condensability of B is higher than A, it will tend to be solubilized better than A, hence having $\alpha_S > 1$. These two parameters will tend to cancel each other resulting in a difficult separation. A good result, instead, is usually achieved when both parameter are in accordance with each other or if one of the two is significantly predominant respect to the other.

In more detail terms, when dealing with a rubbery polymer, meaning that it is operating at a temperature higher than its glass transition temperature (T_g), its matrix will behave, in thermodynamic terms, similarly to a liquid. This is to be understand as the fact that its chains and overall aggregation are fairly mobile and in an equilibrium state and they are provided with a large volume available for diffusion. Hence, being the diffusivity fairly high for all molecules, the α_D will be close to unity for most penetrants. What actually determines the higher or lower permeation rate of a certain chemical species will be theirs solubility, namely the α_S parameter. For glassy polymers, instead, the matrix is in a non-equilibrium state, with the polymeric chains frozen in a fixed state, having very little mobility. In this case, the opposite respect to a rubbery film occurs, with diffusivity being usually the most common discriminating factor between the different penetrants.

For these films the trade-off between occurs since polymers with high free volume will usually present high diffusivity and high permeability, but are not usually capable of sieving different molecules based on their kinetic diameter due to the large average size of the diffusion sites. On the other side, polymers with carefully sized free volume tends to have low permeability and high selectivity.

All these considerations, though, have a validity until a pure physical transport is concerned; the addition of specific functionalities within a membrane can determine an entirely new of dealing with separation processes, as it will be explained in the next paragraph.

1.2 *Facilitated transport*

Having seen the intrinsic limitation, that traditional gas separation membranes usually show, a new kind of promising materials has been gaining a growing interest during the last decade. This is represented by Facilitated Transport Membranes (FTM), a family of selective layers, in which are embedded functional groups, that are capable of reacting with one or more target compounds, facilitating its transport through the film, as already briefly mentioned in the introduction of this work.

Prior to being seen as an interesting industrial process, facilitated diffusion exist since billion of years within the normal biological functioning of a living organism. Each cell needs to acquire

several components from its surrounding medium and not always these can permeate through the cell wall via a diffusion process controlled simply by a concentration gradient. As pictured in Fig. 1.4, molecules can bind with a membrane-embedded channel (or carrier protein) and in this bound state are then transported inside the cell. This is useful for a living cell, since its wall is internally composed of hydrophobic phospholipids, which hinder the transport of polar molecules and ions, dissolved in the aqueous medium.
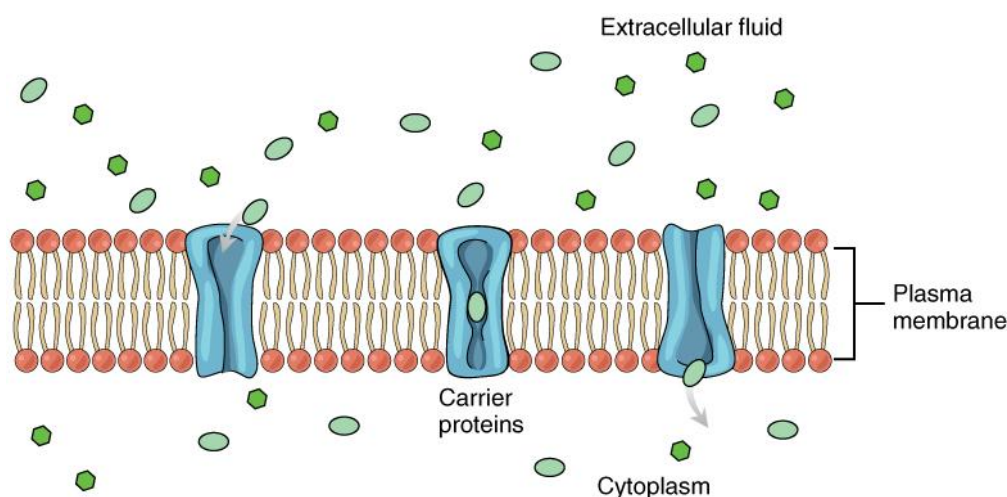

Figure 1.4: schematization of facilitated transport through a cell wall. Adapted from [31].

Other biological examples of facilitated transport can be found in the oxygen being carried in the blood stream via hemoglobin and several small molecules being transported thanks to specific carrier proteins.

Following this idea of a carrier molecule, the first example of a synthetic membrane with these characteristics was developed by Ward and Robb in the late 60s [10] and it consisted of an immobilized aqueous solution of carbonate-bicarbonate dedicated to the separation of CO_2 and O_2. This same approach of a liquid membrane, with some variation, was then replicated a few times [12].

In more mathematical terms, the transport of a reactive species in a facilitated transport membrane occurs via the usual solution-diffusion mechanism (seen in the previous paragraph) and a *carrier-mediated* mechanism, which applies for only one gas (or group of gases with similar chemical behavior), increasing its permeability. To obtain this outcome, FTMs must have a complexing agent embedded in their matrix, which can react reversibly with the target species following a reaction scheme like the following (Eq. 1.19):

$$Penetrant(i) + Carrier(C) \rightleftharpoons iC \qquad (1.19)$$

Hence, the total transport of the component A will be result of both the Fickian diffusion and the facilitated diffusion via carrier. Considering Fick's Law for the compound i and rendering explicit the two contributions it will be obtained:

$$J_i = -D_i \frac{dC_i}{dx} = \frac{D_i}{dx}\left(C_i^u - C_i^d\right) + \frac{D_{iC}}{dx}\left(C_{iC}^u - C_{iC}^d\right) \tag{1.20}$$

$$C_i = S_i p_i \tag{1.21}$$

Here, J_i represents the flux of the component i, C_i is its concentration, while C_{iC} is the one of the i-C complex. As before, the differences are calculated between the values at the upstream side (u) and the downstream one (d). D_i represents the Fickian diffusion coefficient for the species i, while D_{iC} is the same quantity referred to the penetrant-carrier complex. This carrier can be both a mobile one (as in the supported liquid membranes mentioned before), fixed (as in a Fixed Site Carrier membrane) or part of a functionalized nanoparticle in a mixed matrix membrane. Unlike in the solution-diffusion mechanism, where the flow's driving force is represented by the difference in partial pressure on the permeating species across the membrane, in the case of facilitated transport, the flow will depend on the difference in concentration of the complexed target species at the two sides of the film. Thus, if the contribution of the solution-diffusion can increase along with the differential pressure without a theoretical limit other than the mechanical integrity of the film, in the case of facilitated transport the carriers can actually become saturated, limiting the application of this technology at high pressure (e.g. natural gas sweetening).

Overall, the research dedicated to FTMs for industrial applications has been mainly revolving around the selective separation of CO_2, having this molecule a quite different chemical behavior (polar and acidic) than other typical incondensable gases found in the process industry (N_2, CH_4, H_2). For this separation, the most common type of moiety used is nowadays represented by aminated groups, hence relying on a acid-base reversible reaction for the facilitation. The reaction mechanism, that describe the interaction of carbon dioxide with these is still a matter of debate in some cases, but it usually accepted, that the path taken by the reaction depends on the degree of substitution of the amine group [32,33].

Specifically, in the case on a non hindered amine, the CO_2 will follow a reaction with formation of carbamate with a zwitterion mechanism, initially proposed by Caplow [34]. Firstly, carbon dioxide will react with the unhindered amine to create a zwitterions intermediate:

$$CO_2 + R - NH_2 \rightleftharpoons R - NH_2^+ - COO^- \tag{1.22}$$

The zwitterions is subsequently deprotonated by the amine itself to form the carbamate ion:

16

$$R - NH_2^+ - COO^- + R - NH_2 \rightleftharpoons R - NH - COO^- + R - NH_3^+ \qquad (1.23)$$
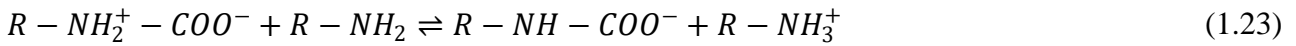
This way, the carbon dioxide will actually be moving through the film by constantly forming and breaking bonds, which allow the formation of a carbamate ion. In the case of a hindered amine (as in a substituted one), the mechanism is different and involves the presence of water.

$$CO_2 + R_1 - NH - R_2 + H_2O \rightleftharpoons R_1R_2 - NH_2^+ + HCO_3^- \qquad (1.24)$$
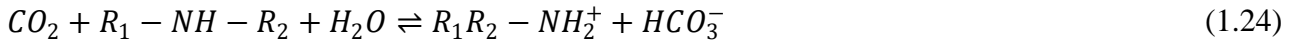
Another mechanism, proposed by Hägg and Deng [35] sees the formation of the hydrogen carbonate ion also in the presence of a non substituted amine:

$$R - NH_2 + H_2O + CO_2 \leftrightarrow R - NH_3^+ + HCO_3^- \qquad (1.25)$$

Moreover, also within this theoretical framework, the amine moieties would also concur as a catalyst in the hydration reaction of CO_2:

$$H_2O + CO_2 \leftrightarrow H^+ + HCO_3^- \qquad (1.26)$$
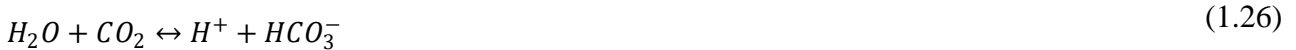
Along this last explanation the overall transport of CO_2 within an aminated fixed site facilitated transport membrane would be the one schematized in Figure 1.5.
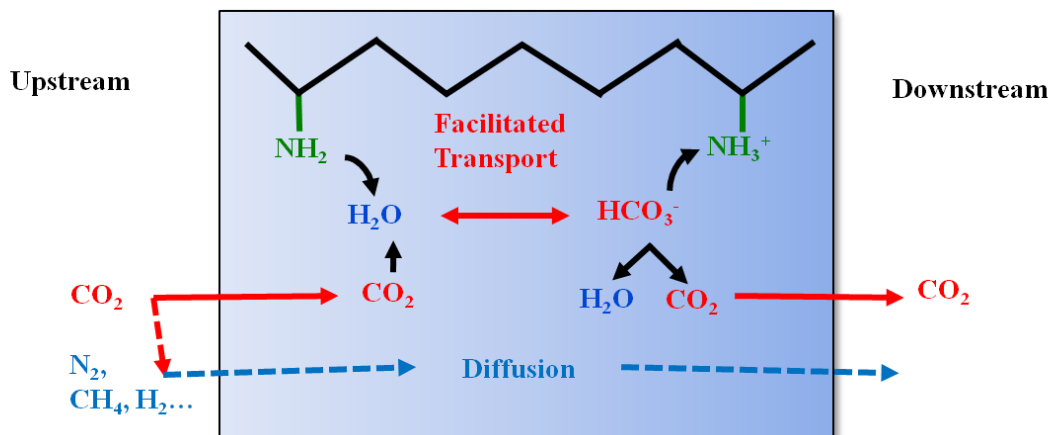

Figure 1.5: scheme of the facilitation process of carbon dioxide in an aminated fixed site facilitated transport membrane as proposed in reference [35].

Kim et al. [36] found the large influence that pH can have on the permeation performances of these films, showing how CO_2 can increase up to one order of magnitude depending on the alkalinity of the casting solution. This is due to the fact that, in order to react with carbon dioxide, the amine group must be in its free form and not the ionic one.

Chapter 2. Materials and Methods

The following chapter will be dedicated to illustrate the reagents employed in the preparation of the membrane films involved in the project and the apparatuses utilized in order to assess their properties. In particular, a series of hydrophilic polymers was used as matrix, while the fillers varied from nanocellulose to functionalized inorganic nanoparticles. The different composite materials were obtained by using different protocols to prepare the polymeric solutions and to cast the films. The latter have been characterized through the evaluation of their gas permeability, the sorption of water and through the analysis of their infrared spectrum.

2.1 Reagents

A series of polymers and reagents, listed in table 2.1, have been utilized in the project in order to prepare different typologies of membranes. Amongst the polymer used, we can find:
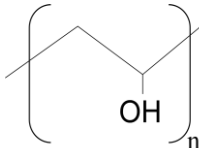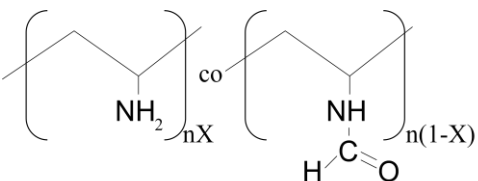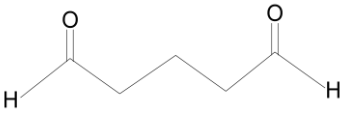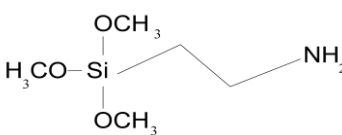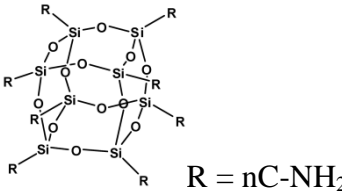
- Polyvinyl Alcohol (PVA), purchased at Sigma Aldrich under the commercial name Mowiol® 28-99, with an average molar weight of 145000 g/mol and a degree of hydrolysis of 99.0-99.8 %, in form of solid white flakes. In a different part of the project, PVA was utilized in powder form with a molecular weight of 89000-99000 g/mol (87-89% hydrolyzed) and it was also supplied by Sigma Aldrich.

- Polyvinyl Amine (PVAm), which has been kindly donated BASF Italy (Cesano Maderno, Italy) as a commercial polymer named Lupamin® in two different forms, 9030 and 9095. The two polymers were obtained via hydrolysis of Polyvinyl Formamide, in particular Lupamin® 9030 is hydrolyzed at a 30 % degree, while Lupamin® 9095 at 95 % and

commercialized respectively in a 15-17 wt% and 20-22 wt% water solution. The commercial solution also contains a significant amount of Sodium Formate, residual salt derived from the hydrolysis process; in the case of Lupamin® 9095 this percentage is around 66 wt% of the total solids. The very same polymer possesses a molar weight, which has been measured by Chen et al. [37] to be ~340000 g/mol. These polymers have been used both in their as received form and after a purification process, which will be thoroughly described later on. For simplicity, during this work Lupamin® 9095 will be directly named PVAm or polyvinylamine, even though the commercial solution has other components in it.

These polymers have been combined with a series of nano scaled materials to improve their performances. Amongst these, Nano Fibrillated Cellulose (NFC) has been employed coming from two different producers;

- Innventia AB (Stockholm, Sweden) that, through the person of Prof. Tom Lindström, donated Nanocellulose G2 (Generation 2) samples obtained a commercial sulfite softwood dissolving pulp (Domsjö DissolvingPlus, Domsjö Fabriker AB, Sweden) with a hemicellulose content of 4.5 wt%, and lignin content of 0.6 wt%. This cellulose pulp was then subjected to a carboxymethylation process, followed by the high pressure homogenization in order to obtain the nanofibrils; the whole process has been thoroughly described by Wågberg et al. [38]. The final diameter of the fibrils was reported to be in the range of 5 – 15 nm, with a length of several micrometers and a surface energy density of ~586 μequiv/g [38]. The fibrils were received as a water suspension with a solid content of 2.17 wt%.

- Centre Technique du Papier (CTP, Grenoble, France) from which a 2 Pass nanocellullose (obtained by passing the nanocellulose in the high pressure homogeneizer 2 times) was purchased. The nanofibrils were received as a 2 wt% water suspension; the density of the fibers was estimated to be ~1.5 g/cm3, with a surface charge density of about 30 μequiv/g. Thanks to a mechano-enzymatic pretreatment of birch bleached kraft pulps, followed by two high pressure homogenization steps, the NFC fibers achieved a diameter of about 20 nm and an average length of 1000 nm.

- Apart from nanocellullose, a different type of functionalized inorganic particles has also been used as a polymeric filler. In particular a proprietary mix of amine functionalized Poly Oligo Silsesquioxanes has been provided by SINTEF Materials and Chemistry under the name HAPS in a 2-Butoxyethanol solution with a solid content of 51.6 wt%.

Table 2.1: list of main reagents used during the project and their characteristics

Name	Structure	Notes
Polyvinyl Alcohol (PVA)		Solid Flakes 145000 g/mol, 99.0-99.8 %, Hydr. 89000-99000 g/mol, 87-89 % Hydr.
Polyvinylmine (PVAm)		Water Solution Lupamin 9030 X = 0.30 Lupamin 9095 X = 0.95 340000 g/mol
Glutaraldehyde		Water Solution 50 wt%
Aminopropyltrimethoxysilane (APTMOS)		Liquid, 97 % pure
HAPS **(Poly Oligo Silsesquioxanes)**	 $R = nC\text{-}NH_2$	2-Butoxyethanol solution 51.6 wt%

Beyond the polymers and fillers a series of compounds have been employed in order to modify or purify these materials. Glutaraldehyde (50 wt% in water solution) was used as a cross-linking agent, while 3-aminopropyltrimethoxysilane (APTMOS, 97% purity) was employed as a source of amine groups. Both compounds have been purchased from Sigma Aldrich and used without any alteration. Other chemicals of common laboratory use have been utilized, such as Potassium Hydroxide (KOH) and Sodium Hydroxide (NaOH) in solid pellets to prepare alkaline solutions. Hydrochloric acid (HCl) was utilized in a 33 wt% fuming solution. As solvent for all preparation involving polymers, deionized water available in the laboratory has been used.

Methanol (98 %), Ethanol (both 96 % and absolute) and Acetone (98 %), all purchased form Sigma Aldrich, have been used, without any further purification, in different laboratory procedures going from precipitation of polymers such as PVAm to solvent extraction procedures.

2.2 Experimental systems

2.2.1 Permeation setups

Throughout the project a number of different apparatuses have been utilized to assess the permeability of a number of gases in various conditions. The following paragraphs will be dedicated to the presentation of the characteristics of these permeometers.

2.2.1.1 Humid gas permeation

Due to the need of absorbed water in the matrix to achieve an efficient facilitated transport, all the permeation tests have been performed with some kind of humidification in the system. A typical setup used for this purpose is a fixed volume, variable pressure humid permeometer, whose layout can be seen in Figure 2.1.

This apparatus relies on a barometric technique, which evaluates the permeability of a film through the pressure variation in the downstream volume V_d (highlighted in Fig. 2.1) [39]. The sample is placed in a Millipore sample holder, with a diameter of 4.7 cm and a filter area of 9.6 cm^2.
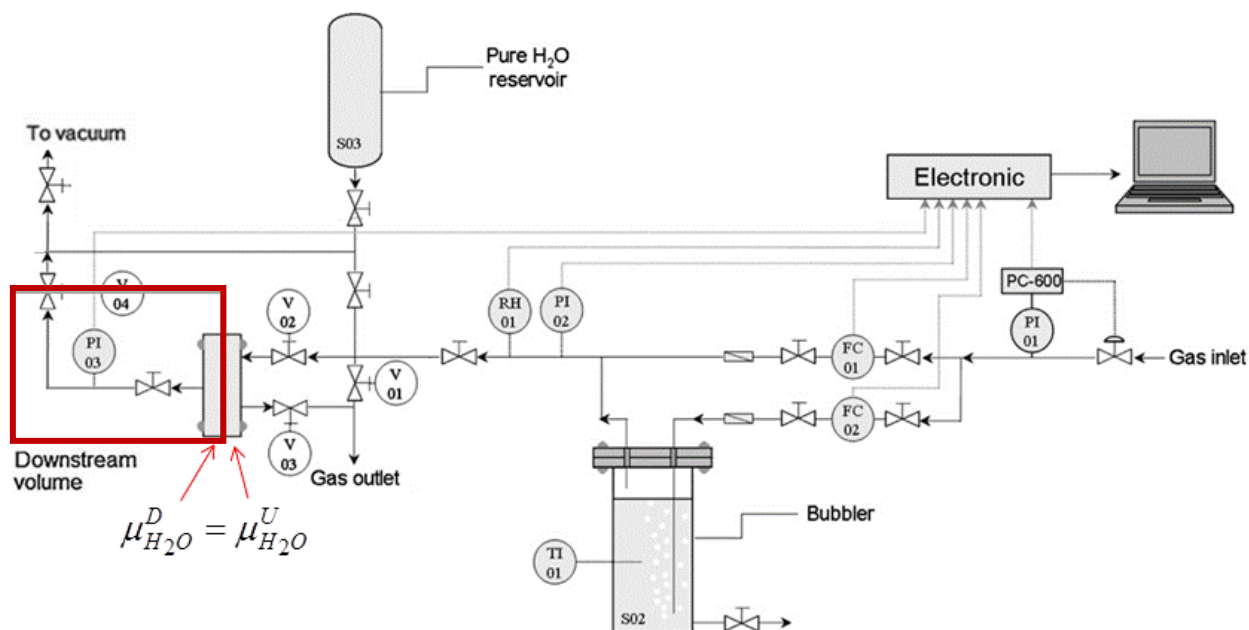

Figure 2.1: Layout of the humid permeation apparatus

In order to maintain a steady temperature, the whole system is built inside an incubator, which allow a temperature range between 25 and 50 °C, with an accuracy of ± 0.1 °C. In a different version of the same setup, a thermostatic bath is used for the same purpose.

Once the sample is in place and a good seal is achieved, valves V04, V03, V02 and V01 are opened and dynamic vacuum is pulled for a few hours until all pollutants are removed from the system. It must be noted that Lupamin® based membranes do not cope well with full dynamic vacuum for prolonged time, since they tend to become extremely brittle in a dry state. For this reason, these films have been subjected to vacuum, while periodically feeding a small amount of water in the system. Once the pollutants are removed, the valve leading to the water reservoir S03 is opened for a brief time (around 30 s) to strip out possible gases dissolved in the liquid. The valve leading to the vacuum pump is then closed, while keeping downstream and upstream volume in contact. In order to humidify the film, the valve from S03 is opened and both humidity (via the humidometer RH01) and total pressure (via PI03) are measured. When the pressure and the humidity measured are stable over time and have reached a desired level, the water activity inside the membrane will have also achieved a known and steady condition, being in equilibrium with the vapor phase. Valves V02, V03 and V04 are then closed, sectioning the calibrated downstream volume, whose capacity is usually 23 cm^3, but can be increased up to 87 cm^3, when dealing with high permeating gases.

A gas stream is then flown through the system at a rate of usually 1000 cm^3(STP)/min in total and split into two branches; one is kept dry, while the other one is humidified via a bubbler. The flow-rate in the two branch is controlled by two flow controllers, one per branch, thus allowing to fix the humidity of averall stream which is then also monitored via the hygrometer RH01. Once the humidity of the stream matches the one of the film, valves V02 and V03 are opened and V01 is closed, exposing the cell to the gas flow. The humidified gas will start to flow through the polymeric film and into the downstream volume, increasing the pressure measured by PI03. Being the activity of the water in the upstream, equal to the one in the downstream ($\mu^U_{H20} = \mu^D_{H20}$), the resulting increase of pressure in the volume V_d will be eventually only due to the permeation of the incondensable gas. Figure 2.2 shows the typical trend of the downstream pressure and its derivative.

$$P_i = \left(\frac{dp_i^D}{dt}\right)_{t\to\infty} \cdot \frac{V_d}{R \cdot T \cdot A} \cdot \frac{\delta}{(p_i^U - p_i^D)} \tag{2.1}$$

The asymptotic pressure derivative can be used to calculate the permeability of the gas through the Equation 2.1. Figure 2.3 summarizes the steps of equilibration and permeation in terms of activity of the chemical species involved.
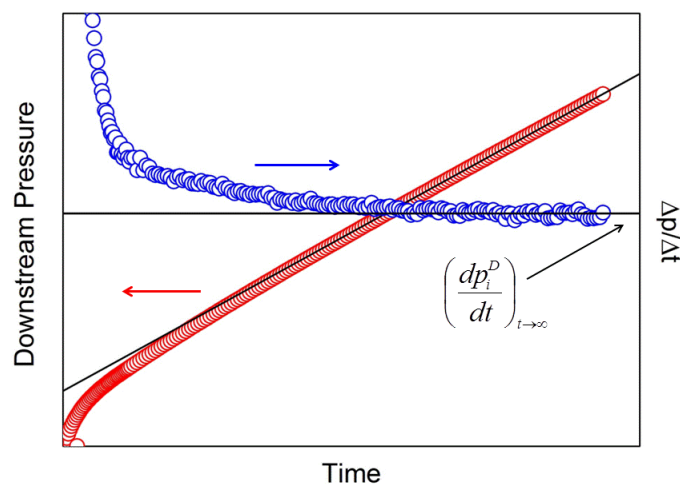
Figure 2.2: output of a permeation experiment, pressure (red) and pressure derivative (blue) over time

Once a steady state condition is achieved for a given humidity, the procedure is repeated by pulling vacuum and equilibrating the system at a higher water content. Eventually it will be possible to build a curve expressing permeability as a function of relative humidity (or water activity).
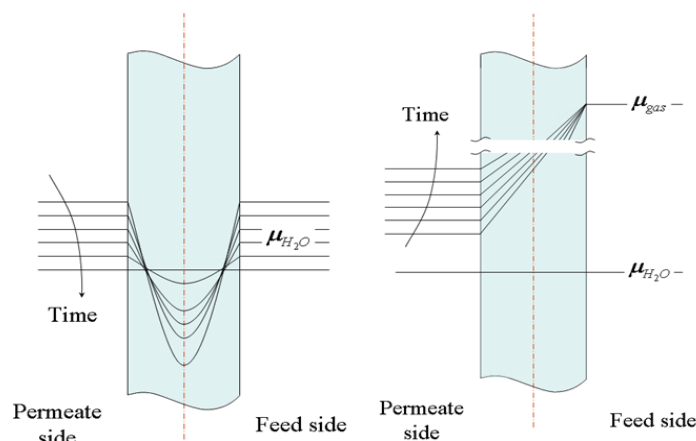

Figure 2.3: equilibration of water in the membrane film (left), permeation of the gas through the film (right)

2.2.1.2 Mixed gas permeation

Another permeometer was used to gain information regarding the permeability of mixtures, in particular for cross-linked PVA membranes. From the layout of the system presented in Figure 2.4 it can be seen how the apparatus can be fed with mixture prepared via two flow controllers (Bronkhorst Flow Meters). These are used to mix the incoming gases in a single stream, which, as in the previous system, is then split in two branches, for humidification purposes. One of the branches indeed lead to a bubbler (S01) where it is saturated before rejoining the other one. The ratio between the two streams and thus the feed RH is modified via a manual regulation valve (V2). The now humidified gas is then fed to the sample holder, which is immersed in a thermostatic bath

to ensure thermal stability. Before entering the membrane cell, an indicator measures the temperature and relative humidity of the stream. The cell has a diameter of 47 mm, a permeating area of 9.6 cm^2 and I characterized by a radial flow on the gas which on obth side I fed from the center and leave the cell from the sides of the membrane. On the downstream side a flow of nitrogen as a purge is used to maintain a low partial pressure of the permeating gases; the permeate is collected via a tube in tube system and its temperature and humidity are measured by a second hygrometer (TI-2, RH-2).
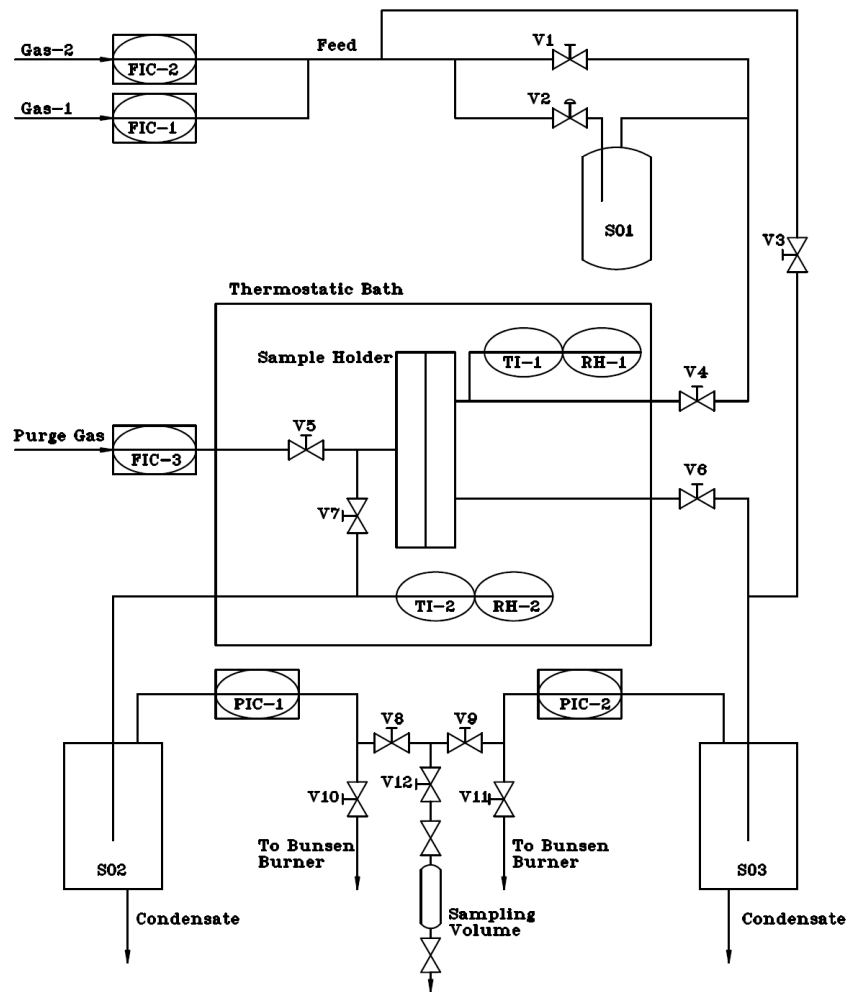

Figure 2.4: layout of the mixed gas permeation setup

The pressure on both downstream and upstream sides is controlled via two pressure indicator and controllers (Bronkhorst Pressure Meters) and usually kept slightly above atmospheric pressure in the permeate and around 3–4 bar in the retentate. To preserve the two controllers, the streams' water content is reduced via two knock-out drums (S02 and S03) kept at a lower temperature and the condensate collected periodically. In order to analyze the composition of the different flows a five way valve is set at the end of the apparatus, connected to a sampling volume. When the permeate is

to be analyzed, valves V9 and V12 are opened allowing the flow to pass through the volume up until the point, in which the concentration is uniform; this happens usually after 20-25 minutes. For the permeate, the situation will be similar, except valves V8 and V12 are open. If the feed composition is to be evaluated, V1 and V2 are closed and the bypass valve V3 is high opened, allowing it to flow in the retentate line.

Once the sampling volume is filled with the desired composition a series of gas samples are taken from it via a gas syringe and injected in a gas chromatograph (Agilent Technologies Inc.); on average 3 injections are performed for each analysis. Permeability of the sample is then evaluated by calculating the molar flow of the permeating gases in the permeate stream via the Equation 2.2

$$P_i = \dot{n}_{Purge} \cdot \frac{y_i}{1 - \sum_j^{n \neq purge} y_j} \cdot \frac{\delta}{A \cdot (p_i^U - p_i^D)} \tag{2.2}$$

Each humidity setting is kept until stability of the permeability of all the gases involved is reached; the ratio between the two gas streams is then changed and a new experimental point found. This system, contrary to the fixed volume humid permeometer, is useful when dealing with membranes, which can guarantee a reasonably high permeating flow, since a small concentration cannot always be detected by the gas cromatograph.

A similar setup (Fig. 2.5) has been used also at the MEMFO laboratories Norwegian University of Science and Technology in Trondheim (Norway). The main different resides in the gas analysis, which is performed online through a micro-GC (Varian 490) directly connected to the outlet of the various streams and that the temperature is controlled through an incubator rather than a thermostatic bath.
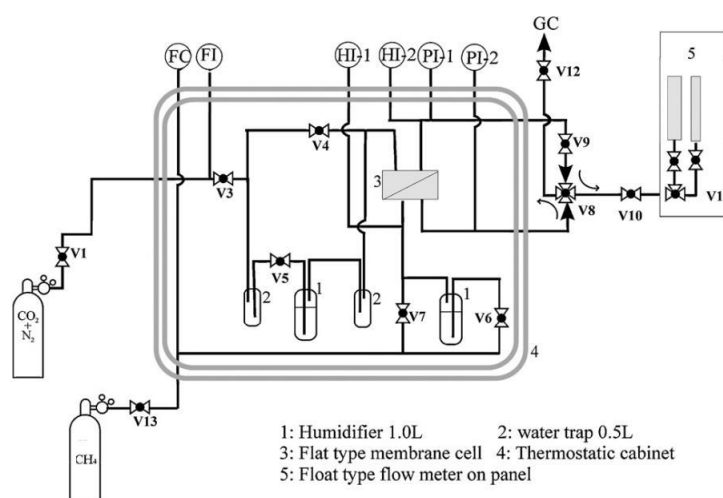

Figure 2.5: Mixed gas permeation setup at MEMFO.

2.2.1.3 High temperature mixed gas permeation

This apparatus was originally developed to measure the permeability of cylindrical metallic membranes for hydrogen separation [40]. During this project, it has been modified, in order to be able to house flat sheet polymeric membranes via the substitution of the sample holder and the tubing connecting it to the rest of the system. The main characteristic of this system is the fact that the entire permeation cell is contained inside an oven (as shown in Figure 2.6), which can reach temperature above 600 °C, even though for the purposes of this work no temperature higher than 120 °C has been investigated.
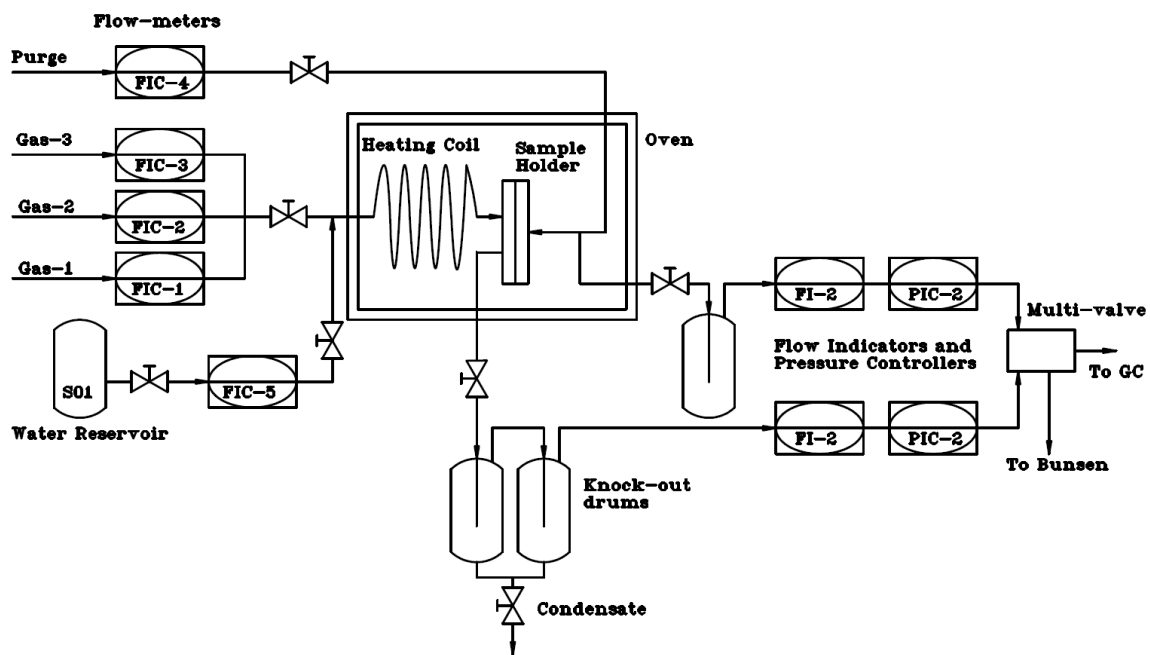

Figure 2.6: layout of high temperature mixed gas permeation setup

Up to three gases can be fed at the same time via flow controllers (Bronkhorst Flowmeters), but for the most part a CO_2 humidified stream has been adopted for testing. In order to humidify the gas, liquid water is fed directly into the stream thanks to a pressurized reservoir (S01) and a liquid flow controller (FIC-5). The whole mixture is then fed inside the oven and the water is vaporized thanks to a heating coil before reaching the membrane. Here the partial pressure of the permeating gas on the downstream side is kept low thanks to a flow of nitrogen used as a sweep gas, whose flow is controlled by FIC-4. Both retentate and permeate flows pass through knock-out drums, in order to reduce the water content before being sent to the gas cromatograph. The pressure of the downstream and upstream section is controlled by two controllers placed after the water removal step and paired with two flow indicators. All gas streams are then fed to an automatic multi valve, through which a specific stream can be selected and sent to analysis, while the remaining ones are fed to a Bunsen

burner. The gas cromatograph is directly in line and is capable of performing automatically periodical analyses on the gas stream. For a given gas, the permeability is given by a calculation similar to what previously seen for the mixed gas permeometer, but with the actual permeate flow known from the indicator (Eq. 2.3).

$$P_i = \dot{n}_{Permeate} \cdot y_i \cdot \frac{\delta}{A \cdot (p_i^U - p_i^D)} \tag{2.3}$$

2.2.2 Water absorption setups

Here will be presented the apparatus mainly used, in order to assess the water uptake of a film as a function of the activity of the penetrant in the vapor phase. This kind of tests allow a more extensive comprehension of the influence of the concentration of water on the performances of a membrane, a parameter, which results quite significant, when dealing with facilitated transport membranes.

2.2.2.1 Quartz Spring Balance

This apparatus is used to evaluate the solubility of a penetrant in a polymeric film and also to estimate its diffusivity in a wide range of activities and at a variable temperature. A detailed explanation of the setups has been performed by Piccinini et al. [41]. It consists of a jacketed glass column, whose temperature can be controlled via a circulating thermostatic water bath with an accuracy of ± 0.5 °C. A quartz spring of known elastic constant is hanged at the top of the column and it is free to extend towards the base. A sample of known weight is attached to the bottom of the spring and drives the extension of the spring with its weight variation, due to the uptake of the penetrant. From Fig. 2.7, it can be seen that the sorbing species, demineralized water in the present case, is stored in a tank (S02) in its liquid form.
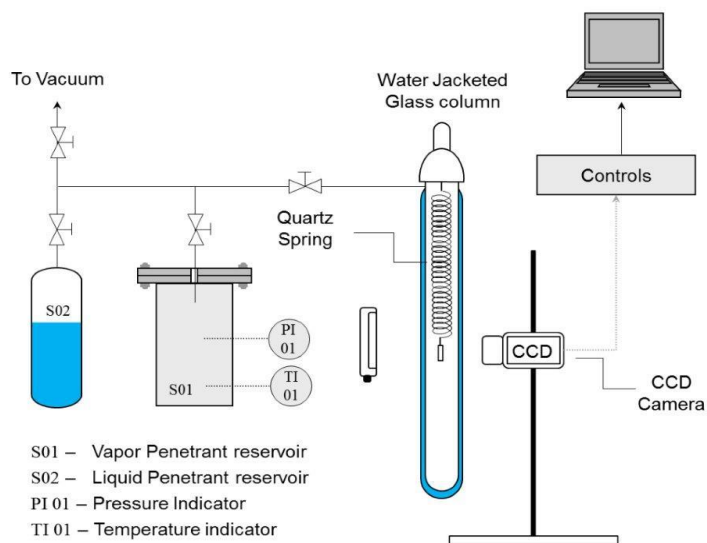

Figure 2.7: layout of quartz spring balance water sorption setup

Before the beginning of each test, dynamic vacuum is applied to the column containing the sample via a system comprised of a vacuum pump and a liquid nitrogen water trap. This eliminates all foreign compounds from the film and sets the starting point of the sorption test. Once the sample is evacuated, the column is isolated thanks to a valve and the water reservoir is opened in order to allow the liquid to vaporize in the 4 L expansion tank (S01). Here, pressure and temperature are measured, so that the vaporization can be carried on, up until the desire vapor activity is reached. This is calculated as simply the ratio of the partial pressure of the gas (equal to the total pressure) and its vapor pressure at the temperature measured (Eq. 2.4)

$$a_w = \frac{P_w}{P^*(T)} \tag{2.5}$$

Once this loading process is completed, S02 is isolated once again and the column exposed to the penetrant. The displacement of the film is recorded via a CCD Camera (Series600 Smartimage sensors) manufactured by the DVT corporation (Norcross, GA). In order to achieve a better reading of the elongation, an aluminum foil reference of well known dimension is attached near the sample; the camera is set to record its displacement. Figure 2.8 presents a screenshot of the view from the CCD camera, where the rectangular aluminum reference is quite visible, as well as the sample hanging at the bottom of it. The long axes measure the total displacement of the reference and are pointed downwards, in order to give a positive signal when mass is gained. The smaller lines measure the width in pixels of the reference, hence allowing the conversion from this unit of measurement to millimeters.
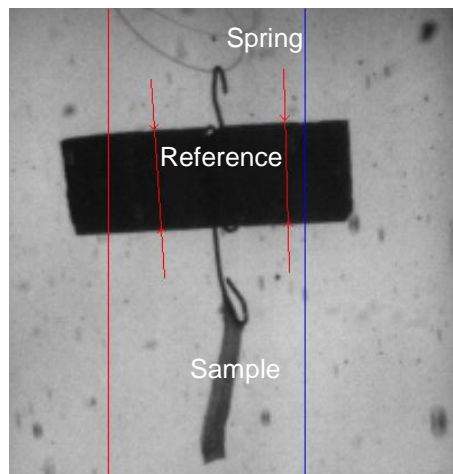

Figure 2.8: screenshot of the view from the CCD camera of the quartz spring balance, which includes reference and sample hanging from the quartz spring during a water sorption test.

The signal is sent to a computer and the image elaborated through the software Framework, also form DVT. After a certain time, equilibrium conditions will be reached and the protocol can be repeated by isolating the column once again and loading a higher pressure in the expansion tank.

The variation in length of the spring can be used to calculate the mass gained by the sample during the ith step, via the application of Hooke's law, as shown in Equation 2.6.

$$\left[m_{penetrant} \right]_i = k \cdot \frac{(h_i - h_{i-1})}{g} \tag{2.6}$$

Here, k represents the elastic constant of the spring, while h_i is the spring height at the ith step; by summing all mass contributions up to a certain step, the total mass of penetrant absorbed can be found. The contribution of the buoyancy force has been neglected, in view of the very low pressure, at which the tests are conducted.
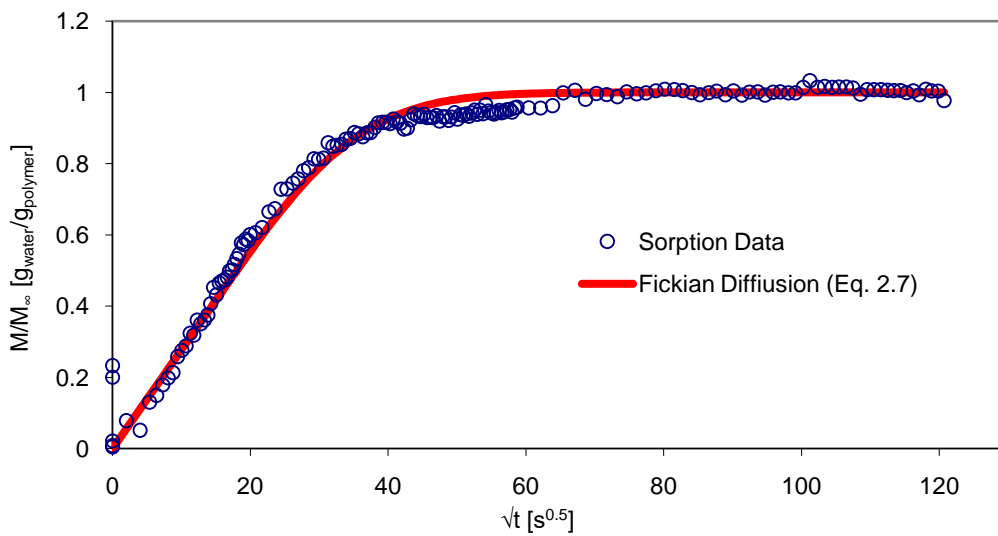

Figure 2.9: example of the analysis of the transient phase of a sorption test. The mass gain is expressed as the ratio respect to the fickian equilibrium mass and plotted with the square root of time.

Through the analysis of the transitory phase of the saturation curve (Fig. 2.9), the diffusion coefficient of the penetrant can be also estimated. Equation 2.7, developed by Crank [42], has as only incognita, once all geometric parameters are introduced, the diffusivity $\mathcal{D}$, which can be then guessed in order to fit the experimental curve.

$$\frac{m_{sample}}{m_{sample\,,t\to\infty}} = 1 - \sum_n \frac{8}{(2n+1)^2 \pi^2} exp\left[\frac{-\mathcal{D}(2n+1)^2 \pi^2 t}{L^2}\right] \tag{2.7}$$

2.2.3 Fourier Transform Infrared Spectroscopy (FTIR)

As a way to assess the modification performed onto the polymers employed, Fourier Transform Infrared Spectroscopy (FTIR) has been usually performed. This analysis method relies on the transmission of an infrared beam through a sample of the material and measure the radiation transmitted via a detector. As a result an absorbance (or transmission) spectrum is obtained (Fig. 2.10), where the different position and shape of peaks can be related to the presence of specific

functional groups. An advantage of this technique relies in a quick result output, but this is commonly used for qualitative assessments, rather than quantitative ones.
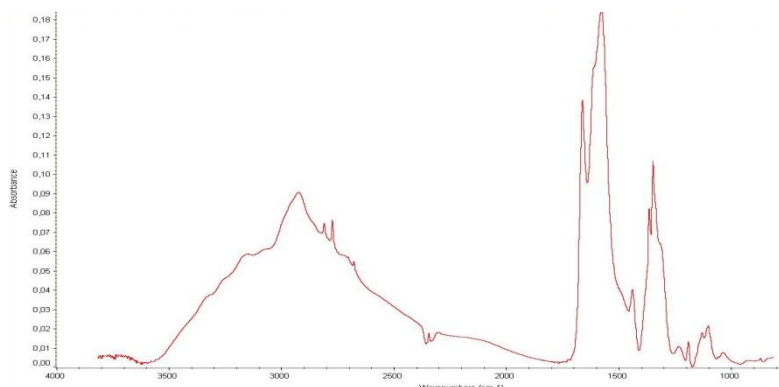

Figure 2.10: example of the FTIR spectrum of Lupamin® 9095 as seen in the Omnic software

For the analysis performed during this project, a FTIR spectrometer Nicolet 380 from Thermo Scientific was used in the MEMLAB laboratories at the DICAM, University of Bologna.

In general, in a IR spectrometer the radiation is emitted from a black body-like source and passes through an aperture that fixes the amount of energy that the sample will receive. This specific apparatus uses the EverGlo technology as source for the beam and a Helium-Neon laser as a reference. Before reaching the sample, the radiation is further regulated by an *interferometer* and a KBr *beamsplitter*. When the beam reaches the sample part of the radiation is absorbed, while the rest passes through and is detected. The signal is then converted from analogue to digital, sent to a calculator for Fourier transformation and can be visualized as a series of energy peaks as a function of the wavenumber (Fig. 2.10).

The molecules in the sample under study will only absorb radiation when the incoming infrared radiation has the same frequency as one of the fundamental modes of vibration of their fundamental groups. This happens, since the atoms in a molecule or functional group undergo relative movements around their equilibrium sites, leading to variations of the bond's length or orientation. An output signal in the IR spectrum can be representative of a single particular bond between two atoms inside a certain molecule.

There are several types of vibration modes (Fig. 2.11), involving variations on the bond lengths (stretching) or angles (bending). These movements can take place with the atoms in phase (symmetric stretching and rocking) or out of phase (asymmetric stretching and scissoring). In molecules with planar conformations, atoms can also vibrate outside this plane, resulting in out-of-plane bending designed as wagging or twisting, depending if the atoms are moving in phase or not,

respectively. Other types of vibrations, called skeletal vibrations, involve larger parts of the molecules, and this may be relevant in the case of polymers or oligomers.
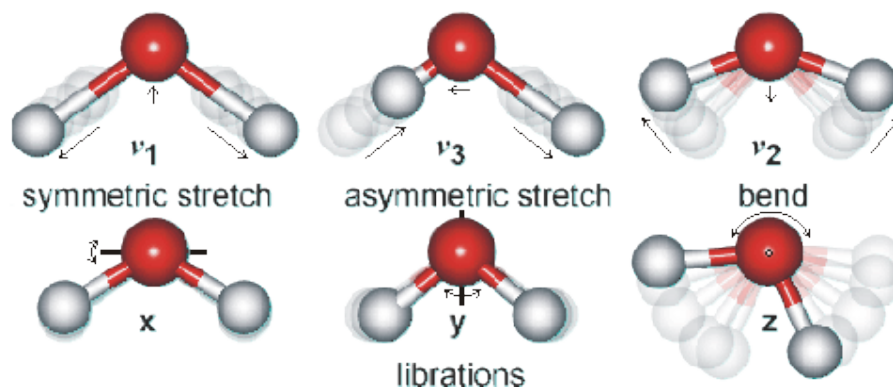

Figure 2.11: types of molecular vibration occurring during an FTIR analysis

Inside the crystal, the beam is trapped by total reflection and bounces a number of times, which depends on its geometry, and is absorbed by the sample on the surface of the ATR element. Each time the infrared beam reaches the crystal surface indeed and evanescent wave is formed and propagates in the film, for a depth ranging from 0.5 to 2 µm, allowing the infrared absorption. and the formation of an ATR spectrum at the exit of the instrument (Fig. 2.12). Since only a small portion of the sample is interested by the absorption process, the resulting absorption signal is significantly reduced and more reliable.

During the project, most ATR analyses have been performed using a MIRacle™ Single Reflection ATR from Pike Technologies, which employs a ZnSe crystal. This specific add-on for the IR spectrometer allows the infrared beam to bounce a single time inside the sample, before being sent to the detector. For the materials analyzed, this allowed an even clearer output signal.

Before each series of analyses with this technique, liquid nitrogen was poured into a specific reservoir into the spectrometer: this is used by the apparatus to cool its detector to an optimal temperature. Subsequently a background spectrum was acquired, by performing an analysis without any sample onto the crystal. Once the backgrounds was acquired drop of a solution containing the polymer of interest was used to cover the crystal. Usually, less than a milliliter of solution was sufficient for this purpose. The solution was then dried with the aid of a hot flow of air run over it in order to vaporize all solvent and guarantee in such way a optimal adhesion to the crystal.
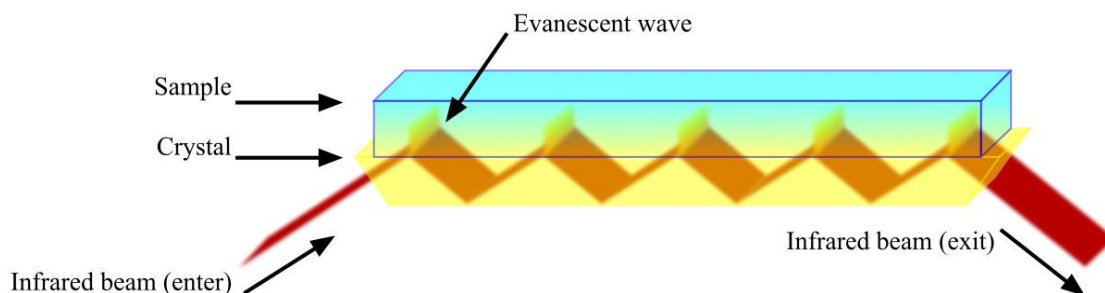
Figure 2.12; path of an infrared beam through an FTIR-ATR crystal

This is, in fact, a critical aspect of ATR spectroscopy, since a non optimal adhesion of the sample to the crystal results in strong interferences from the surrounding atmosphere. A few spectrum were acquired per sample, mostly to verify the volatilization of all solvent, since a satisfying one was obtained. Once the analysis was completed on a sample, the residual polymer was washed with a proper solvent (usually water was enough, since any acidic substance can react with the crystal), to prepare it for the next acquisition. The acquired spectra have been analyzed via the software Omnic, provided along with the spectrometer and the acquisition method used employed 32 scans per spectrum and a resolution of 4 cm^{-1}.

2.2.4 Other apparatuses

Micrometers

To assess the thickness of the casted films, two different micrometers have been employed. The first one is a digital micrometer (Mitutoyo Absolute Series 227-221), with a sensitivity of 0.001 mm, a range of 0-0.15 mm and a measuring force between 0.5 and 2.5 N. The second is a mechanical pin micrometer (Huggenberger, Zurich) with a sensitivity of 0.001 mm. This second one was the least used, since it tends to deform the soft rubbery samples by compression, resulting in an underestimation of the actual thickness.

Three roll mill

This device was used to achieve a proper dispersion of the nano phases in the polymeric solution, especially nanocellulose. The mixing is performed by three steel cylinders, called rollers, which rotate at a given speed, while the solution blend is poured between two of these. Thanks to the viscosity of the solution and the very small distance between the rollers, the fluid does not fall and coats the cylinders, being mixed by the shear stresses developed by the rotation. The model used is an EXAKT 35 (Norderstedt, Germany), provided with rollers of 3.5 cm in diameter (Fig. 2.13).
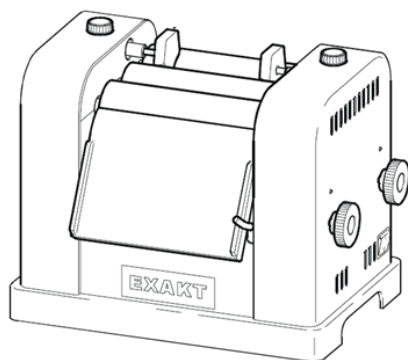
Figure 2.13: three-roll mill used for solution mixing

By varying the gap between the rollers a finer or rougher mixing can be achieved. Once the solution was rolled for a sufficient amount of time, a scraper was used to collect it. When necessary, a second passage was performed, in order to improve the mixing.

Sonication bath

As way to remove air bubbles or improve the contact between the nano-phases and the polymeric matrix, solutions were often sonicated, by placing them into a sonication bath. The apparatus used is from Lavo Srl (Model ST-25) and worked with a frequency between 38 and 25 kHz. During the sonication time, the temperature was kept within a reasonable range by removing hot water from the bath and replacing it with cold one.

Knife-coater

The realization of a portion of the membranes involved the need to cast a thin film of polymer solution onto a porous support. To achieve this, a BYK-Gardener Film Casting Knife was used. This applicator consists of two end plates joined via a bridge, which supports an adjustable blade underneath it. Two micrometers (Mitutoyo) extend through the bridge up to the upper part of the blade allowing it to be positioned at the required height for the operation with 10 μm increments. The two lateral end plates allow the containment of the solution during drawdown.
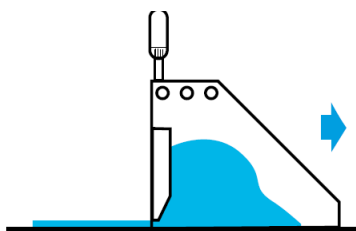

Figure 2.14: casting of a polymeric solution via a coating knife

Scanning Electron Microscope

In order to assess the thickness of the supported membranes, an electron microscope was used at the MEMFO laboratories of NTNU University. The model used is a Hitachi Tabletop Microscope TM3030, capable of a magnification from 15 to 60'000x and the micrographics were acquired with a 15 kV method.

2.3 Solution preparation and film casting

Here, the different methodologies regarding the preparation of polymeric solutions and blends for casting will be discussed. A few techniques have been employed to achieve a permeating film, whose permeability could be tested, ranging from a supported film onto a porous medium to a self-standing film. The various techniques will be divided according to the reagents employed.

2.3.1 Cross-linked polyvinylalcohol films

This section of the work represents a first approach to the realm of facilitated transport membranes, which have been performed within the MEMLAB research group. In order to have an initial point of reference, the activity was modeled around the results achieved by Prof. Ho from Ohio State University (Ohio, USA). In particular, these membranes consist of a matrix of cross-linked polyvinyl alcohol, onto which aminopropyltrimethoxysilane (APTMOS) is grafted as a source of amine groups. The solution was subsequently casted onto a micro porous Polysulfone support in order to test its permeability in humid conditions for CO_2 and H_2.

PVA was received as solid flakes, which have been added to deionized water, in order to achieve a 10 wt% solution. To ensure total dissolution of the solids, the mixture has been stirred under reflux in a thermostatic bath at 90 °C overnight. Following the work of Ho et al. [43], once a clear solution was obtained, APTMOS was added in a 1/16 molar ratio respect to the repetitive unit of PVA to attach the amino silane to the polymer chain. This reaction, reported in fig. 2.8 and schematized in figure 2.9, involves three different steps. In the first one the APTOMS added to the solution, is stirred for 5 minutes to have methoxy groups hydrolyzed, producing methanol and leaving hydroxyl groups in their place (step 1 of Figure 2.15). This step increases the silane reactivity thus allowing its reaction with the PVA. This is achieved by adding hydrochloric acid in a solution at 37 wt% as a catalyst and conducting the reaction under reflux for 80 minutes at the temperature of 80 °C (step 2 of Fig. 2.15).

The last step of the reaction is the modified PVA crosslinking performed with Glutaraldehyde (GA) in alkaline environment. To that aim, an aqueous KOH solution (1:2 base-water ratio) is prepared, mixed with the modified PVA solution and homogeneized by stirring for 15 minutes. Glutaraldehyde is then added as a 50 wt% solution in water in three different steps, 15 minutes apart each other, while stirring and keeping the temperature at 80 °C (step 3 of Fig. 2.15).
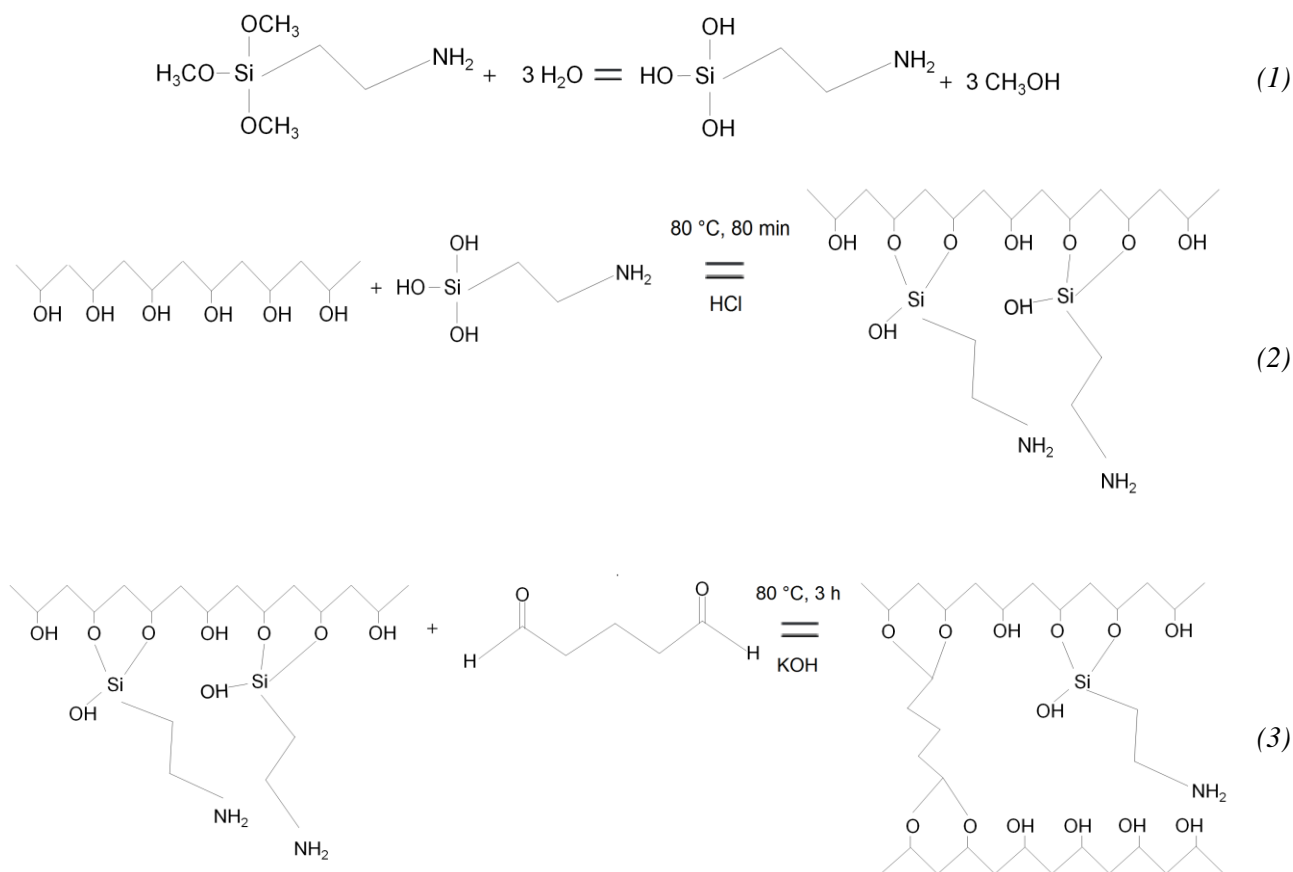

Figure 2.15: reaction scheme of PVA grafting and cross-linking, including (1) methoxysilane hydrolysis,(2) methoxysilane grafting,(3) glutaraldehyde cross-linking.

In total, a quantity of GA needed to achieve a 60 % cross-linking degree is added, assuming each molecule reacts with 4 hydroxyl groups and all molecules react. This 3 step procedure, combined with the high temperature and the constant stirring is needed in order to not cause a sudden increase in the viscosity of the solution, which would result in a gelation of the system. After 3 hours at 80 °C the reaction is completed, as also indicated by a change in color of the solution, which turns from transparent to a dark brown.

The membrane support was microporous polysulfone (PSf) with a pore diameter of about 0.01 μm and a total thickness of 145 μm, comprehensive of a non-woven fiber layer for added mechanical resistance. To prepare it for casting, it was washed with deionized water for a few minutes and dried

with a dry gas flow. It was subsequently taped to a glass sheet, in order to guarantee a flat surface. A few milliliters of the cross-linked PVA solution were placed onto the PSf via a Pasteur pipette and then spread via a coating knife (Fig.2.16).
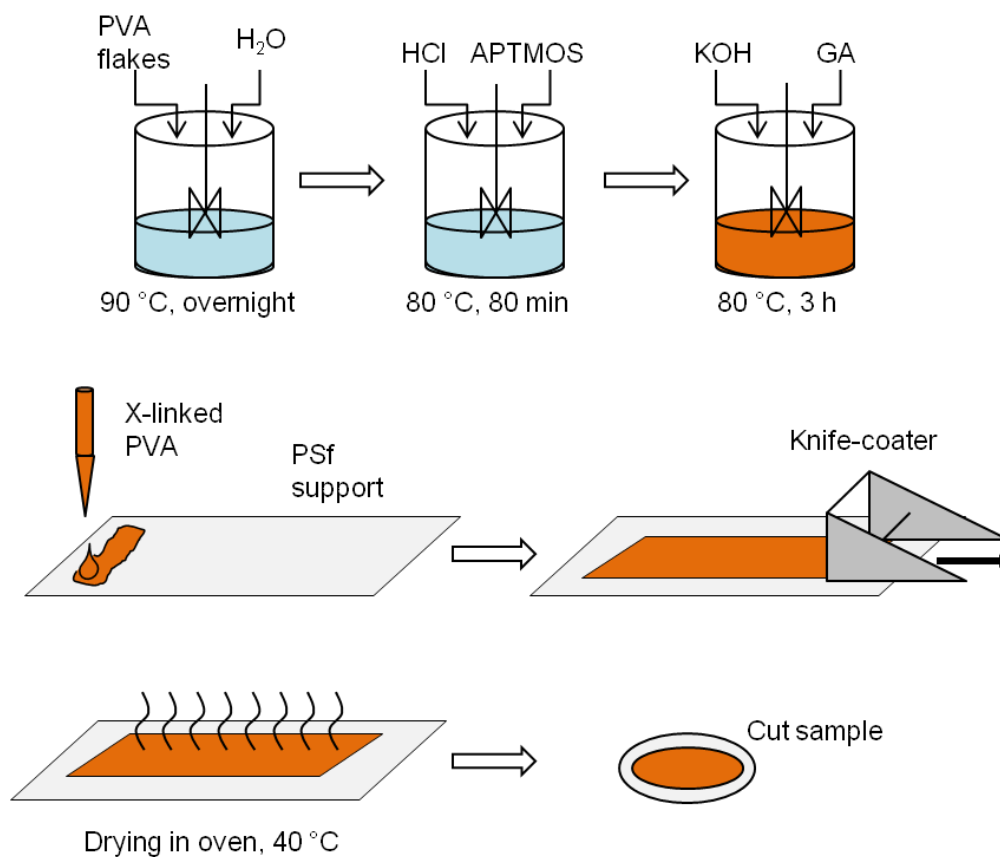

Figure 2.16: scheme of the synthesis and casting of cross-linked PVA.

Once coated, the membrane was dried in an oven at 40 °C for a few hours. The dried film was prepared for the permeation test by cutting it with a punching die of 46 mm in diameter. Its thickness was assessed via a flat head micrometer to be 15 μm.

2.3.2 PVA based amino functionalized nano-composites

This section of the work has been developed at the MEMFO laboratories in the Department of Chemical Engineering at the Norwegian University of Science and Technology (NTNU) in Trondheim. The group, lead by Prof. May-Britt Hägg, has been researching facilitated transport membranes for CO_2 separation for over a decade and it is considered one of the most advanced facilities in the field.

During the period spent at NTNU, a series of membranes were synthesized by adding amine-functionalized nano-particles to a polyvinyl alcohol (PVA) matrix. The solution was then cast via dip-

coating on a Polysulfone (PSf) support and subsequently the permeation properties assessed thanks to a mixed gas permeation setup, while the thickness of the coating was analyzed through a scanning electron microscope (SEM). This experiments had the aim to evaluate the influence of different loadings of amine-functionalized nano-particles on PVA, in the hope that the amine groups, in combination with the humidified matrix, would achieve facilitated transport of CO_2 through the film. They have been carried on under the European project HiPerCap (High Performance Capture), dedicated to create high permeance membranes for the separation of CO_2 form flue gas.

The procedure chosen to create a thin film onto a porous support was developed by Deng and Hägg [44] and starts by preparing a 10 wt% stock solution of PVA in water. PVA powder (89000-99000 MW, 87-89 % hydrolyzed) as a solid powder was added to deionized water and the whole mixture was left at 90 °C under reflux for 7 hours to ensure a proper dissolution. Moreover, in order to limit the formation of bubbles, while keeping the system homogeneous, the bottle was left rolling overnight at slow speed.

The nano-particles used belong to the family of compounds called polyoctahedral silesquioxanes (POSS); these consist of a cage-like structure, represented in Fig. 2.17, built by silicon-oxygen bonds with Si atoms at the vertexes. This kind of structure can be engineered in different geometries, like cubic or orthorhombic, which are usually classified by the total number of vertexes. The synthesis process starts commonly by single silane molecules, which carry the desired substituent group and are then condensed in an oligomeric structure, that arrange itself in one of the afore mentioned geometries.
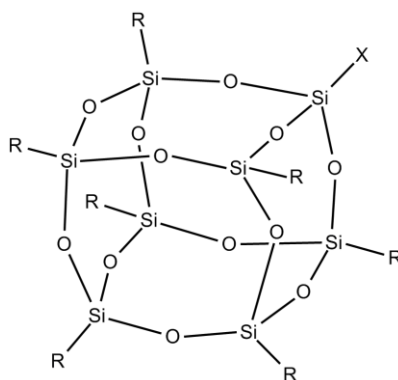

Figure 2.17:Example of a cubic functionalized silesquioxane

In the case of the HiPerCap project, the nanoparticles were provided by SINTEF Materials and Chemistry, which synthesized them via a proprietary technology called FunzioNano®. These were functionalized with –NH$_2$ terminated alkyl chains and used as an organic solution under the name HAPS.

In a series of 100 mL bottles the 10 wt% PVA stock solution was added and then diluted with water. Then, the HAPS solution was added drop wise and for each bottle the amount was calculated in order to have a concentration of PVA+HAPS equal to 1 wt%. What was varied amongst the

bottles prepared, was the ratio between the polymer and the nano-particles, varying from pure PVA as control and a 1:0.8 PVA:HAPS ratio summarized in Table 2.2.

Table 2.2: ratios of PVA:HAPS for the different solutions prepared

Solution mass [g]	Solution concentration [wt%]	PVA:HAPS
100	1	1:0 (Pure PVA)
100	1	1:0.05
100	1	1:0.1
100	1	1:0.2
100	1	1:0.4
100	1	1:0.8

All substances have been weighed inside the bottles and right after this operation, these have been stirred at 500 rpm for 2 hours to achieve a good homogenization of the components. While keeping the stirring a small amount of NaOH 1 M solution was added, in order to have a final pH of the casting solution of 12. All the mixtures were then passed through a 5 µm syringe filter to remove possible impurities collected during the weighing process. As a final mixing, the bottles were left rolling overnight.

To guarantee a proper support to the polymeric film, micro-porous Polysulfone (PSf) has been chosen, with a molecular cut-off of 20000. This choice has been made, in order to minimize the possibility of the polymer dripping inside the support's pores having it a molecular weight significantly higher than the MWCO. PSf was taped, using masking tape, to a glass sheet of 10x20 cm and few millimeters in thickness. Afterwards it was left inside a large amount of deionized water for 1 hour, in order to remove its protective coating.

Once the supports were ready, the PVA mixtures were poured in custom made rectangular glass containers and the glass sheet with the PSf taped onto it was dipped in the liquid for 30 seconds and then removed. Once the first coating was completed, all films were left on a steep inclined plane, to allow the solution in excess to flow off for 1 hour at room temperature. Once this first drying step was complete, the membrane were put inside an oven and heated at 90 °C for 1 hour. After this time, the whole procedure was repeated once more, this time dipping the support upside down respect to the first time. This is done in order to minimize the differences in thickness of the selective layer. This same exact procedure was repeated for all PVA:HAPS solutions.

The effectiveness of the coating process was assessed via Scanning Electron Microscopy, in particular, a piece of the membrane was cut and then freeze dried in liquid nitrogen, in order to induce a brittle crack in the film. Once cracked, the specimen was placed on a sample holder using carbon tape, aimed at keeping it vertical, and gold plated to make the surface conductive. Fig. 2.18

shows the micrographs resulting from this analysis. In each one it is quite visible the porous PSf support, whose porosity increases on its way down, while on top of it, the polymeric selective film can be distinguished. Using the built-in software of the microscope, it was possible to measure the selective layer to be around 3 μm thick.
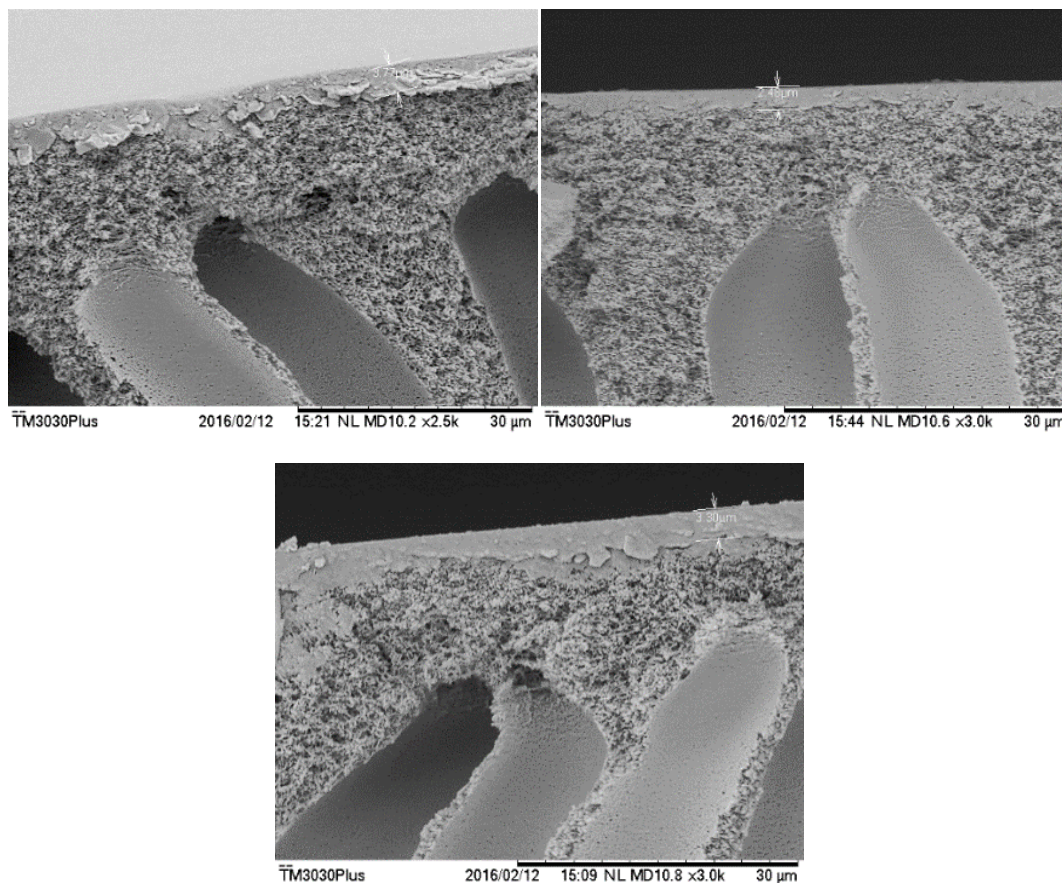

Figure 2.18: SEM micrographs of the cross sections of: Pure PVA (left), PVA:HAPS 1:0.05 (right) and PVA:HAPS 1:0.1 (bottom) composite films.

2.3.3 Nano Fibrillated Cellulose and PVAm blends

As a source of PVAm, the already presented Lupamin® 9095 solution was used, while the nanocellulose was acquired from the Centre Technique du Papièr (CTP) and its details can be found in the paragraph 2.1. Thick film membranes have been prepared via a solvent casting technique, by mixing the two components and then drying out the solvent. The initial mixture was obtained by weighing different amounts of the two commercial solution in a glass beaker, in order to obtain different ratios between the two solids contents, summarized in Table 2.3. To reduce the viscosity of the solutions, deionized water was added in the reported amounts.

Table 2.3: characteristics of the NFC/PVAm solution prepared for casting

NFC/PVAm Weight Ratio	Reagents Mass [g]	Water Added [g]	Final Concentration [wt%]
30/70	20	7	4 %
50/50	20	5	3 %
70/30	20	7	2 %
100 (pure NFC)	3	/	2 %

The calculations were performed by considering the net solid content given by the supplier. Initially, the mixture was stirred via a magnetic stirrer for a few hours at 1500 rpm to achieve a good macroscopic mixing; during this phase water was added to reduce the overall viscosity and allow a better handling of the solution (Fig. 2.19). To achieve a good mixing at a microscopic level between the phases, the solution was passed twice through a three roll mill and maintained for a total residence time of about two minutes. The final solution was then poured in PTFE petri dishes, each one containing around 5 g of the mixture. Extreme care was taken in order to spread the viscous liquid as evenly as possible, to avoid any imperfection in the final film. To evaporate the solvent, the dishes have been left under a fume hood at 35 °C.
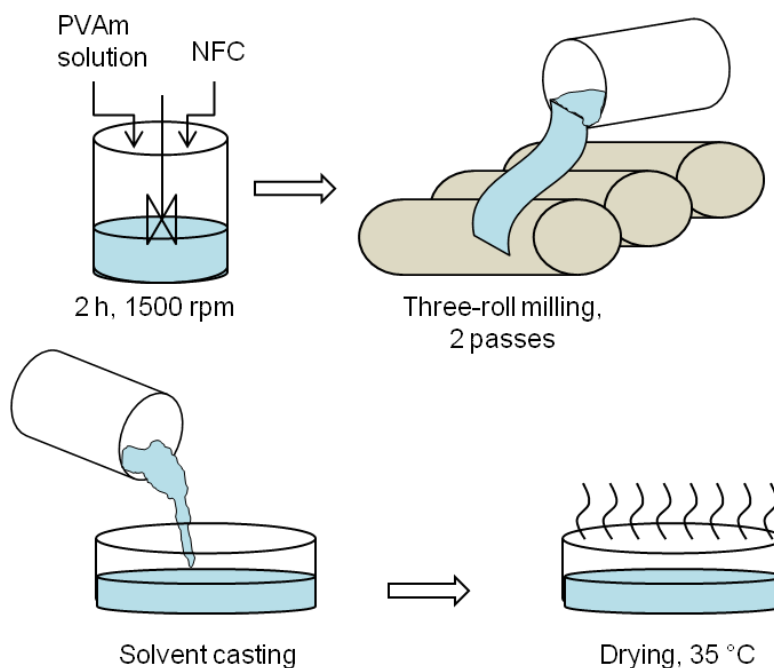

Figure 2.19: film preparation for NFC/PVAm blends, consisting of mixing, milling in a 3-roll mill and solvent casting in a Teflon petri dish.

Beyond the mixture with PVAm, a series of pure NFC films have been also casted as a reference, by pouring the commercial solution directly into the petri dishes and letting them dry in similar conditions. Once dried, the final films showed a thickness of about 50 μm, with a variability within 15 % amongst the different samples prepared. Pure Lupamin®9095 did not show enough mechanical resistance to be casted in a self standing film, hence, to obtain water sorption data, a small amount of solution was spread onto an aluminum foil support and dried in oven at 40 °C. The variation in weight of the sample before and after the spreading was used as the sample mass for the data elaboration.

2.3.4 Carboxymethylated NFC and PVAm

Differently from the previous series of films, the nanocellulose used here was kindly donated by Innventia AB (Stockholm, Sweden) under the name of G2 and was obtained via an acidic chemical pretreatment of a commercial dissolving pulp, followed by the carboxymethylation step and finally a pressure driven homogenization.

Both self-standing films of pure NFC and NFC-PVAm blends have been made and separately tested. This specific kind of nanocellulose presents a higher superficial charge, which is believed to enhance the interaction both with carbon dioxide and polyvinylamine. Moreover, the films were also subjected to a curing procedure at high temperature, in order to increase the stability in high humidity conditions.

Specifically, pure NFC films were obtained by pouring a small amount of the as received suspension in a polystyrene petri dish of 8.5 cm in diameter. The water was then evaporated by placing the dish in an oven at 40 °C on a leveled plane and leaving it overnight. Once sufficiently dried, the film was peeled off with a pair of tweezers and its thickness was measured to be about 30 μm.

A 50:50 weight ratio between the solid contents was chosen, when preparing the blend of nanocellulose and PVAm solution (Fig. 2.20). The NFC suspension (2.17 wt%) was mixed directly with the Lupamin® 9095 solution (21 wt%) in a medium glass beaker and the final solid concentration was calculated to be around 4 wt%. This blend was then stirred with a magnetic Teflon stirrer at 1500 rpm to ensure a first macro homogenization. As a further improvement to the intimate contact between the two phases and the dispersion of NFC, the mixture was placed in a closed bottle and put in a sonication bath for 2 hours, keeping the temperature low b y continuously replacing the water of the bath. Following a similar procedure to pure NFC films, the solution was poured a into polystyrene petri dish and dried in a ventilated oven at 40 °C overnight.
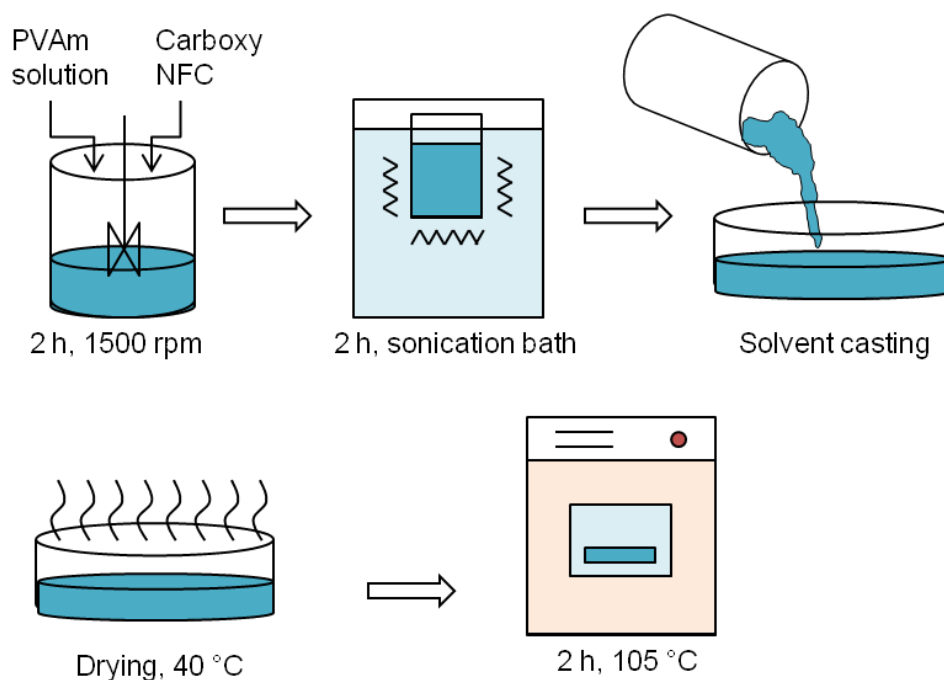
Figure 2.20: mixing, casting and thermal treating of carboxymethylated NFC and PVAm solution

The resulting film was then subjected to a thermal treatment in a vacuum oven at 105 °C for 2 hours. The final thickness of the membranes resulted to be of about 45 μm with variation not exceeding 10 % for the different samples used for the tests.

2.3.5 Nanocellulose/PVAm cross-linking

As it will be further discussed in the next chapter (§ Par 3.3.2), the films prepared with the procedure previously shown do present good characteristics in terms of permeability, but tends to suffer from swelling at high humidity. This is an undesired fact, since it can reduce the selectivity towards unwanted gas species. For this reason, a protocol aimed at introducing a degree of cross-linking in the polymeric matrix has been developed. The principle behind this operation was developed on the same bases, on which the cross-linking of PVA showed in Par. 2.3.1 stands. Specifically, an external molecule has been introduced in the system, equipped with highly reactive functional groups on both sides of it, that could be able to react with two or more polymeric chains at the same time. Since glutaraldehyde (GA) proved itself to be adapt for this kind of function for PVA, the same molecule was used to induce cross-linking in the nanocellulose/polyvinylamine blends. As exemplified by Figure 2.21, the aim is creating a series of bridges between chains of PVAm, via reactions of the carboxylic carbon with the amine groups. This represents the most likely reaction, due to the high concentration of amine groups, but GA could also react with the superficial hydroxyl groups present in nanocellulose.
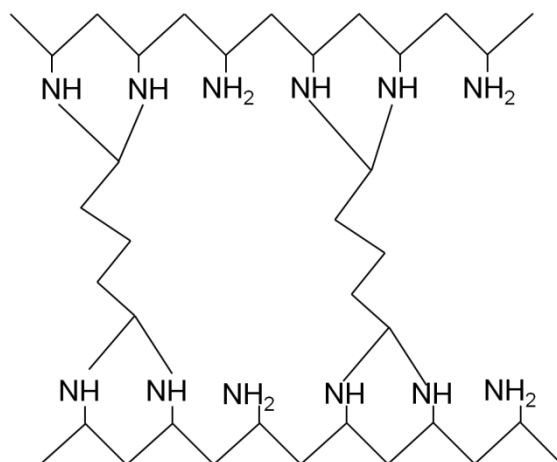
Figure 2.21: effect of glutaraldehyde cross-linking on a PVAm matrix

The first part of the preparation protocol is exactly the same one followed in the previous paragraph and was used to obtain a self-standing film. Since this series of tests was dedicated to explore the viability of this kind of methodology and its effectiveness rather than preparing a high performance film, only a single blend composition was analyzed, specifically the 50/50 NFC/PVAm.
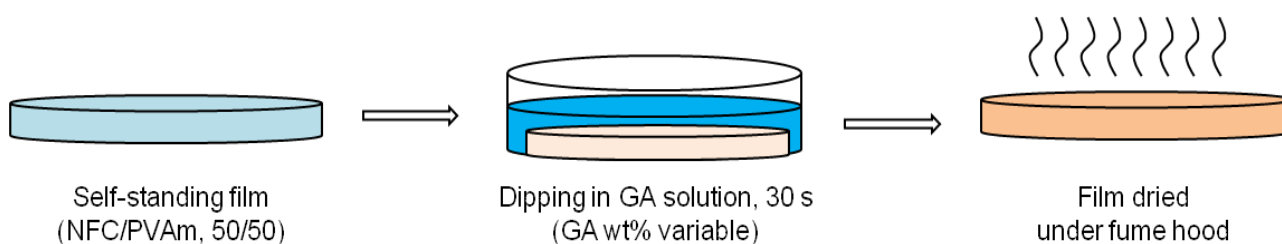

Figure 2.22: cross-linking protocol for a self-standing film of the NFC/PVAm blend. Film is dipped in a glutaraldehyde (GA) solution for 30 s and then dried in air under fume hood.

Once the film was casted and dried, a water solution containing glutaraldehyde was prepared. In this one, the film was dipped for a total time of 30 seconds and then removed (Fig. 2.22). The superficial solution still present on the film was damped using absorbing paper and the residual solvent and aldehyde left to dry under a fume hood. As a way to control the degree of cross-linking, different concentration of glutaraldehyde were used. This protocol was applied under the assumption that, being the blend highly hydrophilic, the water based solution is quickly absorbed along with the GA within the matrix. Here the reaction takes place and most likely continues to happen also once the film is removed from the solution. This is also confirmed by the change in coloration of the film over time, which varies from white/transparent to a more orange/brown one. To avoid any aldehyde contamination, the soaked films have been left to dry under a fume hood overnight. Once dried, it could be observed an increase in stiffness of the material.

The different concentration of glutaraldehyde solution used throughout the project are 1, 5, 10, 25 and 50 wt%.

2.3.5 Polyvinylamine purification and film preparation

As previously stated in paragraph 2.1, Lupamin® 9095 is a commercial solution, which is provided with a large presence of residual Sodium Formate ($HCOO^-$ Na^+) salt. This compound is present, due to the fact that polyvinylamine is synthesized via hydrolysis of poly(N-vinylformamide) (PVNF) via an acidic or alkaline reaction [45]. When sodium hydroxide is used, sodium formate is formed, as shown by Fig. 2.23. On a commercial level, this compound is not removed from the final solution and can interfere with the synthesis of functionalized films.
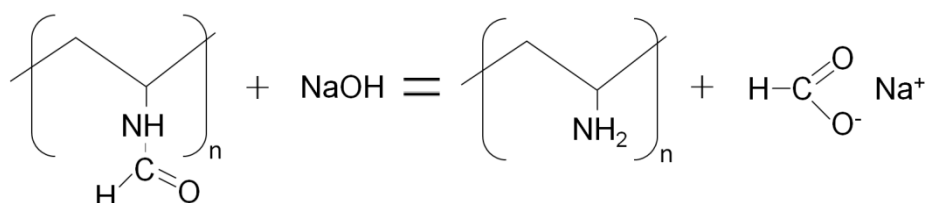

Figure 2.23: reaction scheme of PVNF hydrolysis via sodium hydroxide

For this reason, some of the materials presented in this work have been prepared by using PVAm, which was previously purified by removing the salt from the solution. The purification process used hinges on the fact that PVAm is not soluble in ethanol, while the formate salt is. Because of this, the commercial solution was poured into an excess of 96 % ethanol in a beaker: a volumetric ratio of about 1:4 between the polymeric solution and the alcohol has been used. Due to its low solubility, PVAm precipitate as a white solid, while the salts tends to remain in the solution. The polymer is recovered via a spatula and placed in a Teflon petri dish. Subsequently, the solid was dried overnight at 50 °C in a ventilated oven. Once dried, the polymeric solid was cut into small pieces in order to enhance the exchange area and a Soxhlet extraction with acetone was performed. This procedure consist of a continuous solid liquid extraction, where the liquid is constantly renewed via a evaporation/condensation process.
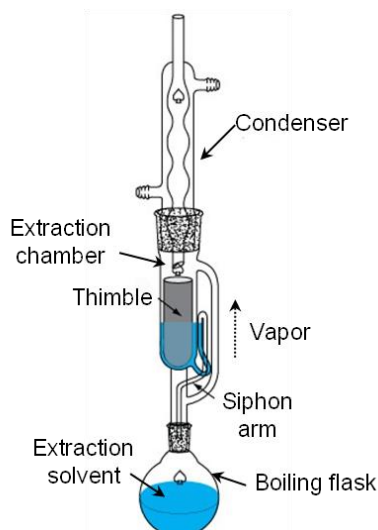
Figure 2.24: diagram of a soxhlet extractor and all its main components

As Fig. 2.24 shows, the solids to be purified are inserted in a thimble, located in the center piece of the equipment, while the solvent s placed in a boiling flask at the bottom. This one is heated up to the boiling temperature of the liquid (56 °C for acetone) and its vapors are directed through the external tube directly towards the head condenser, which is cooled by water flowing in the outer shell. Here, the solvent condenses and drips into the thimble, starting the extraction process. The liquid piles up in this section and at the same time fills the external siphon arm. When the level in the siphon reaches the maximum, the siphon is triggered, the whole volume of solvent its discharged back into the flask and the cycle starts again. Each cycle, the extraction is performed with "fresh" solvent, since the low volatile impurities are accumulated into the flask and do not transfer significantly in the vapor phase. This whole process is left running for 48 h and once it's completed, the polymer is dried under a fume hood overnight. The final step involves a washing with absolute ethanol, to remove possible residual salt, prolonged for 1 hour. The purified polymer was recovered via a filtration by gravity and dried in oven at 55 °C overnight.

In order to have a viable solution for casting, the polymer was dissolved in deionized water in a concentration of 10 wt% depending on the batches. To guarantee a full dissolution, water and polymer have been left stirring in a closed bottle overnight at room temperature, until a limpid solution was obtained. Subsequently, self-standing films have been prepared in the same way described in Par. 2.3.2 (excluding the thermal treatment), by mixing the newly prepared PVAm solution and NFC in a weight proportion of 50:50. Once properly homogenized, the solution was sonicated for 2 hours and then casted into a Teflon petri dish. Due to higher viscosity of the purified PVAm solution, the drying occurred under a fume hood for a few days at room temperature, to avoid the formation of vapor bubbles, trapped due to a too high evaporation rate. The thickness of

the films obtained in this way was assessed by a flat head micrometer to be around 50 μm and it must be noted how these purified films presented a higher flexibility than the one realized with the commercial solution and higher tendency to not degrade or dissolve in high humidity conditions.

Section 2:Experimental Results and Discussion

.

Chapter 3. *Polyvinylalcohol based films*

Here, the work involving Polyvinylalcohol (PVA) based films will be presented. This series of experiments has been mainly considered as an introductory part to the field of facilitated transport membranes, which was previously not dealt with by the research group. Firstly PVA has been used as a cross-linked matrix, onto which amine functionalities have been grafted to promote transport facilitation. The solution obtained was casted onto a porous support and its permeation properties assessed in a mixed gas permeation setup with a mixture of CO_2 and H_2.

In this same chapter, will be also discussed the work regarding PVA thin films loaded with amine functionalized nanoparticles obtained through dip coating. These tests have been conducted at the MEMFO laboratories at the Norwegian Technical University (NTNU) in Trondheim under the supervision of Prof. May-Britt Hägg. This series of tests was part of an international experience carried on during the PhD program, to promote the internationalization of the research. Once casted, these films were tested in a mixed gas permeometer in humid condition using a mix of CO_2 and N_2.

3.1 Cross-linked polyvinylalcohol films

This section of the work represents a first approach to the realm of facilitated transport membranes, which have been performed within the MEMLAB research group. In order to have an initial point of reference, the activity was modeled around the results achieved by Prof. Ho from Ohio State University (Ohio, USA). In particular, these membranes consist of a matrix of cross-linked Polyvinyl Alcohol, grafted with aminopropyltrimethoxysilane (APTMOS) as a source of amine groups. The solution was subsequently casted onto a micro porous Polysulfone support and its

permeability tested in humid conditions for CO_2 and H_2. The description of preparation and casting procedure has been described thoroughly in the previous chapter (§ 2.3.1).

3.1.1 Mixed gas permeation

The membrane samples, cut to the desired dimension form the cast films were mounted into the Millipore cell and the seal guaranteed by a rubber O-ring, which comes into direct contact with the films. The complete setup of the permeometer can be seen in the paragraph 2.2 of Chapter 2. All permeation tests on this materials have been performed at a temperature of 35 °C. CO_2 permeability has been tested both as a single gas and in a 50:50 volumetric mixture with H_2, always in humid conditions. During the experiments a total feed flow of 300 cm^3(STP)/min has been maintained in the feed side, while the flow-rate of nitrogen, used as a sweep gas, was kept at 10 cm^3(STP)/min. The relative humidity was measured both on the upstream and downstream side and the humidity of the film was assumed to be an average of the two values, which did not particularly deviate significantly one from each other in view of the high water permeability of the membrane. A range of relative humidity between 49 and 71 % was investigated, since below this values, the concentration of gases in the downstream side was too low for a reliable measurement through the GC, while the system was not capable of reaching higher humidity values.

Table 3.1:summary of single and mixed gas permeation results for cross-linked PVA

Single Gas		Mixed Gas (50% CO$_2$-H$_2$ mixture)		
RH	**Perm CO$_2$ [Barrer]**	**RH**	**Perm CO$_2$ [Barrer]**	**Perm H$_2$**
0.49	9.5	0.52	15.7	6.8
0.58	70	0.71	179.4	21
0.62	79			
0.66	114			

Figure 3.1 shows the results of the permeation tests for both single gas and mixture for both carbon dioxide and hydrogen. The permeability are also reported in table 3.1 for the sake of completeness. The results, as expected indicate a very strong dependency of the permeability to the water activity, with increment of more than one order of magnitude in the narrow relative humidity range investigated. In particular, the CO_2 permeability resulted to be as low as 9.5 Barrer at the minimum RH investigated (49%), while it reached the value of 179.4 Barrer at 71 % relative humidity.
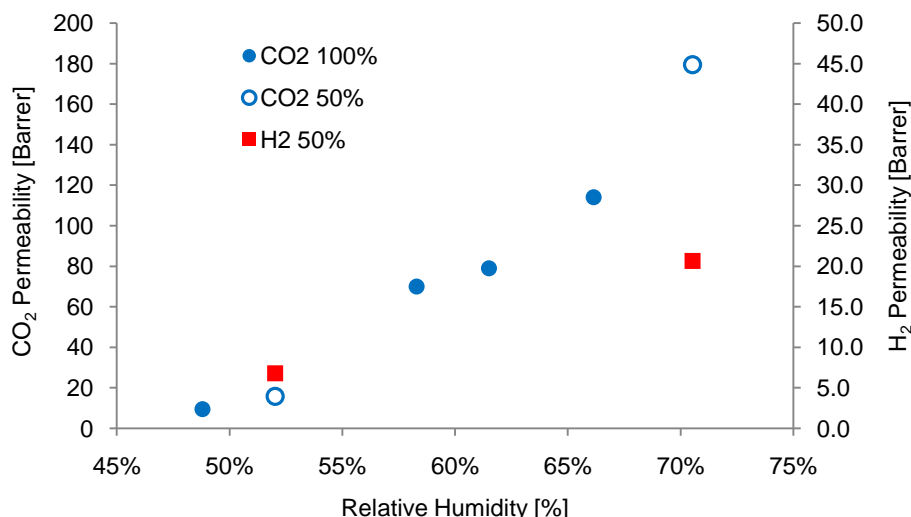
Figure 3.1: permeability of cross-linked PVA respect to CO_2 as single gas (blue dots) and in a mixture (blue squares) and of H_2 as a mixture (red squares)

For hydrogen, the permeability range is smaller and varies from 6.8 to 21 Barrer at its maximum. An interesting thing, that could be noted, is represented by the fact that permeability results do not seem to be particularly affected by the presence of a second gas. A worse performance, when dealing with mixtures rather than single gases, is a typical drawback of most solution diffusion membranes, since the two (or more) gases tend to compete for the free volume.
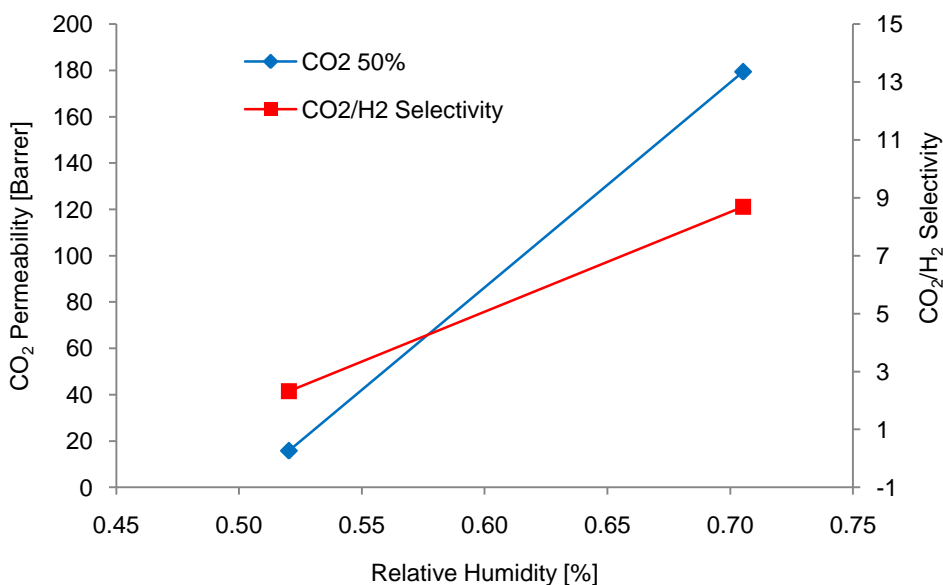
Figure 3.2: CO_2/H_2 selectivity (red) and mixed gas CO_2 permeability (blue) of cross-linked PVA as a function of relative humidity.

In the case of facilitated transport membranes, this phenomenon is greatly reduced, since the carbon dioxide can diffuse through the membrane via a mechanism available only for itself; hydrogen, on the other hand, will simply diffuse via the solution-diffusion mechanism, with minimum interference with the facilitated transport of CO_2.

51

Another fact, which suggests the presence of facilitated transport relies on the fact that both CO_2 permeability and selectivity towards H_2 increase with relative humidity. In particular, the selectivity jumps from 2.3 at 52 % relative humidity up to 8.7 at 71 % (Figure 3.2). This is expected, since the increase of carbon dioxide's flow through the membrane is not equally matched by the one of hydrogen. Facilitated transport is capable of targeting a single species, incrementing only its permeability, while keeping relatively steady the one of the non facilitated gas. An increment of H_2 permeability is nevertheless present, probably due to a minor swelling of the polymeric matrix, despite the cross-linking.
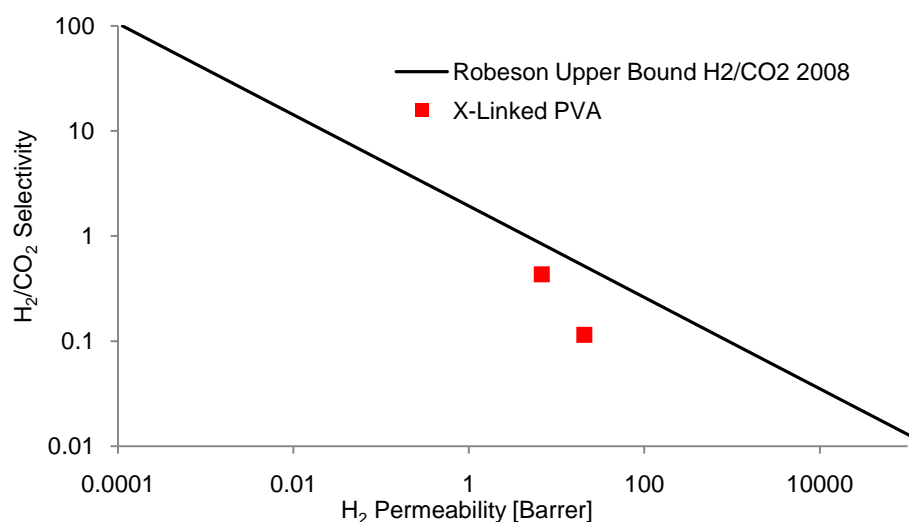

Figure 3.3: cross-linked PVA selectivity compared to Robeson 2008 upper bound [9]

As reference, the performances of the membrane prepared have been compared to the upper bound presented by Robeson in its 2008 work [9]. This kind of chart shows the selectivity as a function of the permeability on a double logarithmic scale for what is considered the state of the art in terms of separation performances for a certain couple of gases. It can be seen how the points obtained from the film prepared lay very close to top performances.

Overall, this first set of experiments was considered to be deliver interesting and successful results, which represented a useful initial step towards the elaboration of an optimized and original film for the separation of CO_2 via facilitated transport.

As per the original paper, which inspired this first phase of the work, Xing et al. [43] tested their films at high temperature (105-115 °C), a fact that does not allow an immediate comparison of the data. In these conditions of high temperature they were able to obtain CO_2 permeability between 800 and 1100 Barrer in a relative humidity interval of 60-90 RH%. These are of course much higher values than the 180 Barrer obtained in this work, but it must be also taken into consideration the

fact that in our case the membranes synthesized did not contain any mobile carrier, since these are considered to represent a source of long-term stability issues for the material. Instead, in the cited paper in the matrix of the film was also added an alkaline mobile carrier, specifically aminoisobutyric potassium salt (AIBA-K), which most likely improved drastically the facilitation of the transport.

3.2 PVA based amino functionalized nano-composites

The following section will discuss the work performed at the MEMFO laboratories at the Norwegian Technical University (NTNU) of Trondheim (Norway). This experience was an integral part of the doctoral program aimed at expanding the overall baggage of knowledge regarding the topic of transport facilitation. MEMFO group was chosen for this project thanks to the vast experience preset, which lead it to become one of the most influential and important research group in this particular field. This project was carried on under the supervision of Prof. May-Britt Hägg and within the european project HiPerCap (High Performance Capture). The specific work presented here follows a few promising results previously obtained by mixing a particular type of functionalized nano-particles in a hydrophilic PVA matrix. Via gas permeation tests in different conditions, the aim of the work was to assess the actual performances, that these particles might have in a systematic way.

3.2.1 Mixed gas permeation

To assess the permeation properties of the membranes prepared as in section 2.3.2, a mixed gas permeation apparatus was used, like the one described in paragraph 2.2.2. As feed gas, a premixed, commercial cylinder of 90 vol% N_2 and 10 vol% CO_2 was used, kept at an absolute pressure comprised between 1.1 and 1.2 bar a. As a sweep gas, pure CH_4 at 1 bar a was employed, while the temperature was 25 °C throughout all the permeation tests. Each sample was tested at three different humidity degree: 50, 75 and 100 %. Before each test, the film was equalized at the right humidity by feeding a stream of pure CO_2 at the water activity corresponding to the one of the upcoming experiment. The regulation of the humidity was performed via a manual control valve fitted onto the dry branch. A flow of about 500 cm^3/min was then fed to the film and the composition of permeate and retentate evaluated via MicroGC. Being these thin film membrane endowed with a very high flow and an uncertain value of thickness, rather than permeability, a permeance was usually measured and adopted as the target value. This was calculated by dividing the permeation flow by the partial pressure differential, thus not considering the thickness of the selective film, and expressed as m^3(STP)/m^2 bar h (for reference a membrane with a permeance of 1 m^3(STP)/m^2 bar h corresponds to 370 Barrer for a 1 μm thick film).

The results for the permeance of CO_2 at different degree of humidity and HAPS loading are summarized in Figure 3.8. As expected, permeance is highly influenced by the amount of water in the system as it usually is for hydrophilic systems such as PVA and PVAm [46] and its value increases by two orders of magnitude from 50 to 100 RH%. In fact, at 50 RH%, permeance is in the

order of $1 \cdot 10^{-2}$ m^3(STP)/m^2 bar h, at 75 RH% steps up to $1 \cdot 10^{-1}$ m^3(STP)/m^2 bar h and at saturation it reaches values up to 0.4 m^3(STP)/m^2 bar h. The point corresponding to the blend PVA:HAPS 1:0.4 at 100 RH%, reported for the sake of true, is considered to be an outlier and should be ignored for the current analysis.
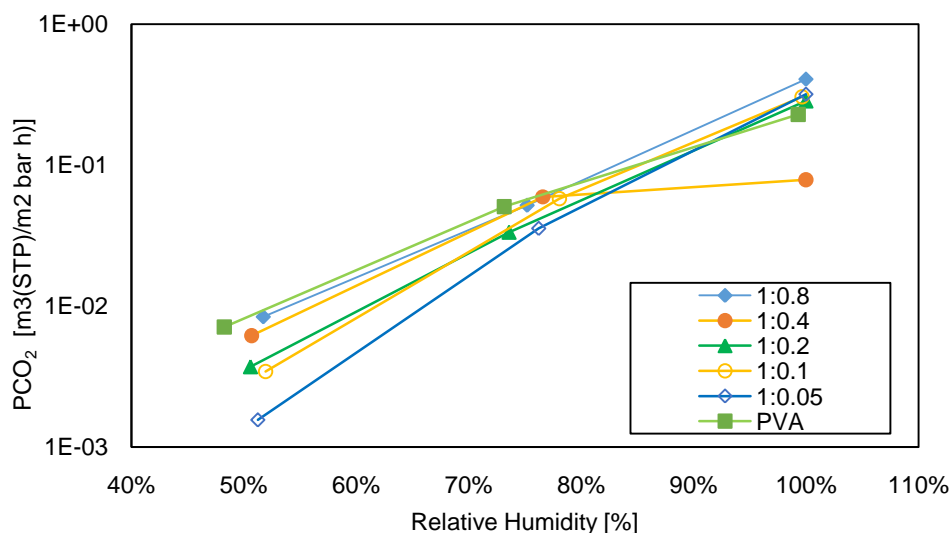

Figure 3.4: permeance of CO$_2$ for the PVA:HAPS blend films at different humidity and polymer : nano-particles ratios.

For this class of membranes, the controlling factor for permeation is usually represented by the gas solubility in the matrix. Since carbon dioxide possesses both the lowest kinetic diameter and the highest condesability respect to nitrogen, its permeability will be always higher than the second gas in these type of materials [7]. This strong correlation of permeance and humidity is typical for hydrophilic films, especially for CO$_2$. In fact, a higher humidity leads to a higher concentration of water inside the polymeric matrix. Being carbon dioxide highly soluble in water, it is quite logical that its transport will be faster if its solubility in the film increases (Equation 3.1):

$P = S * D$ (3.1)

Subsequently, the influence of the leading of HAPS on the separation performances of the films can be taken into consideration. Figure 3.5 presents the permeability of CO$_2$ as a function of the weight concentration of the nano-particles at different degrees of humidity, while Figure 3.6 shows the real selectivity of carbon dioxide over nitrogen also as a function of both particle loading and relative humidity. Since during the tests performed at 50 RH% the concentration of nitrogen in the downstream side was very close to the sensitivity of the gas chromatograph, the resulting permeability was deemed not particularly reliable, hence the absence of the 50 RH% selectivity curve. From these charts, it can be noted how the selectivity is highly influenced by relative humidity: at 75 RH% it is clearly higher, reaching values up to 120, while at 100 RH% it is limited around 60.
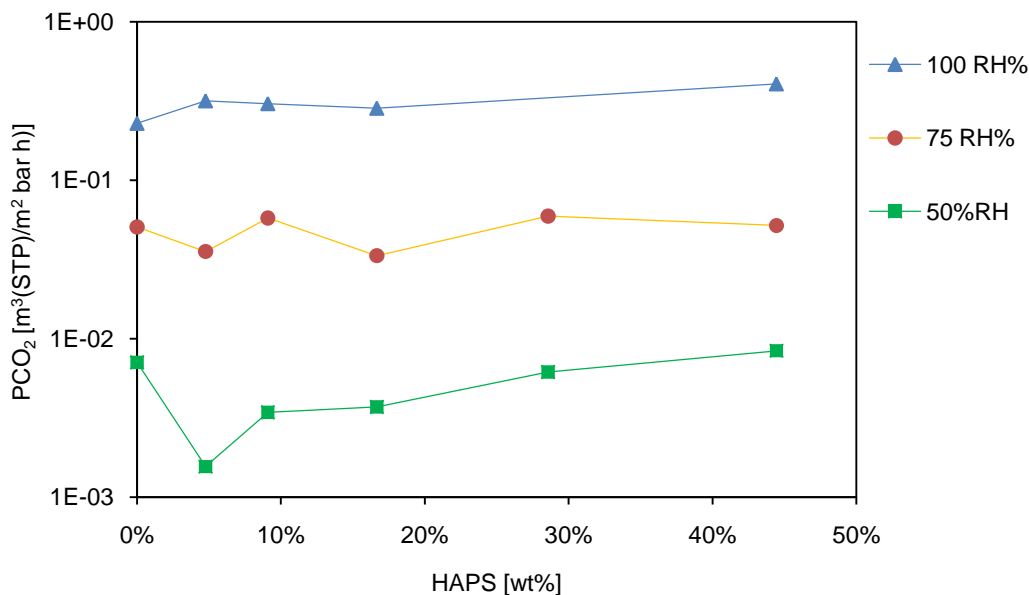
55

Figure 3.5: CO₂ permeance (left) and CO₂/N₂ selectivity as a function of HAPS concentration for different degree of humidity.

One thing, which can be observed in the graph, is the fact that for both humidity levels, selectivity increases when HAPS is introduced in the system, but after this first increment, the value appears rather stable or decreasing. In particular, at 75 RH% the selectivity increases from 51 of pure PVA to 120 of the blend with 5 wt% of HAPS. This increment, though, appears to be short-lived, since at higher values the selectivity stays relatively constant and finally drops around 85 at high HAPS loadings.
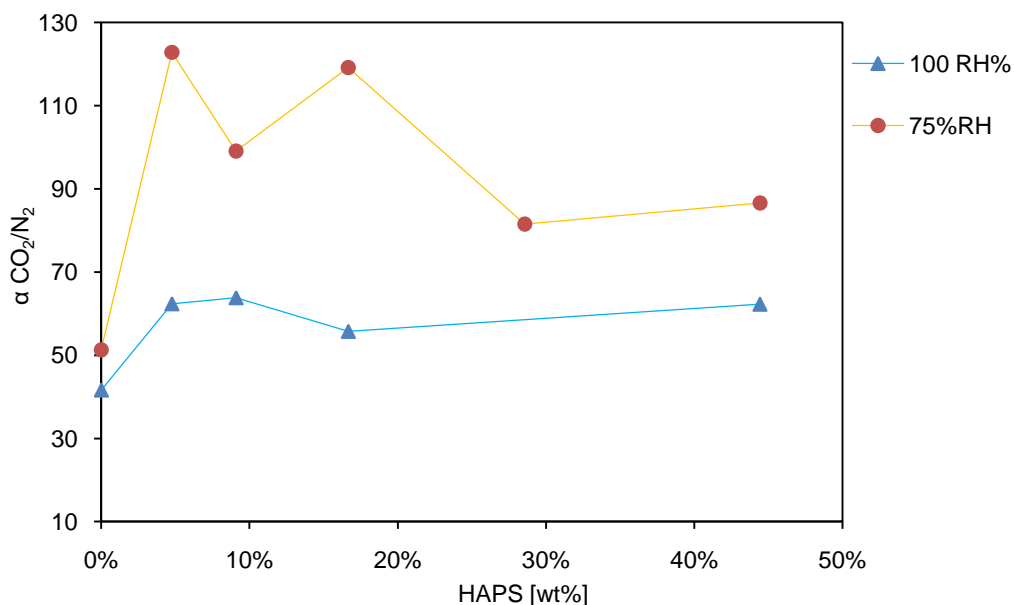

Figure 3.6: CO₂ permeance (left) and CO₂/N₂ selectivity as a function of HAPS concentration for different degree of humidity.

At lower humidity, the permeance does not appear to be significantly influenced by the content of the amine-functionalized nano-particles, with values constantly oscillating between 0.04 and 0.06

m^3(STP)/(m^2 h bar). On the other hand, the behavior of the membranes at high humidity is more encouraging: starting from a value for pure PVA of 0.22, the permeance increases, with some oscillations, up to 0.4 m^3(STP)/(m^2 h bar). For a 3 μm thick film, this corresponds to around 420 Barrer in permeability.

Overall it appears that the nanoparticles, rather than directly improving the permeability of CO_2, tend to slow down the flow of nitrogen, by increasing the tortuosity of the diffusion path. This effect appears to be more relevant for nitrogen, most likely because the amine functionalization of the particles made them more affine to carbon dioxide. The drop in selectivity observed at high loadings, hence, could be due to a poor dispersion of the particles, which created voids between them, deteriorating the separation properties.

Chapter 4. Polyvinylamine and Nanocellulose composites

The following paragraphs will be dedicated to the presentation of the main work performed during the PhD program and are considered the principal advancement achieved during the work. This type of nano-composite have been prepared by mixing polyvinylamine (PVAm) and Nano Fibrillated Cellulose (NFC), also known as Microfibrillated cellulose (MFC) or Cellulose Nanofibers (CNF), in different proportions and with different characteristics. This part of the work relied on the study of the influence of different amounts of the filler (NFC) on the commercial polyvinylamine performances. Here the characterization will be showed of several films, casted from solution with different ratio of NFC and PVAm. For this section of the research, a plain, commercial non carboxymethylated nanocellulose was used as obtained from the Centre Technique du Papier, CTP (§ Par. 2.1).

4.1 FTIR analysis

As a way to assess the functional groups involved in the different materials and blends, a characterization via FTIR-ATR spectroscopy (§ 2.2.3) was performed. The resulting absorbance spectra of both the pure PVAm and NFC commercial solution and their blends are presented in Figures 4.1 an 4.2, where, in order to better visualize the differences between the curves, the whole range of frequencies has been split into two charts. It must be also said that, in order to avoid excessive overlapping of the curves, these have been shifted on different levels of the Y-axis. In Figure 4.1, where the high frequency fraction of the spectrum is shown the broad, medium height

peak at 3300-3400 cm^{-1}, corresponding to the stretching of the O-H bond, can be easily identified in the pure NFC spectrum as a consequence of the of the presence of numerous hydroxyl groups on the surface of the cellulose fibers. This specific peak does not seem to be transferred to the spectra of the blends containing this material, which, instead, do show the broad peak related to the stretching of the N-H bond, belonging to the polyvinylamine. The reason that this peak can be associated to the amine group, rather than the hydroxyl one, is to be found in the relative size of it between the different blends and it is quite clear how its height grows according to the weight fraction of the Lupamin®.
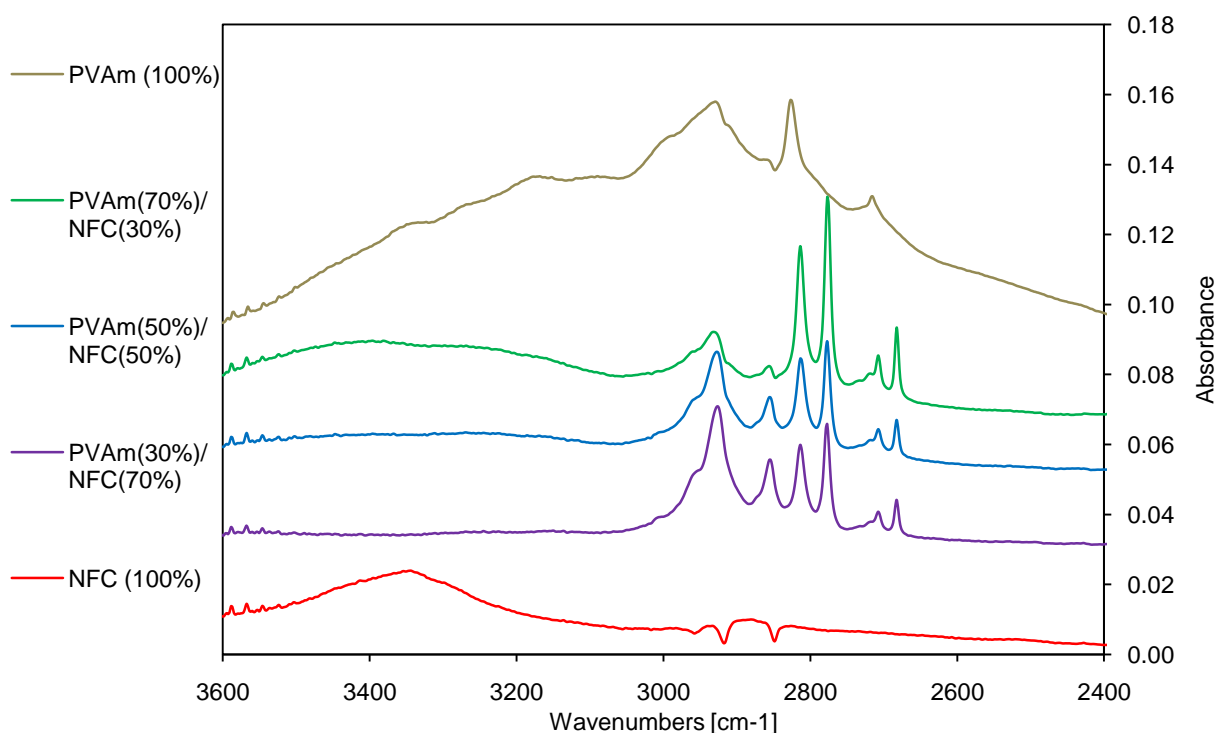

Figure 4.1: 3600-2400 cm^{-1} interval of FTIR-ATR spectra of commercial PVAm (Lupamin® 9095), Nano Fibrillated Cellulose (NFC) and their blends (70/30, 50/50 and 30/70).

For example for the 70 wt% PVAm blend, this characteristic peaks is more pronounced than the one observed for while for the 30 wt% blend this value stays below 0.005. As it would be expected, the largest peak for this specific functional group belongs to pure Lupamin®.

Moving to lower frequencies, a sharp peak between 3000 and 2800 cm^{-1} can be observed, which is in common with all PVAm containing blends. The nature of this one could be debatable, but an hypothesis can be made regarding it being originated by a N-H stretching not as a free group, but rather as a saline form, most likely formed between a NH_3^+ group and the formate anion. A peculiar fact concerning this peak is due to the fact that, despite being obviously related to the presence of the PVAm solution, its relative amount in the various blends has an opposite trend respect to peaks

form the same origin, possessing the highest value for the 30 wt% PVAm blend and the lowest one for the 70 wt% one.

At 2930 cm^{-1} the sharp peak observed for all PVAm based film can be associated to the stretching of the C-H bonds present in its polymeric chain. Also nanocellulose presents a small peak related to the stretching vibration of its C-H groups in the same range of frequency. In the vicinity of 2800 cm^{-1}, two small sharp peaks are present and these, instead, can be associated to the presence of the PVAm solution, specifically to the one of the sodium formate salt, as it can be seen in the spectrum shown in Fig. 4.3.
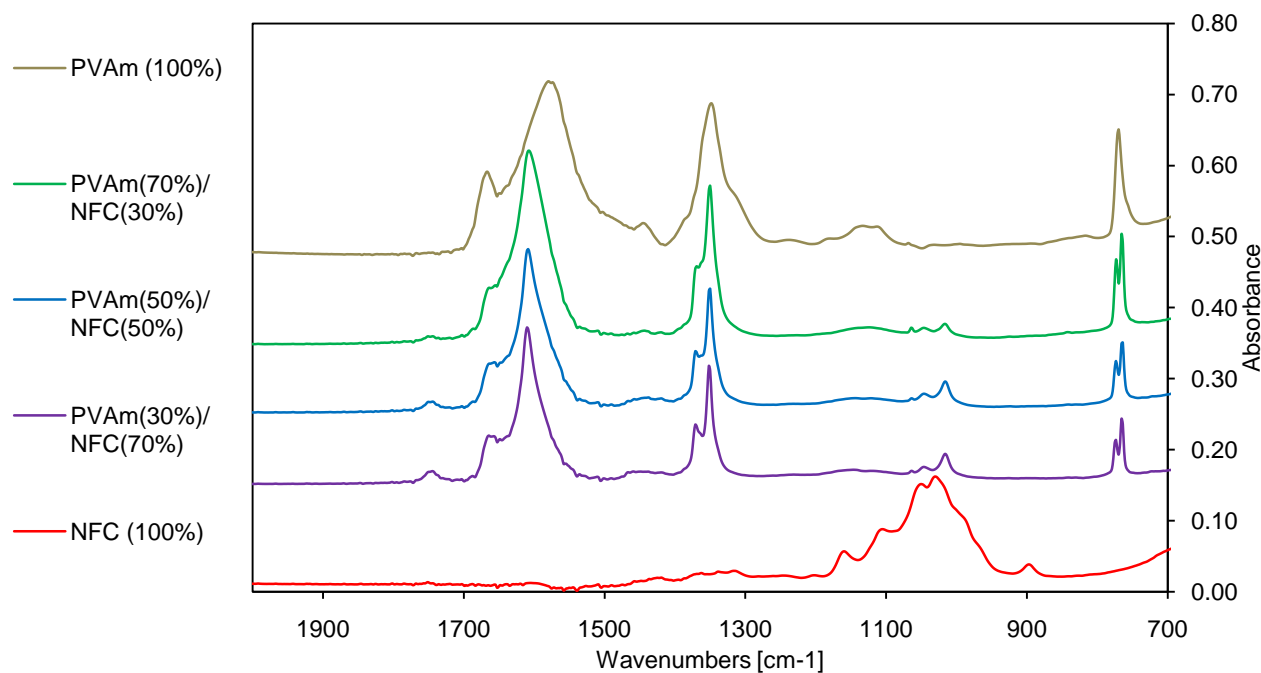

Figure 4.2: 1900-700 cm^{-1} interval of FTIR-ATR spectra of commercial PVAm (Lupamin® 9095), Nano Fibrillated Cellulose (NFC) and their blends (70/30, 50/50 and 30/70).

The doublet of peaks can be related to the stretching of the C-H bond for a carboxylic carbon. Similarly to the broad N-H stretching peak at 3400 cm^{-1}, the trend of the height closely follows the percentage of PVAm solution added to the blend. In figure 4.2, instead, the spectra from a frequency of 1900 down to 700 cm^{-1} are presented; the first peak to be encountered going from high to low wavenumbers, is the sharp and intense one at 1600 cm^{-1}, which is very likely related to the stretching of the C=O bond. This specific functional group, can have two different origins, both of them contributing to it: the first one is associated to the residual 5 mol% of formamide groups on the backbone of the polymeric chain, which have not been hydrolyzed during the synthesis process. Another compound, which can contribute to this one, is the residual formate ion, with its carbonyl group. A confirmation to this last assumption, as well as the same one regarding the peak at 1400 cm^{-1}, can be found once again in the spectrum of pure sodium formate (Fig. 4.3). This last signal is

probably due to the absorption via bending by the C-H group of the carboxyl carbon. The same considerations can be made for the small sharp peak at 750 cm^{-1}, also related to the presence of the formate ion.
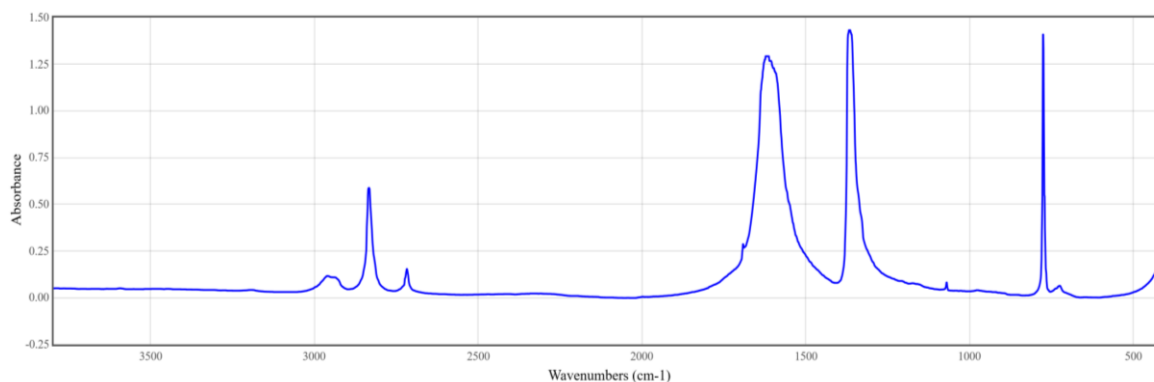

Figure 4.3:infrared absorbance spectrum of sodium formate for reference [47]

Lastly, a series of peaks between 1350 and 900 cm^{-1}, represent the main fingerprint associated to the presence of nanocellulose. The main peak, at 1000 cm^{-1} is probably originated by the stretching of the C-O bond, while the ones at higher frequency can derive from the bending of C-H bonds.

In general, as it would be expected, in the composite films can be found specific features characteristic of the two phase of which they are composed. Qualitatively, though, it appears as though the peaks related to pure nanocellulose and also the polymeric chain of the Lupamin solution are much smaller than it would be expected by looking at the spectra of the pure materials. In fact, the sharpest and most intense peaks present in the nanocomposites appear to be the one related to the presence of the sodium formate salt, even though its overall amount should not be high enough to justify this kind of behavior. An explanation to this can be found in the fact that this salt tends to segregate on the surface of the casted films as outlined by a SEM analysis performed in the previous work on this kind of materials by Ansaloni et al. [48]. Since the FTIR spectra have been acquired via an ATR technique, which analyzes only the first few microns of the blend, a higher concentration of the salt in this region might have resulted in the curves, that can be seen here.

4.2 Water absorption

The isotherm curves presented in Figure 4.4 represent the water intake data for the various blends of NFC and PVAm and also the respective pure films. From a first look to the data, all collected at 35 °C in a water activity range between 0 and 0.8, it can be seen the clear influence that NFC has on the system. Water concentration largely vary depending on the proportion of the two component.

By itself, nanocellulose never showed a water intake higher than 10 wt%, topping at 0.097 absorbed water at an activity of 0.82. This behavior is consistent with what was found by Minelli et al. [39] and also in a previous work [49]. Despite being highly hydrophilic, nano fibrillated cellulose does not show a particular tendency towards swelling in presence of water, even at high activity. On the other side, pure Lupamin® presents a minimal water uptake at low activity, which quickly increases in an exponential manner, when values of relative humidity above 25-30 % are reached.
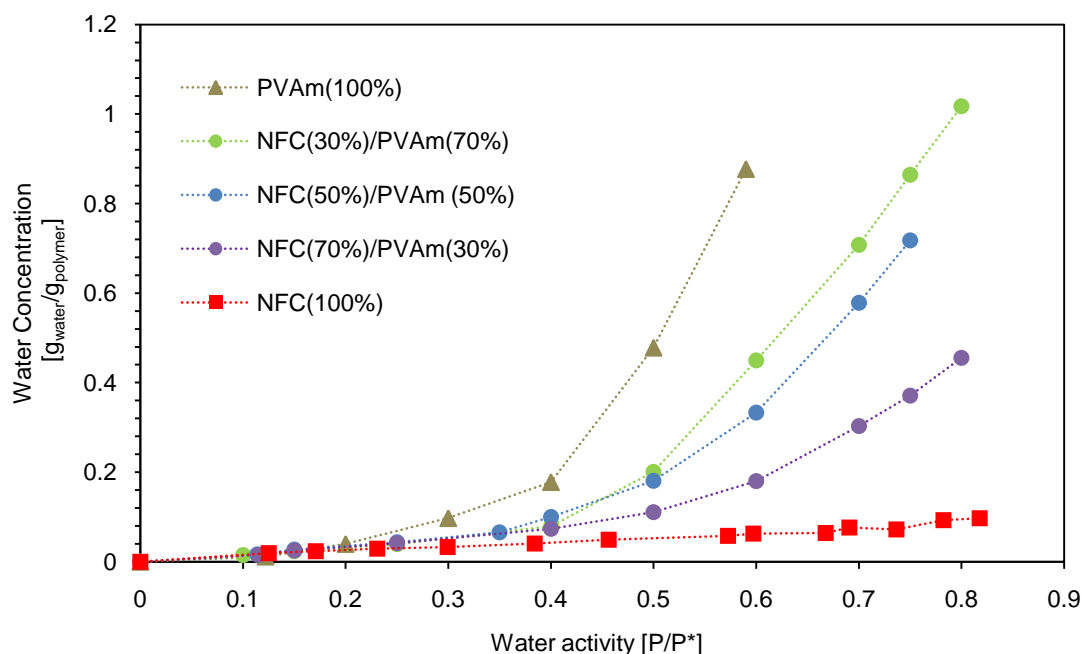

Figure 4.4: water absorption isotherms at 35 °C of the different blends of NFC and PVAm, compared to pure NFC and Lupamin® 9095.

In particular, at an activity of 0.12 it showed a water concentration of 0.012 $g_{water}/g_{polymer}$, which is actually lower than what presented by pure NFC. Instead, at the maximum activity, that was possible to investigate in this case, 0.59, the water uptake reached a value of 0.88 $g_{water}/g_{polymer}$. This extremely high value can be explained by considering both the high hydrophilicity of amine groups in PVAm and the large fraction of sodium formate in the system, which is also highly hygroscopic.

As it would be expected, the films made by a blend of the two polymers showed values of water uptake intermediate between the curves previously described, presenting a strong dependency from the content of Lupamin® added to the nanocellulose. Up until an activity of around 0.4, the three different curves show very similar values (between 0.015 and 0.01 $g_{water}/g_{polymer}$) and a trend substantially equal to the linear one observed for nanocellulose. Beyond this point, the sorption isotherms experience a sudden increase, which is normally associated to the onset of a swelling behavior and the beginning of a large water clustering [50]. This swelling, according to the data presented, takes place at a humidity of around 50% and at a water content between 0.1 and 0.2,

depending on the NFC/PVAm ratio considered. After this point, the curves present a trend, which closely reflects the one shown by pure PVAm. As it could be expected, being Lupamin® the most hydrophilic phase in the material, the overall uptake of water is closely related to its amount respect to nanocellulose.

In comparison with literature values for pure nanocellulose, Belbekhouche et al. [51] found water sorption values for a similar type of cellulosic nano fibers between 0.05 and 0.15 g of water per g of dry nanocellulose in a water activity interval of 0.2 and 0.8. These are values overall slightly higher than what measured here, but disparities can be due to a difference in the casting method and the temperature of the test; the literature values were obtained at 25 °C, instead of the 35 °C of our experiments. In terms of trend (Fig. 4.5), like many other hydrophilic polymers, NFC presents three main phases during its water sorption process (less than linear, linear and exponential). In the case of our data, the first two are arguably present, while the third one has not been recorder, since the measurements stopped at 0.8 $g_{water}/g_{polymer}$.
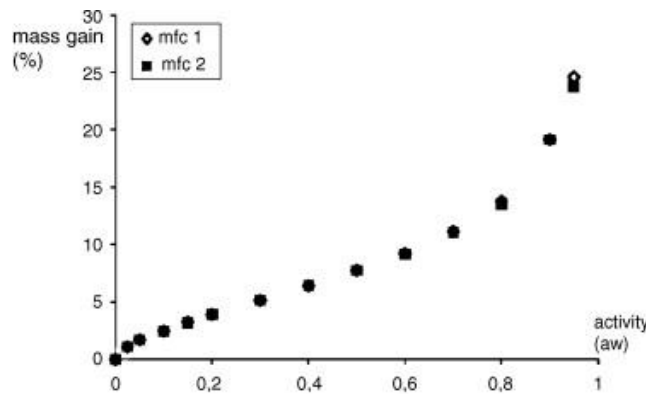

Figure 4.5: typical water sorption isotherm for two different types of nanocellulose found in literature [51]*, acquired at 25 °C.*

To further understand the influence of the addition of the nanocellulose to polyvinylamine it has been calculated the theoretical water sorption, by adding the single contributions of the two components, weighed on the weight fraction, as presented in Eq. 4.1.

$$\omega_{H2O,IDEAL,i} = \omega_{H2O,NFC,i} \cdot \omega_{NFC} + \omega_{H2O,PVAm,i} \cdot \omega_{PVAm} \tag{4.1}$$

Here, *i* represents the value of water activity at which the concentration of two single phases has been calculated, $\omega_{H2O,i}$ is the mass concentration of water respect to the mass of the polymer at the activity *i* and ω_{NFC} is used to indicate the mass fraction of the specific phase in the film. This simple additive model assumes that both phases absorb the same amount of water as if they were pure; it thus represents a situation where nanocellulose has no further effect on PVAm beyond it's simple presence as a low water intake phase. When compared to the actual results (Fig. 4.6), it can be noted

how all the "ideal" curves predict a significantly higher water uptake than the one actually observed on the final films.
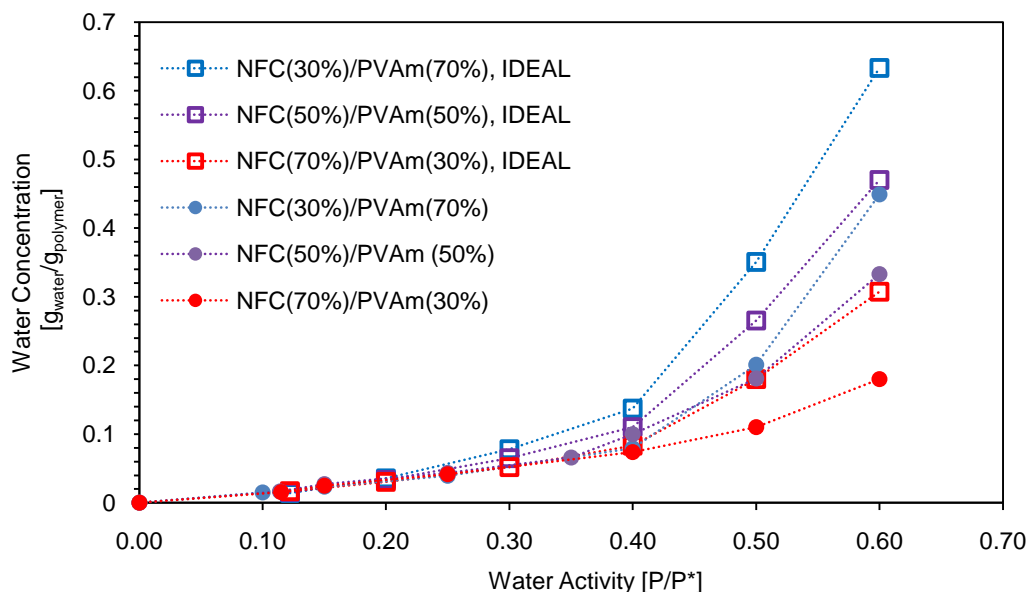

Figure 4.6:comparison of experimental (dots) and theoretical (squares) NFC/PVAm blends water absorption isotherms calculated via the additive model.

This effect clearly shows that NFC has an active effect towards the polymer water solubility, possibly related to the formation of a three-dimensional lattice [23], inside the polymer matrix that limits the PVAm volumetric swelling thus preventing it from absorbing an excessive amount of water. Table 4.1 summarizes the values of water concentration calculated by the model and the difference between these and the experimental ones.

Table 4.1: water concentration values of NFC/PVAm films predicted by the additive model and their difference respect to the experimental ones.

	70 % NFC		50 % NFC		30 % NFC	
Water Activity	Conc. (model) [$g_{H20}/g_{polymer}$]	Difference [%]	Conc. (model) [$g_{H20}/g_{polymer}$]	Difference [%]	Conc. (model) [$g_{H20}/g_{polymer}$]	Difference [%]
0.20	0.030	-8.2%	0.033	-6.3%	0.036	14%
0.30	0.052	-0.4%	0.065	18.7%	0.078	48%
0.40	0.083	12.8%	0.110	10.4%	0.137	73%
0.50	0.180	63.4%	0.265	46.6%	0.351	74%
0.60	0.307	70.7%	0.470	41.1%	0.633	41%

At low activity, when also PVAm tends to absorb less water, the difference is minimal and in some cases the predicted concentration is lower than the observed one. At higher activity, instead, the gap between the two curves appear to be widened, in correspondence to the onset of the swelling phase of pure Lupamin®, which starts around a humidity of about 30 %. Apart from one or two outlier this trend appear to be respected for all of the three compositions, giving more credit to the interpretation given.

To gain more insight on the properties of the analyzed films, the sorption curves have been processed through Eq. 2.7, which allowed to estimate the Fickian diffusivity presented for the investigated systems in Figure. 4.7, as a function of water content.
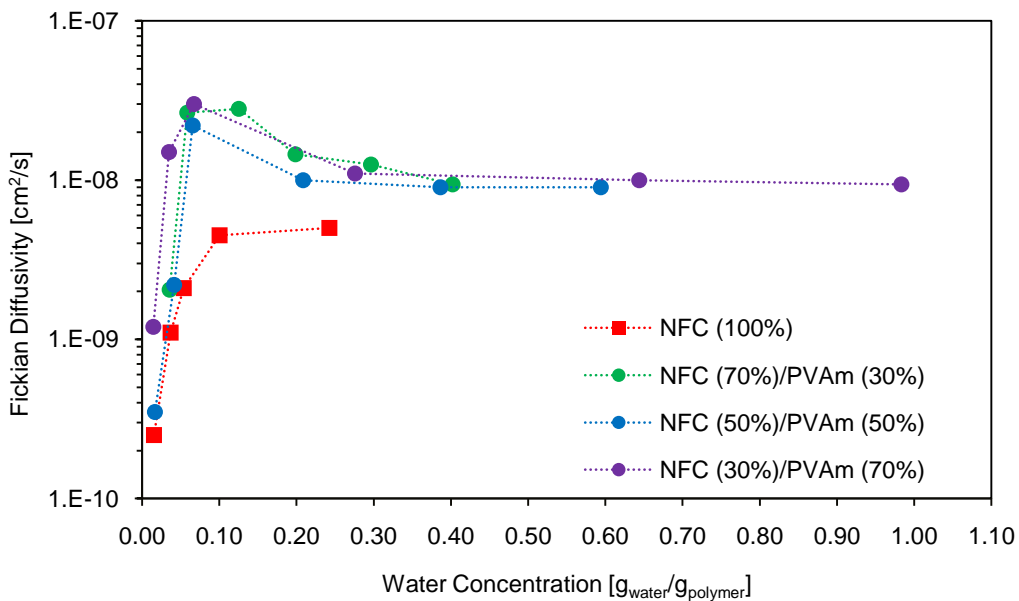
Figure 4.7: Fickian diffusivity of NFC/PVAm blends as a function of water concentration at 35 °C.

For all blends containing PVAm, diffusivity increases quite rapidly at low water activity, going from $3.5 \cdot 10^{-10}$ cm^2/s at a concentration of about 2 wt%, to a maximum of $3 \cdot 10^{-8}$ cm^2/s at around 7 wt%. From here the diffusivity slowly descends towards an asymptotic trend, which settles at $1 \cdot 10^{-8}$ cm^2/s. Pure NFC shows a similar behavior at low concentrations, eventually settling at a final diffusivity of $5 \cdot 10^{-9}$ cm^2/s. This strengthens the assumption that at low water activity all blends behave similarly to the nano-cellulosic phase, a trend that disappears once the swelling takes place. Beyond that point, PVAm appears to contribute exclusively by increasing the volume available for water to be absorbed into.

4.3 Gas permeability

Permeability of the films prepared as described in Par. 2.3.3 has been assessed via the humid permeation protocol outlined in Par. 2.2.1.1. Overall, the tests involved three different gases, CO_2, N_2 and CH_4, all tested in as a single gas in presence of humidity at a temperature of 35 °C. This is, in fact, the most common testing temperature for gas separation membranes and this also allowed the comparison with the parallel acquired water sorption data.

In the following charts the permeation curves regarding the blends of nanocellulose and the commercial solution Lupamin® 9095 will be presented. Out of simplicity, as done also in the previous paragraphs, this component will be indicated simply as PVAm, even though more components are present.

Throughout a previous work within the same research group, the gas permeability of the 50:50 blend was already assessed (Ansaloni et al. [48]) following the same protocols described here; hence, to avoid redundancy, these data were not repeated during this work and the published data are reported for completeness sake to give a complete overview of the system behavior.. Starting from this basic blend, the aim of these series of tests consisted of understanding how a different ratio between Lupamin and nanocellulose would affect the transport of different gases. Moreover, the permeation data have been elaborated with the aid of the water sorption tests, in order to obtain a better insight of the influence of the actual water content in the polymeric matrix, since this is usually the parameter that actually affects the transport properties in the case of hydrophilic polymer [44].

Figure 4.8 shows the permeation isotherms for the nanocellulose blends for the main target gas of the work: carbon dioxide. Permeability is expressed in Barrer on the Y-axis and it is reported as a function of relative humidity, expressed as a percentage on the X-axis. Due to the extremely large variation of the permeability along the humidity spectrum, its values are reported on a logarithmic scale. At low humidity, in fact, the differences between the various films are limited and all of them present a permeability in the order of 10^{-2} Barrer. Specifically, the blends containing 70 and 30 wt% Lupamin present a value of respectively 0.0079 and 0.0057 Barrer at a humidity of about 25 %, thus inferring that, at least for CO_2, both behave as a barrier material at low humidity.
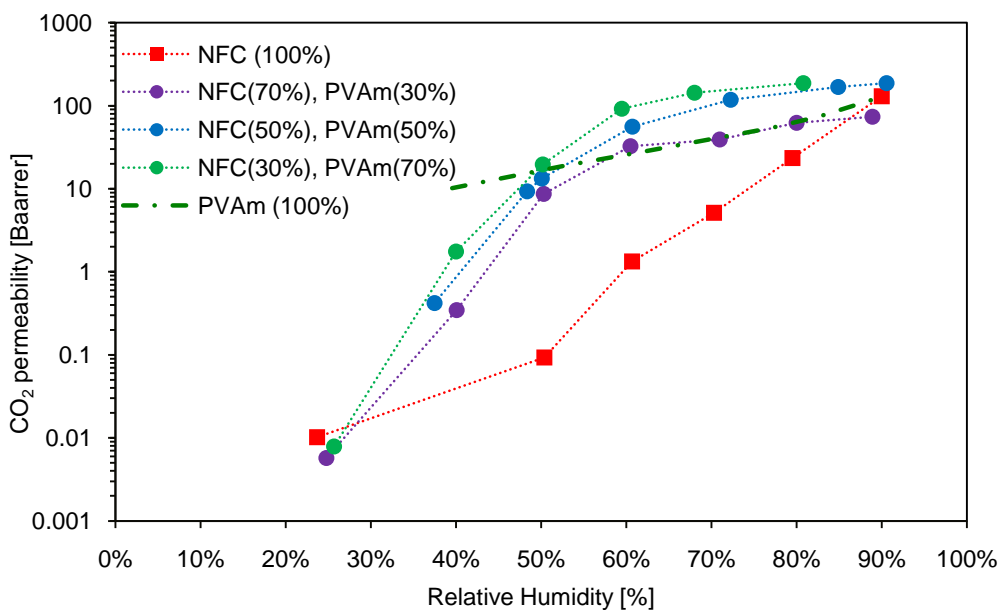
Figure 4.8: CO$_2$ permeability of NFC/PVAm blends as a function of relative humidity [48], *compared to pure NFC and pure PVAm* [36].

Once the water content of the system is increased, the gap between PVAm containing blends and the pure cellulose starts to widen. In particular, the films prepared using Lupamin show a very sudden increment of one order of magnitude between 20 and 40 RH%, arriving at 0.34 Barrer for the 30 % PVAm blend and 1.76 Barrer for the 70 % PVAm one. As it would be expected the film with an intermediate amount of polyvinylamine settles for values that are between the two previously mentioned blends. This growing trend shows the same exponential slope for all three blends up to a relative humidity of about 50-60 %. CO$_2$ permeability, at this point, reached values of 92.3, 55.9 and 32.4 Barrer for the films with respectively 70, 50 and 30 % Lupamin. From this point on, the exponential slope appears to be decrease in a similar manner for all systems. Up until the end, however the curves show a monotonous trend, always associating an increment in relative humidity to a one for permeability, as it is usual for hydrophilic materials. At the highest relative humidity inspected, the 70 % Lupamin film showed the highest permeability recorded at 187 Barrer at 81 RH%, while the 30 % film reached 73.8 Barrer at 89 RH%. At an intermediate humidity of 85 RH%, the 50:50 blend showed a value of 168 Barrer. It is quite reasonable to assume that a further increment in the water content would have resulted in an even higher permeability, but this was not achieved due to an intrinsic limitation of the apparatus, which, due to poor temperature control was not able to reach too high humidity without showing condensation problem in the system. This fact together with the risk that liquid water reaching the membrane, could result in an excessive water swelling and consequential loss in continuity of the film, lead to the decision of limiting the RH range to values which did not show any evidence of condensation in the system.

For the sake of comparison, a curve reporting the permeability of a pure polyvinylamine film [36] is also present. This one shows a more uniform trend throughout the humidity range, presenting a higher permeability at a low-intermediate water activity, paired with values similar, if not lower in some cases, to the NFC-Lupamin blends at high humidity.

Looking back to the nanocellulose curve, instead, it can be seen how its exponential slope appears to be fairly constant in all the activity range inspected, with permeability which increases consistently from values around 0.010 Barrer at 24 RH% up to 129 Barrer at 91 RH%. Reaching values close to that of the different blends and even higher than those observed for the 30% PVAm-NFC films.

It's well known that NFC in the dry state is an extremely effective gas barrier due to its structure of densely packed, hydrogen bonded, nanofibrils, which leaves little to no free volume available for permeation. Once water is introduced into the matrix, however, it reaches the interstitial spaces between the fibers and bonds with available hydroxyl groups thus releasing and softening their connections. This way, the network is expanded and water channels are created throughout the matrix, allowing gases, and in particular polar CO_2 to permeate easily thus justifying the loss of barrier properties reported in the open literature and the exponential increment showed by the data.
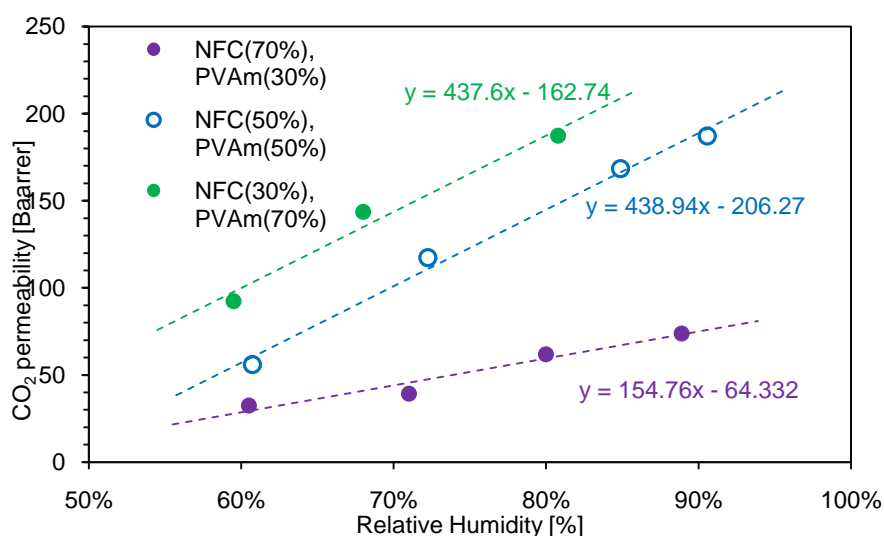
Figure 4.9: carbon dioxide permeability as a function of relative humidity for NFC/PVAm blends after the swelling point. The linear trend of the curves is highlighted.

As to why the slope of the permeation isotherm is significantly differently between the blends and nanocellulose, the answer can be found analyzing the results given by the water sorption experiments (Fig. 4.4). Here, as already pointed out, it is quite visible the presence of two phases of the water intake process: the first one occurs at low-intermediate water activity and has a linear-like behavior and it was common to all film tested, both with and without polyvinylamine, while the second one is peculiar to only the PVAm containing films and takes place at high humidity and has

a more exponential-like behavior. Apparently, this phenomenon appears to translate into a different slope of permeability before and after the swelling point. In fact, before the swelling takes place (20-50 RH%), the growth of CO_2 permeability is exponential, while after it bends down to a more linear-like curve, as highlighted by Fig. 4.9.

Moreover, the permeability curves, acquired as a function of relative humidity, can be translated into functions of the actual concentration of water within the polymeric matrix, thanks to the data measured in Par. 4.2. The results of this elaboration can be seen in Figure 4.10. Here, the difference between the two different trends, before and after the swelling point are even more evident. In particular, the carbon dioxide of the various blends appear to increase exponentially form values around 0.01 Barrer at a water content of 0.05 $g_{water}/g_{polymer}$, up to 20-30 Barrer at a concentration of 0.20 $g_{water}/g_{polymer}$. Beyond this threshold, permeability flattens out, showing minimal increments (at least on the logarithmic scale used here) up to the highest values of water sorption observed for the various nanocomposites.
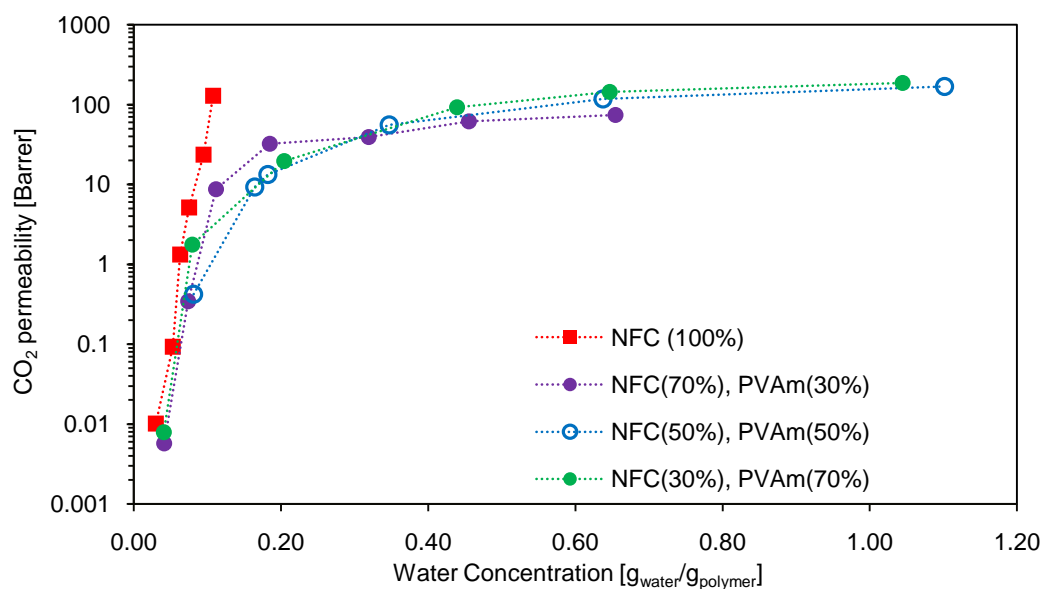
Figure 4.10: CO$_2$ permeability of NFC/PVAm blends and pure NFC on a logarithmic scale as a function of water concentration.

In order to evaluate the performances of gas separation of the films synthesized, permeability tests have been performed using also nitrogen and methane as single gases.

In Figure 4.11 is summarized the nitrogen permeability of the different blends of NFC and Lupamin along with pure NFC. As a reference, the literature values regarding a pure PVAm film are also reported [36]. By analyzing the data it can be noticed that, for this gases, only data at high humidity (RH > 40%) has been reported. Indeed, measuring values at low humidity proved to be quite difficult, since in this range the permeability to a gas like nitrogen is extremely small, resulting in a

downstream pressure increment fairly close to the sensitivity of the instrumentation (§ 2.2.1.1). For low permeating gases such as nitrogen or methane, this effect is usually amplified. This all is to say that it is not possible to completely exclude the presence of a different trend of the values in the low humidity range, even though it is quite unlikely that the trend would be much different than what observed here. As it would be expected, N_2 permeability is overall quite lower than what seen for carbon dioxide. This is a characteristic shared by most gas separation membranes, since nitrogen has both a higher kinetic diameter and lower condensability respect to CO_2 [7]. In different terms, nitrogen is a molecule, which tends to transition towards a condensed state less easily and when it does, its relative size slows down its diffusion process, not being able to exploit all of the permeation volume, which would be available for a smaller molecule.
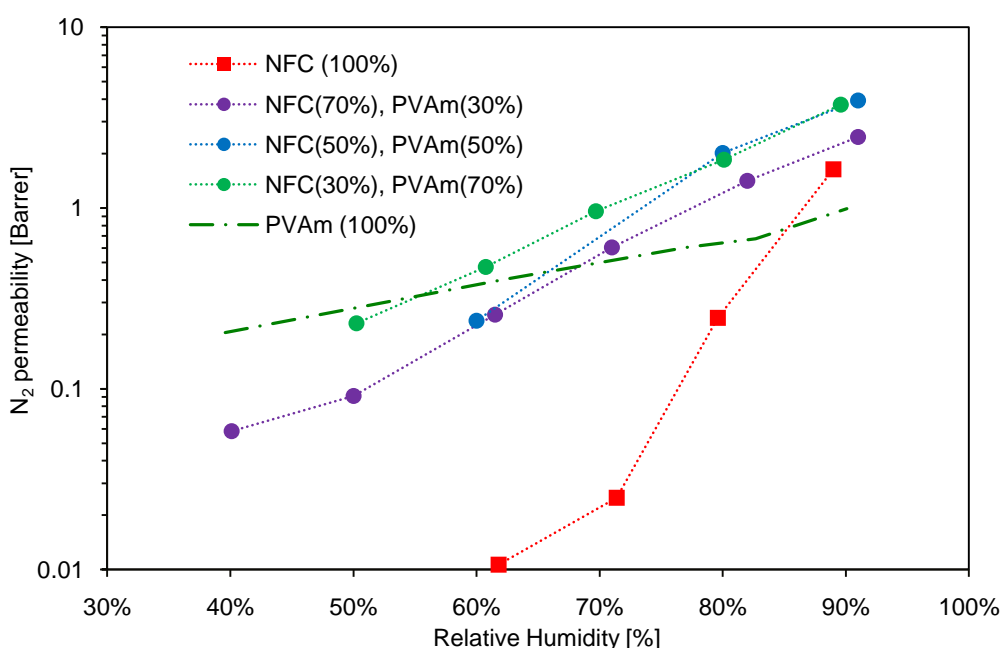

Figure 4.11: N_2 permeability of NFC/PVAm blends as a function of relative humidity, compared to pure NFC and pure PVAm [36].

For a regular glassy polymer, the permeation advantage usually ends here, while in a hydrophilic film, such as PVAm, the presence of water in the matrix also plays strong role. In fact, if the solubility of CO_2 in water is around 1.1 g_{gas}/kg_{water} at 35 °C and 1 atm., for N_2 this value drops down to 0.015 in the same conditions [52]. This difference of around two orders of magnitude is deeply reflected in the permeation data. At low relative humidity, N_2 permeability for the 30 % PVAm blend start from a value of 0.058 Barrer (at 40 RH%). From here, an exponential growth at a constant rate is observed along the humidity spectrum, allowing the gas to permeate at a rate of 2.47 Barrer at 91 RH%. Similarly to what seen for carbon dioxide, the 70 % PVAm blend settles itself for higher values. Specifically, at 50 RH% it shows a permeability of 0.23 Barrer (compared to 0.09 Barrer for the 30 % PVAm film) and increases up to 3.74 Barrer at 91 RH%. The 50:50 blend

appears to present permeation values, which are in between these two curves, as it would also be expected. Similarly to what observed for CO_2 the permeability of pure PVAm [36] grows at a much slower rate with humidity respect to the films prepared here, most likely due to a lower water absorption, especially at high humidity. Analyzing the exponential slope of the two curves (Fig. 4.12), it can be seen how the exponential coefficients are substantially equal and no specific variation of it is present along the humidity spectrum. This highlights a difference in the behavior from what was the one observed for CO_2 beyond the swelling point (Fig. 4.9).
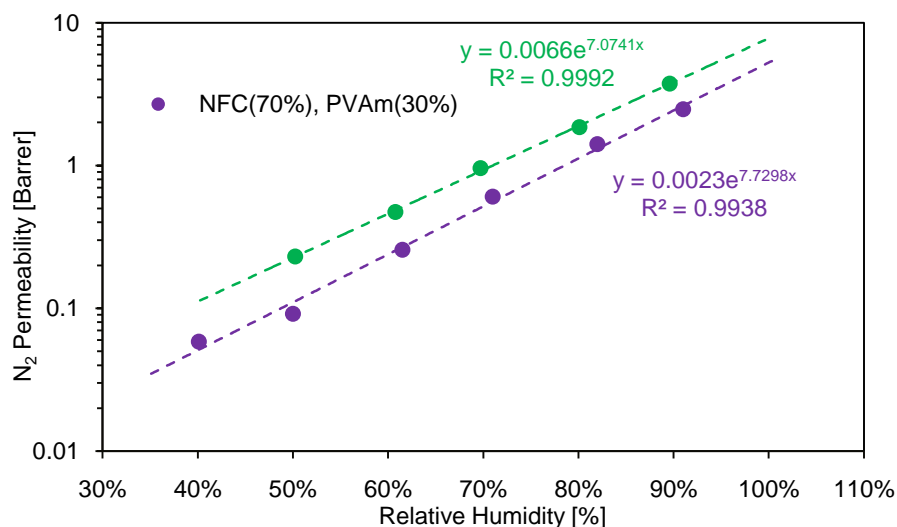

Figure 4.12: nitrogen permeability of the 70 and 30 % PVAm blends on a logarithmic scale as a function of relative humidity. The lines represent the best fitting exponential curves of the data points.

For this last chemical species, in fact, the permeation curves shifted towards a purely linear increment with relative humidity and a higher percentage of PVAm resulted in a higher slope, indicative of transport facilitation. Since no facilitation occurs for nitrogen, being it unable to react reversibly with amine groups, it is quite easy to see why a different concentration of these moieties would not affect the permeability in this sense. But, if the slope itself appear not to be affected by the concentration of PVAm, the absolute value of permeability does increase when this parameter is varied. At first, this could be imputed to the higher presence of water, that a higher concentration of PVAm brings (§ 4.2). In contradiction to this hypothesis, when N_2 permeability is scaled respect to the effective water content of the film (Fig. 4.13), the trend respect to the percentage of PVAm seems to be inverted. Specifically, at the same water concentration the 30 % PVAm film shows a higher permeability than the one with 70 % PVAm. For example, at 0.7 $g_{water}/g_{polymer}$ the nitrogen permeability of the 30 % PVAm blend is 2.47 Barrer, while the one with 70 % is as low as 0.96 Barrer. This inversion is of course related to the fact that the low PVAm blend absorb less water at the same relative humidity as already showed, so its curve appears to be higher, but it also disproves

the hypothesis that the permeation of the non polar species is related simply to the amount of water in the film.

Considering, instead, the behavior of pure nanocellulose, it can be seen how its permeability to nitrogen starts at extremely low values (0.01 Barrer at 62 RH%). This does not surprise, since in other applications it's a material used for its barrier properties towards oxygen [39], a molecule which has transport properties quite similar to N_2. In a matter of a few relative humidity percentage point (from 60 to 90 RH%), its permeability to the gas increases of two orders of magnitude reaching 1.64 Barrer at 89 RH%. A behavior of this kind, can be explained once again considering the nanocellulose film as a densely packed structure of fibrils at low humidity, which in the presence of water tend to separate to accommodate it in a series of microscopic channels along the surface of the fibrils. The overall permeability is naturally much smaller than the one observed for CO_2, being around two orders of magnitude lower, roughly the same different observed for the solubility coefficient.
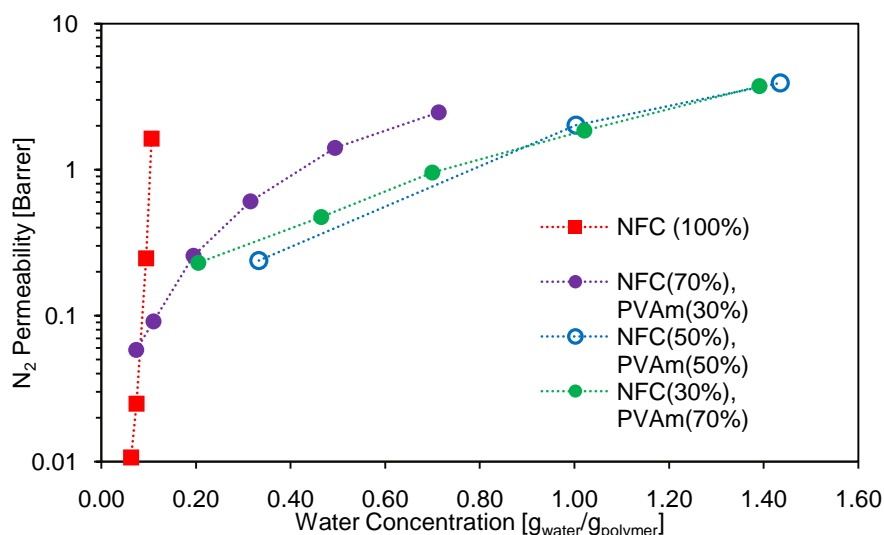
Figure 4.13: N_2 permeability of NFC/PVAm blends as a function of water concentration, compared to pure NFC.

In terms of water content (Fig. 4.13), the increment of the permeability with it is extremely fast and suggests once again that a small increase in water content in the nano fibrillated structure is quite sufficient to extend the water channel network at an exponential rate.

Moving to the analysis of the CH_4 permeability results (Fig. 4.14), it is found a trend very similar to what overall observed for nitrogen. Here too, in fact, the permeability appears to increase at a constant exponential rate with relative humidity, independently form the PVAm content of a given film. Looking at the specific values measured, these are slightly higher than what seen for methane; in particular, for the 70 % PVAm blend a permeability of 0.0.019 Barrer was measured around 25 RH%. At a similar humidity the 30 % PVAm blend showed, instead, a value of 0.009 Barrer. From

this humidity level up to a value of around 90 RH%, the permeability showed an increment of three orders of magnitude, reaching 10.5 Barrer for the 70 % PVAm film and 3.85 for the 30 % one. Overall, the 50:50 blend showed values roughly in between these two curves as it has already been seen throughout this work.
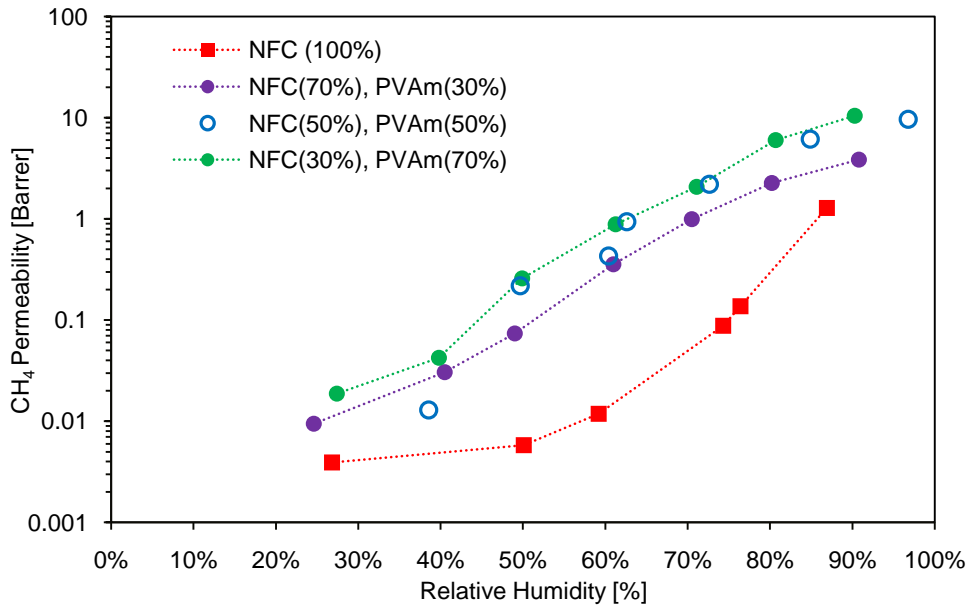
Figure 4.14: CH$_4$ permeability of NFC/PVAm blends as a function of relative humidity (50:50 blend from [48]), compared to pure NFC.

Beyond this, similarly to nitrogen permeability, the trend of the curves does not show any particular flexion along the humidity range (Fig. 4.15), which was a quite characteristic presence in the carbon dioxide isotherms. Here, the absence of a variation in the trend at the swelling point (which occurs around 50-60 RH%) is even more evident respect to the nitrogen data, since these start at lower humidity. This can be seen as an ulterior confirmation that CO_2 and these other two gases follow different permeation mechanisms and N_2 and CH_4 are not negatively affected by the matrix swelling. A behavior of this kind can result in a degeneration of the separation performances, since after a certain value of humidity the permeability increases at a higher pace for the gases that should be mostly rejected by the film.
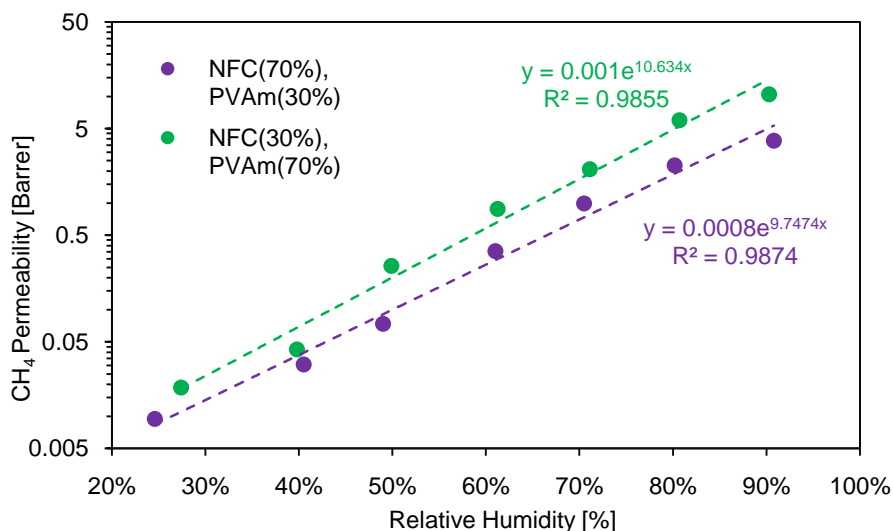
Figure 4.15: methane permeability of the 70 and 30 % PVAm blends on a logarithmic scale as a function of relative humidity. The lines represent the best fitting exponential curves of the data points.

Once again, as a way to further understand the influence of water content, the permeability has been plotted against this specific parameter (Fig. 4.16). As it would be expected, the behavior is fairly similar to the one observed for nitrogen and, respect to the content of PVAm, opposite to the one for carbon dioxide. In fact, here too, the higher presence of NFC, rather than PVAm appears to determine a larger increment of the permeability respect to the water content. Differently than what seen in the permeability versus relative humidity curves, here the presence of a two-stage process is quite evident, with values increasing at a higher rate at low water content and flattening out after the swelling takes place. This is also what most likely happens for the nitrogen isotherm, but due to the lack of reliable data at low permeability, it is not possible to assess it clearly. In terms of absolute values, amongst the PVAm based blends, the one with 70 wt% NFC is once again on the top of the other two showing a permeability of 2.26 Barrer at around 0.45 $g_{water}/g_{polymer}$, while the one with 70 % PVAm present a value of 0.88. As usual the 50:50 blend sits between the two with a permeability of about 1 Barrer.

Pure nanocellulose, as seen before, presents a very fast increment of the permeation properties in a small range of water content, passing from 0.004 Barrer at 0.03 $g_{water}/g_{polymer}$, up to 1.28 Barrer at 0.10 $g_{water}/g_{polymer}$.

In order to better visualize the behavior of pure nanocellulose with the different gases, since the trend is difficult to interpret in such a large scale as the one needed for the PVAm based films, Figure 4.16 collects its permeability results as a function of water content. As suggested before, the trend is exponential with no particular flexing and follows quite closely what was seen by plotting the data against relative humidity.
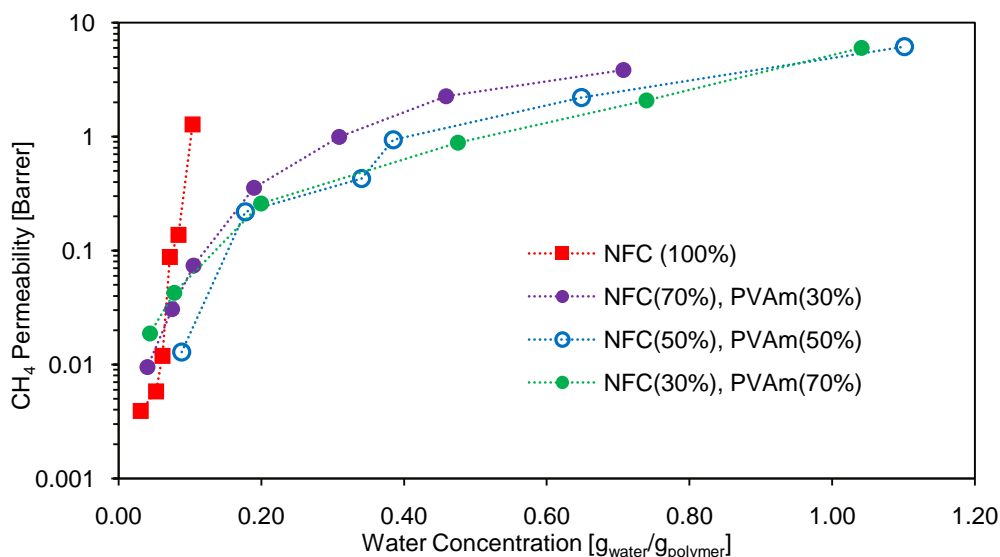
*Figure 4.16: CH$_4$ permeability of NFC/PVAm (50:50 blend from [48]), blends as a function of water concentration, compared to pure NFC.*

This is due to the fact that NFC does not experience any significant swelling phenomenon, even at high humidity, keeping a quasi linear relation between water activity and its mass content inside the film. Between the different gases (Fig. 4.17), no large difference in the trends can be observed and the two curves concerning methane and nitrogen are very close together.
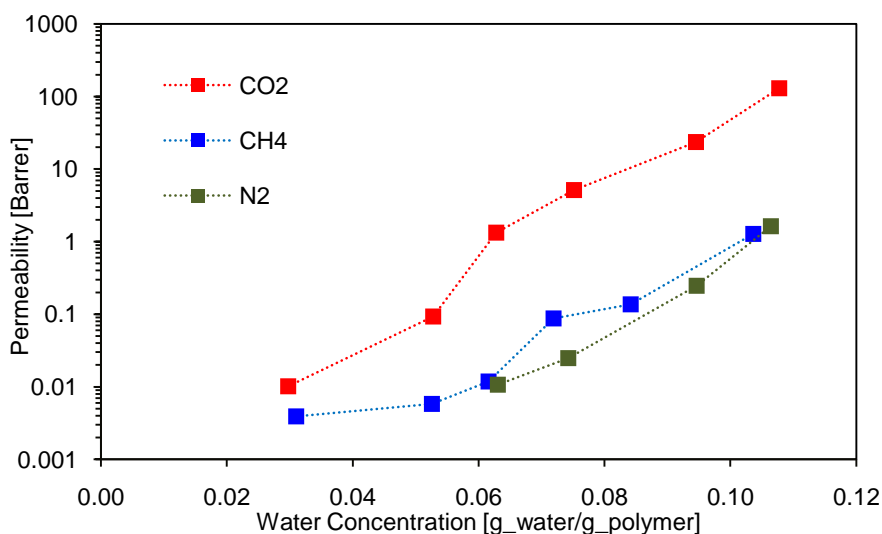
Figure 4.17: comparison between the permeability of pure Nano Fibrillated Cellulose towards different gases respect to the water content of the film

The only variation of the slope that could be argued might be present in the methane curve, which at low water content (0.02-0.05) seems to increase at a lower rate respect to what observed at higher humidity content. Due to the lack of reliable data as such low values for both permeability an water content, it is hard to clearly assess this kind of trend.

Another interesting behavior, which pure nanocellulose showed, lies in the fact that it can apparently reach relatively high gas permeability even though its water content is quite small respect to the PVAm based blends. This difference could be due to the fact that transport facilitation in these last materials is not as present as it would be expected. To gain further insight on the properties of these films, the permeability data have been analyzed to calculate the selectivity respect to the different gases.

4.4 Selectivity

All the results collected up until now give a quite complete picture of how the different gases permeate in films with a variable content of PVAm and NFC, but by themselves are not particularly useful to gain an insight on how the separation performances achieved compare to preexisting materials. A way to assess this, it is first necessary to calculate the separation factor (or selectivity) for each couple of gases; specifically, the interest in the kind of applications concerning these films is to obtain the highest possible selectivity of CO_2 respect to N_2 and/or CH_4. As previously presented in Par. 1.1, if the downstream pressure is low enough selectivity can be assimilated to the ratio of the permeability of each gas in a pure state. Doing this, the possible mixture effects are neglected, but, since carbon dioxide follows a permeation mechanism quite separate from the other two species, relying, at least in large part, on facilitated transport, instead on pure solution-diffusion.

Since the permeability results for each curves were obtained at slightly different relative humidity, an interpolation elaboration was needed to calculate a reliable selectivity for a given point. Specifically, all the permeation isotherms were elaborated, in order to calculated the values corresponding to the permeability at 50, 60, 70 (75), 80 (85) and 90 RH%. At lower humidity the data lack of high reliability due to the very small permeability of nitrogen and methane and are not particularly interesting for any application. The interpolation equation used to obtain the data assumes a natural exponential trend and it is exemplified in Eq. 4.2.

$$\frac{\ln P_{RH*} - \ln P_{RH1}}{\ln P_{RH2} - \ln P_{RH1}} = \frac{RH^* - RH_1}{RH_2 - RH_1} \qquad (4.2)$$

Having calculated the selectivity of the film for the CO_2/N_2 and CO_2/CH_4 separations, these are then plotted against the permeability of the highest permeating gas, here carbon dioxide. This is done so that it is possible to compare these curves to the Robeson Upper Bound [53], presented in Par 1.1. As previously stated, this can be considered the state of the art for a given separation and it is expressed via a double logarithmic chart, which shows the selectivity as a function of permeability.

In the case of the pair of gas considered, the equation of this line takes the form expressed in Eq. 4.3 and 4.4

$$P_{CO_2} = 30\,967\,000 \cdot \alpha_{CO_2/N_2}^{-2.888} \tag{4.3}$$

$$P_{CO_2} = 5\,369\,140 \cdot \alpha_{CO_2/CH_4}^{-2.636} \tag{4.4}$$

The summary of all the selectivity curves for the carbon dioxide/nitrogen separation is presented in Fig. 4.18 along with the Robeson's upper bound for this specific pair. To help correlate these data to the ones showed before, Figure 4.19 presents the selectivity as a function of relative humidity. From the start, it can be seen that all films in both charts, with or without PVAm, present a maximum in the selectivity followed by a more or less rapid decrement. Interestingly, this behavior is shared also with pure nanocellulose, but it is opposite to what was found in literature for pure PVAm [36], which shows a monotonous increase of selectivity with permeability. Looking more in detail at the data we can see how the three curves at different concentration of polyvinylamine achieve an overall increasing trend of both selectivity and permeability, when the amount of the polymer increases. The 30 % PVAm blend presents a maximum selectivity of 135 respect to nitrogen, coupled with a CO_2 permeability of 30.4 Barrer and it is correspondent to a relative humidity of 60 RH%. By itself, this point is already slightly above the upper bound and it can be considered an improvement to the current state of the art. Before this point, the selectivity is 86 and unfortunately, when the humidity increases, it quickly diminishes below this line, while the permeability, as it has been already presented, keeps on incrementing.
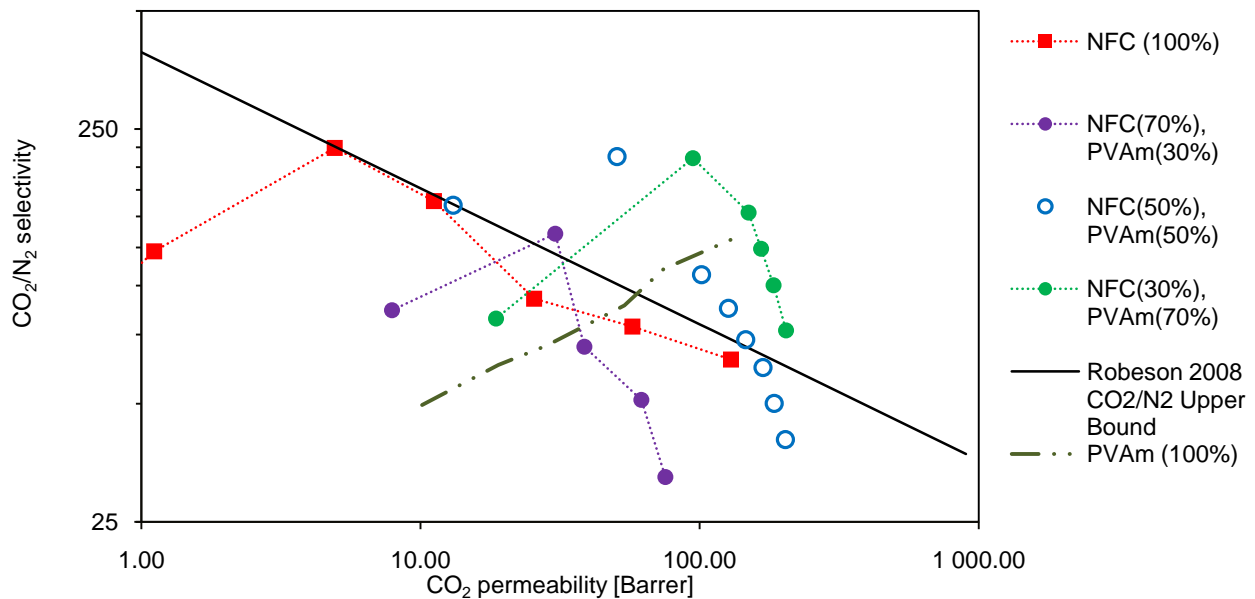

Figure 4.18: CO_2/N_2 ideal selectivity of NFC/PVAm blends as a function of CO_2 permeability (50:50 blend from [48]),, compared to pure NFC and pure PVAm [36].

For example, already at 70 RH%, the selectivity drops to 69.7 and when the permeability reaches an interesting value such as 75 Barrer, the separation factor is as low as 32.5, corresponding to a humidity of 90 %. As seen throughout the rest of the data, the 50:50 blend [48] has values above the 30 % PVAm blend, but below the 70 % one. Specifically, its maximum selectivity is 213, achieved at 60 RH% and a carbon dioxide permeability of 50.6 Barrer., followed by the same sudden drop observed for the 30 % blend.

Moving to the 70 % PVAm film, we can observed the highest values of selectivity and permeability amongst these specific films. In particular, from 50 to 60 RH% the selectivity shows a very sudden increment, going from 82.4 up to 211, with this last point being paired with a CO_2 permeability of 94.7 Barrer. These values represent the highest improvement respect to the upper bound, which was achieved by these films. As seen for the rest of the materials, beyond a relative humidity of 60 %, the selectivity start to decrease quite rapidly. In this case, though, it can be seen how even the point at the highest humidity measured (85 %) is above the Robeson's upper bound, with a value of 76.8 and a permeability of 204 Barrer. It is already quite obvious how all the curves show their maximum around a humidity of 60 RH%, followed by a quick decline after this.
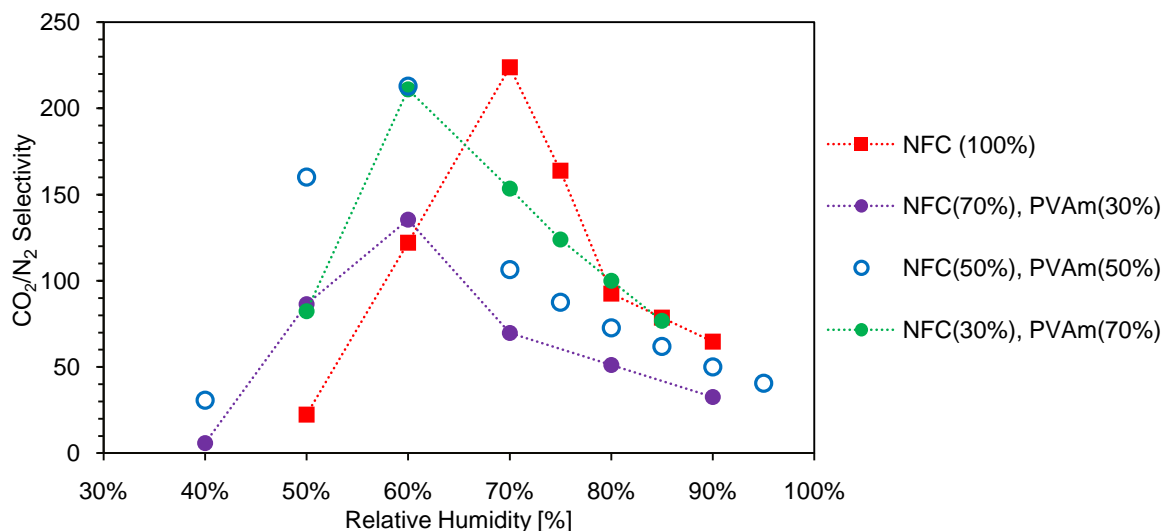
Figure 4.19: CO_2/N_2 ideal selectivity of PVAm based films (50:50 blend from [48]), and nanocellulose respect to the relative humidity

Before starting to analyze this particular behavior, characterized by a maximum and a sudden drop in the separation performances, it seems appropriate to also introduce the selectivity data for the CO_2/CH_4 pair, since the trends observed are fairly similar. As before, the permeability data for both gases have been adjusted via interpolation, assuming an exponential trend (Eq. 4.2), in order to make them comparable at the same level of humidity. The values processed in this way are the one

corresponding to a relative humidity of 50 RH% or more, since below this threshold, the values observed do not spark a particular interest for real life applications.

At a first glance, it can be observed how, similarly to the curves for the nitrogen separation, a maximum is present for all the materials analyzed. As before, in order to further understand the influence of relative humidity on the different systems, the selectivity data are reported both as a function of CO_2 selectivity (Fig. 4.20) and as a function of relative humidity (Fig. 4.21). Starting with the 30 % PVAm blend, at 50 RH%, the selectivity is already quite high being 94.1, but it is coupled with a permeability of only 7.9 Barrer. As for the separation with nitrogen, the maximum is reached at 60 RH%, even though the increment of selectivity respect to the previous point is quite small respect to it. Specifically, the highest selectivity is 81 at a CO_2 permeability of 50 Barrer. From this point on the values start to decrease quite rapidly; at 80 RH% the selectivity is reduced down to 27.8, while the permeability is 61.9 Barrer. Moving up with the PVAm content, the 50:50 blend [48] sits above the previous film, showing a maximum permeability of 121 paired with a CO_2 permeability of 50.6 Barrer, also achieved at 60 RH%. Once again, the film which shows the best properties it is indeed the one containing the highest concentration of PVAm (70 %). Here, at 50 RH%, the ideal selectivity is 71.5 with a permeability of carbon dioxide of 18.6 Barrer, but it is quickly improved moving up to 60 RH%. At this humidity, the selectivity reaches 122 and the permeability of CO_2 is as high as 94.7 Barrer placing this material, in these conditions, well above the Robeson's Upper Bound for this couple of gases.
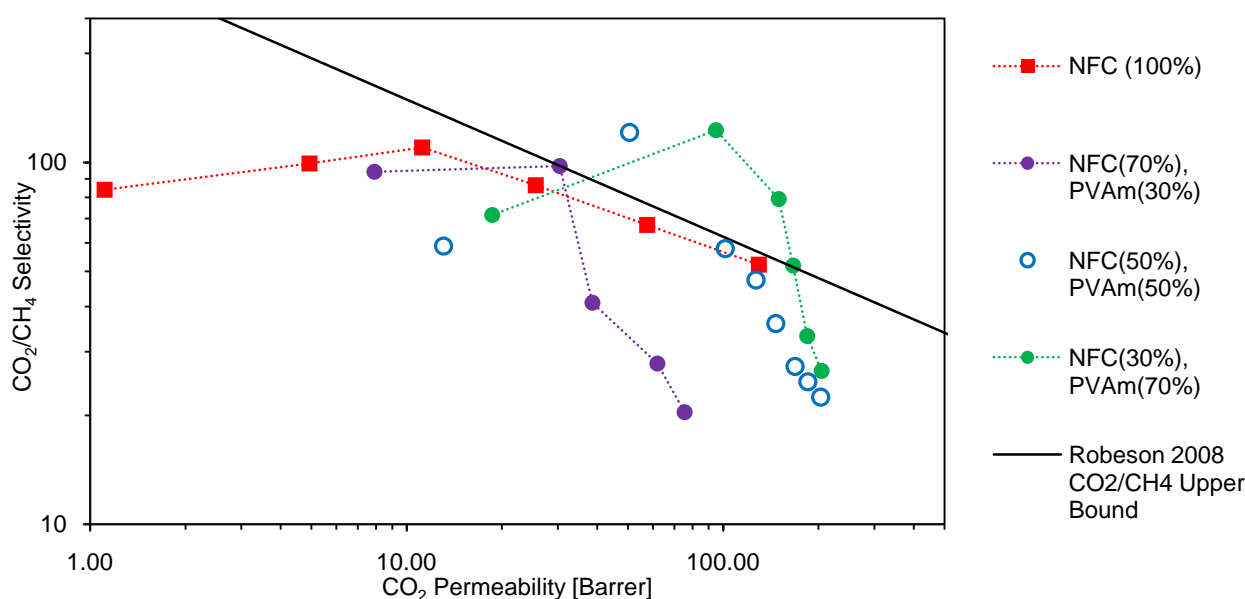

Figure 4.20: CO_2/CH_4 ideal selectivity of NFC/PVAm blends as a function of CO_2 permeability (50:50 blend from [48]), compared to pure NFC.

The same goes for the next point at 70 RH%, even though it is already possible to discern a clear decrease in the separation performances, which continues along with the increment in humidity. As an example, at 85 RH% selectivity is already down to 26.5, almost a full order of magnitude below what was achieved at the maximum, at a permeability of 204 Barrer. Considering pure NFC, instead, we can see how selectivity does not experience the same large variations observed for the PVAm based materials, starting at already 84 at a permeability of 1.1 Barrer (at 60 RH%). This value slightly increases, encountering its maximum of 110 at a permeability of 11.2 Barrer and a relative humidity of 75 %.
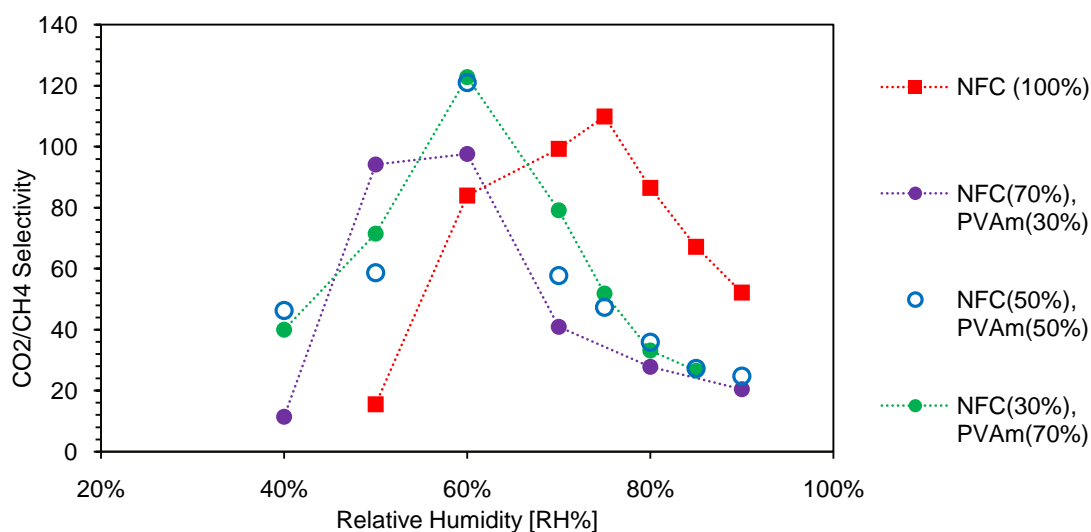

Figure 4.21: CO_2/CH_4 ideal selectivity of NFC/PVAm blends as a function of relative humidity (50:50 blend from [48]*), compared to pure NFC.*

Parallel to its increment, the drop of selectivity is also not particularly steep with values of 86.5 and 52.2 at a CO_2 permeability of respectively 25.6 and 127 Barrer.

What appears to be quite clear after analyzing all the data is that all of the selectivity isotherms acquired for the different materials present the same overall trend, showing a more or less rapid increment al low-medium humidity, followed by a sudden drop when the humidity reaches 60 RH% (or 70-75 RH% in the case of nanocellulose). A way to explain this is to taking into account the presence of the matrix swelling, outlined in Par. 4.2. In the previous section, dedicated to permeability, it has been already made present how this most likely affects the permeability of carbon dioxide in a negative way, diminishing the volumetric concentration of the amine groups, hence not allowing a proper facilitation of the transport of the molecules. While the permeation of CO_2 is hindered by this phenomenon, showing a purely linear growth with water content, the diffusion of nitrogen is not particularly affected by this since it continues to climb exponentially. This change in the trend eventually results in the presence of a maximum, which is located at a relative humidity very close to the onset of the matrix swelling. The 60 RH% turn point, though,

80

does not correspond exactly to the onset of the exponential trend of the water sorption isotherms, associated to the beginning of the matrix swelling (Fig. 4.4). Instead, the shifting from a linear behavior appears to happen at a water activity of 0.4 (40 RH%). So, it appears that the actual threshold for the loss in selectivity is not directly related to the onset of swelling, since a slightly swelled matrix is actually more performing in terms of gas separation than a non swelled one. This leads to assume the existence of a trade-off between the increase in permeability of CO_2 given by a higher content of water intake and the loss of selectivity towards less permeating gas, that the same parameters eventually brings. A reasonable assumption would be that the amount of water content at the maximum value observed would be the same for all three PVAm based membranes. The experimental reality, though, is slightly different, as summarized in Table 3.2.

Table 3.2: Values of water concentration and relative humidity encountered at the maximum selectivity measured. Values rescaled respect to the concentration of PVAm are also reported.

Material	Water Concentration [$g_{water}/g_{polymer}$]	Water Concentration (Adjusted for PVAm content) [$g_{water}/g_{Lupamin}$]	Relative Humidity [RH%]
NFC (100%)	0.072	/	75 %
NFC(70%)/PVAm(30%)	0.180	0.451	60 %
NFC(50%)/PVAm(50%)	0.333	0.590	60 %
NFC(30%)/PVAm(70%)	0.449	0.614	60 %

In this table are reported the hydration conditions of each membrane, at which the maximum selectivity was observed. If we consider only the overall water concentration, it is quite clear how the values are fairly different and do not give any particular explanation to the behavior observed. Instead, if only the amount of water absorbed by the PVAm phase is considered all the values appears to get much closer to each other, even though no single value is noticeable. In order to calculate this specific contribution it has been assumed that the fraction of nanocellulose absorbs the same amount of water in each film as it does in its pure form. This value has been subtracted by the total water intake and the remaining concentration rescaled for the actual amount of Lupamin present in the film as exemplified by Eq. 4.5., where *i* indicates the humidity level taken into consideration and the denominator represents the mass fraction of the PVAm phase in the film.

$$\omega_{H2O,PVAm,i} = \frac{\left(\omega_{H2O,total,i} - \omega_{H2O,NFC,i}\right)}{\omega_{PVAm}} \tag{4.5}$$

Even though a single ideal value for the water content cannot be identified, it is arguable that it must be around 0.5 $g_{water}/g_{polymer}$, and oscillation around this value might be attributable to the active effect of nanocellulose, hindering a higher uptake of water.

As a general analysis of the data collected and in view of the selectivity variations with humidity, it appears that water content is the most controlling factor for both permeation and separation properties. All gases increased their permeance through the various films of several order of magnitude as relative humidity went up. The way this increment happened, though, was different respect to the various gases, with carbon dioxide permeability suffering as a consequence of swelling.

This kind of behavior and also the fact that all gases, not only carbon dioxide, incremented their flow as humidity increased can suggest that the contribution of facilitated transport present in these materials is rather limited. This can be due to a series of factors; the first one is the amount of salt impurities (sodium formate), which reduces the effective amount of functional polymer (hence of amine moieties). Moreover, the amine groups might not be fully available for transport facilitation for interactions with the hydroxyl groups on the nanocellulose surface, which act as an acid. Also the formate ion could shift the balance of the equilibrium between $-NH_2$ and $-NH_3^+$ groups in favor of these last ones. To be able to react reversibly, carbon dioxide needs a free amine group, not its saline form and this could have contributed to a non optimal gas permeation performance.

Beyond this, as previously pointed out, all materials show a point, after which selectivity starts to drop, which also corresponds to the first part of the swelling curve of the matrix. This behavior could also be due to the presence of salt in the matrix. In particular, the salt impurities could tend to segregate on the surface of the film (this is also suggested by the FTIR spectra in Par. 4.1). Once humidity reaches high levels, these segregation might start dissolving, creating discontinuities in the material thickness, which do not have any selectivity towards gases.

Regarding nanocellulose, instead, the high permeability observed, could be due to the casting procedure employed. In fact, comparing this work to the one of Ansaloni et al. [48], it can be seen that treating under vacuum the solution resulted in much higher selectivity (500 for CO_2/N_2) and lower permeability, while in the films prepared here without this protocol, the tendency is the opposite. This suggests that in the microstructure of the cellulose nano fibers are present small defects such as air inclusions, which increase the volume available for the gases to permeate through, but also determine a decrement of the separation abilities.

Overall, the separation properties of these films appear to be highly correlated to a solubility effect, which favors the highly soluble CO_2, while the less soluble gases cannot rely as much on this

phenomenon. Diffusivity most likely plays a smaller role, since at high humidity the diffusion for all species occurs in a water-like state.

During the project the issue related to excessive swelling and selectivity loss has been addressed in a few different ways with quite different outcomes. The first method involved the use of a carboxymethylated nanocellulose paired with a thermal treating of the casted film. The second one consisted of the introduction of a cross-linking agent in the matrix of the films to create additional covalent bonds. Finally, the attention was shifted towards the starting polymer and its purification prior to the membrane preparation process, in order to understand the influence, that this has on the final properties of the blend.

Chapter 5. *Modifications of NFC/PVAm composites*

As seen in the previous chapter, the novel blends of commercial polyvinylamine (Lupamin® 9095) and nanocellulose do show very interesting properties in terms of both permeability and selectivity for carbon dioxide, making it quite attractive for real life applications. Few defects, though, have been highlighted until now, amongst which the loss of selectivity at high humidity appears to be the most compelling to deal with. For this reason, the second part of this section will be dedicated to explore the different methodologies employed to tackle this issue. Since, the lack of separation properties appear to be linked to an excessive water intake, due to swelling, the first two methodologies aimed at reducing the overall amount of water absorbed by the film. Firstly, a thermal treatment on the casted was added to the preparation protocol, with the aim of reducing water sorption and swelling and possibly creating a few cross-linked bonds between the polymeric chains and the cellulosic fibers. With the same line of thinking, a second method employed saw the use of an external cross-linking agent (Glutaraldehyde, GA) on the casted film as a way to chemically induce the formation of a three-dimensional lattice capable of inhibit any form of swelling. Finally, since more than a few of the issues encountered appeared to be related to an excessive presence of salt impurities (sodium formate), efforts were made in order to develop an efficient purification method for the polymer. Once the PVAm was purified, new films were prepared and their permeability tested both at low and high temperature.

5.1 *Thermally treated NFC/PVAm films*

As a way to improve the properties of the membranes prepared, a different type of nanocellulose was employed, whose characteristics are thoroughly described in Par. 2.1 and the casting method outlined in Par. 2.3.4. In a nutshell, this specific NFC has a much higher superficial charge, due to carboxylic groups grafted to its fibers. It is believed that these functionalities can facilitated the interaction of the material with carbon dioxide, being it a polar molecule, and also between the nanocellulose and the polyvinylamine itself, thus increasing the mechanical strength and separation properties of the material at very high RH [49].

To that aim, beyond the use of a different type of nanocellulose, the casted membrane has been also subjected to a thermal treatment at 105 °C. It is indeed known that amines and carboxylic groups can react at high temperature forming amide bonds [54], while the decrease in the water sorption in cellulose fibers subjected to an intensive drying is another phenomenon usually referred to as "hornification" [55]. This seems to be related to fibers shrinkage [56] and cellulose co-crystallization [57], even though a complete and widely accepted explanation of the causes has not been obtained yet. Moreover, a thermal treating of this kind could also trigger the formation of covalent bonds between two chains of polyvinylamine itself, possibly inducing in this way a certain degree of cross-linking. .The curing procedure therefore should improve the stability of the membrane at high humidity, lowering the water uptake and limiting the matrix swelling, which seems to be the main cause of the strong losses in selectivity observed in the previous section. I

The prepared films have been tested in the same way seen previously, assessing both water sorption and permeation properties in single gas tests at different relative humidity but focusing only on a single NFC concentration that is 50%wt of nanocellulose in non purified Lupamin. Here it follows the presentation of the presentation of the results and their discussion.

5.1.1 *FTIR analysis*

Similarly to what previously done for most samples, the blend prepared with carboxylmethylated NFC has been subjected to an FTIR analysis before and after the thermal treatment, in order to assess the presence of any chemical modification the curing process might have induced (Fig. 5.1). It must be noted that these spectra have been acquired with a different ATR crystal than the one used for the films based on unsubstituted NFC, so, even though the technique is the same, the results cannot be compared directly. In Figure 5.1, starting from high wavenumbers, at 3300 cm^{-1} the peak corresponding to the stretching of the N-H bond (and possibly the stretching of also the O-H bond) can be found.
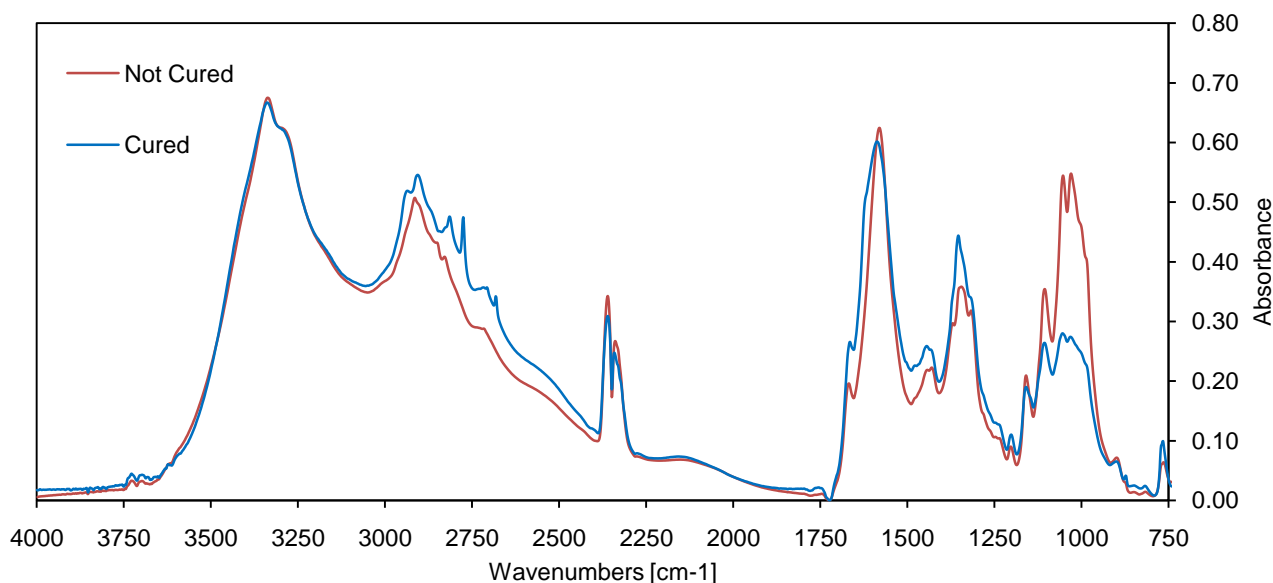
Figure 5.1: FTIR spectra of the 50:50 carboxymethylated NFC and PVAm blends before and after the curing process in vacuum at 105 °C

This one, as well as the peak at 2900 cm^{-1} related to the stretching of C-H bonds, do not appear to be influenced by the curing process in any way. This suggests that, if any bonds were created between amine and carboxylic groups, these involved indeed a relatively small percentage of the various moieties. Moving at lower frequencies, the sharp double peak at 2350 cm^{-1} is most likely related to environmental carbon dioxide and should be ignored as an imperfection of the experimental procedure. Between 1750 and 1200 cm^{-1} all peaks once again appear to be quite similar to each other, at least within the experimental error of the system. These are the peaks related to the stretching of the C=O bond from the modified nanocellulose and the formate salt (1600 cm^{-1}), bending of C-H bond (1450 cm^{-1}) and bending of O-H group (1350 cm^{-1}). What appears to have decreased in absorbance in a significant manner is the double peak at 1000-1050 cm^{-1}, which can be related to the stretching of the C-O bond in the alcoholic groups of nanocellulose. This decrement in absorbance appears to occur only for a peak specifically characteristics of the cellulosic fibers, suggesting that, if modification has actually took place, this is probably within this specific phase.

5.1.2 Water absorption

Once casted, the films' water sorption properties have been assessed via the quartz spring balance apparatus described in paragraph 2.3.1.

In Figure 5.2, the results of this test for the NFC/PVAm blend after thermal treatment are showed. The experiment was run at 35 °C and the water concentration in the polymer was measured to have increased from 0.016 g$_{water}$/g$_{pol}$ to 0.52 g$_{water}$/g$_{pol}$ in a water activity range between 0.15 and 0.86.

In order to give a relatable comparison, Figure 5.1 also shows the absorption curves corresponding to pure NFC G2 [39] and to a PVA/PVAm blend with a Polyvinylamine content of 80 % [44]. This last material have been subjected to a similar thermal treatment at 105 °C to induce cross-linking and it is shown in order to give an example of what the water sorption of a material subjected to these kind of process is like. Moreover, a comparison with the unsubstituted nanocellulose and the untreated 50:50 NFC/PVAm film has been made.
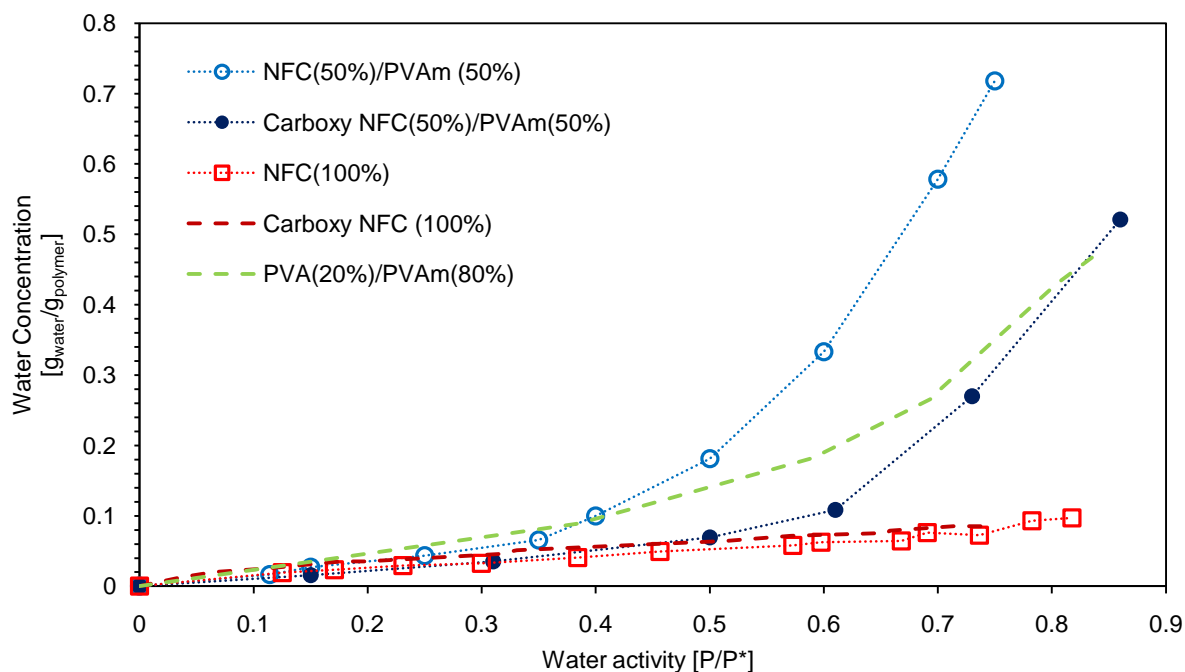

Figure 5.1: water absorption isotherms as a function of water activity at 35 °C of NFC/PVAm 50:50 blend (blue dots, this work), compared to pure carboxymethylated NFC (red line) [39] *and a PVA(20%)/PVAm(80%) blend (green line)* [44]. *The isotherms for pure unsubstituted NFC and the NFC/PVAm 50:50 blend previously seen have been also added for comparison.*

It can be seen how the membrane prepared in this work is laying in between the two curves from literature. In particular, in the activity range from 0 to 0.5, the curves representing pure carboxylmethylated NFC and the 50:50 NFC/PVAm cured blend are substantially overlapping, while higher values of water absorption should be expected for the latter in view of higher PVAm water uptake with respect to NFC. This kind of behavior suggests that NFC fibers in the blends have lower solubility with respect to that of pure NFC. An idea of the efficacy of the curing process can be acquired by comparing the modified film with the original one (Fig. 5.1). After the first low sorption phase, the two curves appear to diverge starting from a water activity of 0.3, with the thermally treated one showing overall a lower uptake than the previous one. Since the two kinds of cellulose nano fibers do not appear to have a significantly difference in terms of water sorption, it can be then concluded that the curing process is quite efficient in reducing the sensitivity of the film

towards water. Specifically, at an activity of about 0.6 the untreated film presented a water concentration of 0.33, against a value of 0.10 $g_{water}/g_{polymer}$ for the cured one at the same humidity. At higher humidity this gap appear to widen even more reaching the top at the maximum humidity inspected for the untreated sample (around 0.75 the concentration values are 0.72 and 0.27 $g_{water}/g_{polymer}$ for respectively the original material and the thermally treated one).

The thermal treatment thus appears to have successfully reduced the material sensitivity to water through the formation of new bonds between the cellulose fibers (hornification [56]) or among amine groups of PVAm and the carboxylic ones on the surface of the cellulose nano-fibrils (cross-linking). In particular, the fact that the water uptake appears to be simply reduced respect the non treated film and not eliminated throughout the humidity range suggests that the number of cross-links, if any, is rather limited inside the matrix and that difference are more related to a densification of NFC network that prevent to some extent the water uptake of the more hydrophilic Lupamin[®] domains.

The overall behavior therefore can be described by considering that the NFC/PVAm films have a microstructure very similar to the one of pure nanocellulose, having PVAm as a secondary dispersed phase. Therefore, the NFC network acts as a constraint for PVAm and hinders its swelling until a critical RH is reached, where the fibrillar network breaks and the whole material rapidly swells due to water intake of polyvinylamine.

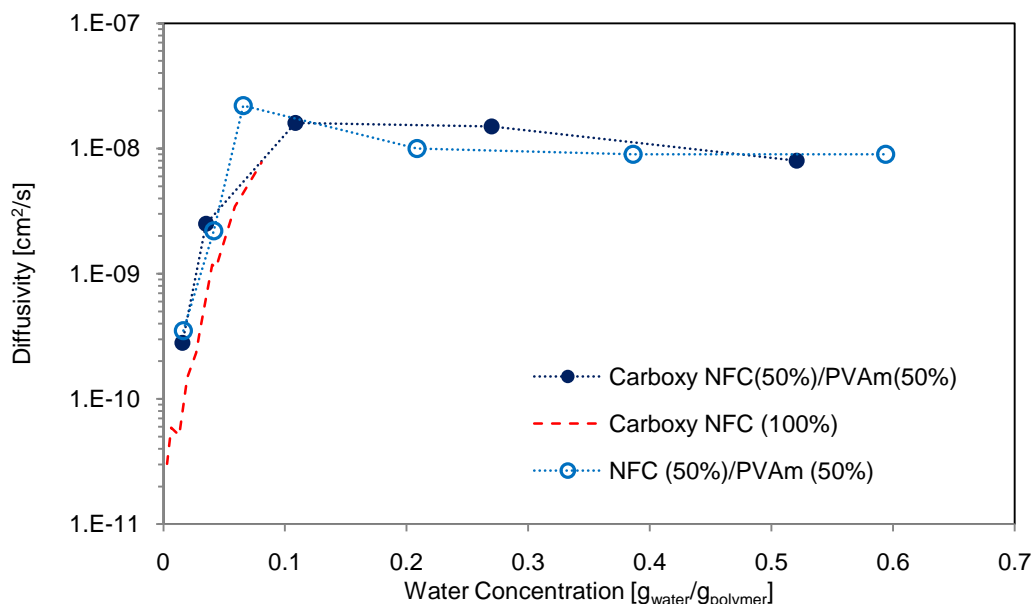*Figure 5.2: Fickian diffusivity of water as a function of water intake at 35 °C of NFC/PVAm 50:50 blend (both treated at 105 °C and not) and pure carboxymethylated NFC (red line) from literature [39].*

As mentioned in Par. 2.2.2.1, sorption tests also allow achieving information of the water diffusivity in the system. The kinetic data were processed through Eq. 2.7 and the results are reported in Figure

5.2, which shows the water diffusion coefficient plotted as a function of the water concentration inside the membrane.

For uptakes up to 0.1 g_{water}/g_{pol} the sample developed in the present work (full blue dots) shows a rapid increment of diffusivity, from 2.8E-10 to 1.6E-8 cm^2/s beyond this point however the diffusivity appears to hit a plateau, since no further significant increment can be observed.

Again, for the sake of completeness, the water diffusivity values of a pure NFC G2 film have also been plotted [39] along with the ones for the untreated NFC/PVAm 50/50 blend also presented before. As per the water sorption curve, the two curves present the same behavior up to the swelling point identified by a water intake of about 0.1 and actually reach the same plateau level of 10^{-8} cm^2/s at the higher concentrations inspected. This is probably due to the fact that after a certain water intake, the system behaves as a gel, where the diffusivity of the various species is very close to the one of water.

5.1.3 Gas permeability

Seen the promising results obtained by the water sorption tests, this paragraph will focus on the assessment of the gas permeation properties of the cured film and its variation respect to the base material. Specifically, gas permeability of the film has been tested for CO_2 and for CH_4 as a reference gas by utilizing the single gas humid permeometer described in paragraph 2.2.1. In this case, since nitrogen and methane showed very similar behaviors in the previous series of tests, permeability has been analyzed only for this second gas in order to minimize redundancies. Like all previous tests, this one was also performed at 35 °C, with a total feed flow of 1000 cm^3/min and RH ranging from 30 to 90%.

The results of the permeation tests are presented in Figure 5.3 and 5.4. In the first one the results for the cured NFC/PVAm blends are shown along the non treated film [48]. As already observed for the other PVAm based membranes, a dramatic increase of gas permeability can be noted with a large variation, that in the present case consists of about 3 orders of magnitude in the investigated humidity range. Throughout the whole range, then, CO_2 appears to be the most permeable gas, showing a permeability up to two orders of magnitude higher than the one obtained for CH_4. For example, at 70 % relative humidity the CO_2 permeability in NFC/PVAm blends has a value of 89 Barrer against 0.8 Barrer for methane, while at 87 % relative humidity a value of 278 Barrer, the largest achieved in the present work, is observed that correspond to a methane permeability of about 10 Barrer. The results for carbon dioxide are substantially similar to what found previously for the untreated films and for methane a small variation can be seen at an intermediate degree of humidity

(50-70 RH%), where the permeability appears to be lower for the cured film respect to the previous one (at 62 RH%, 0.26 respect to 0.93 Barrer).
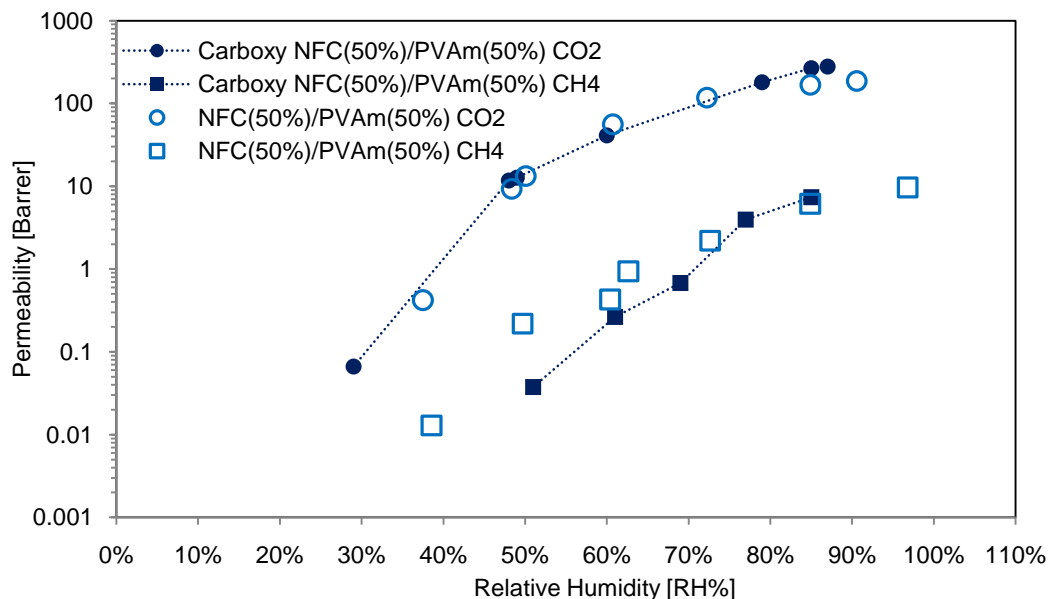

Figure 5.3: CO_2 and CH_4 permeability of the thermally treated NFC(50%)/PVAm(50%) film as a function of relative humidity. For comparison, the results for the untreated blend are also reported [48].

In the case of pure NFC films (both with and without carboxymethylation, Fig. 5.4) CO_2 permeability ranges from around 10^{-2} Barrer at 10 RH%, to 42 Barrer at 82 RH% while that of methane increases from 0.006 to 0.37 Barrer in the same water activity range thus remaining well below that of the other gas.
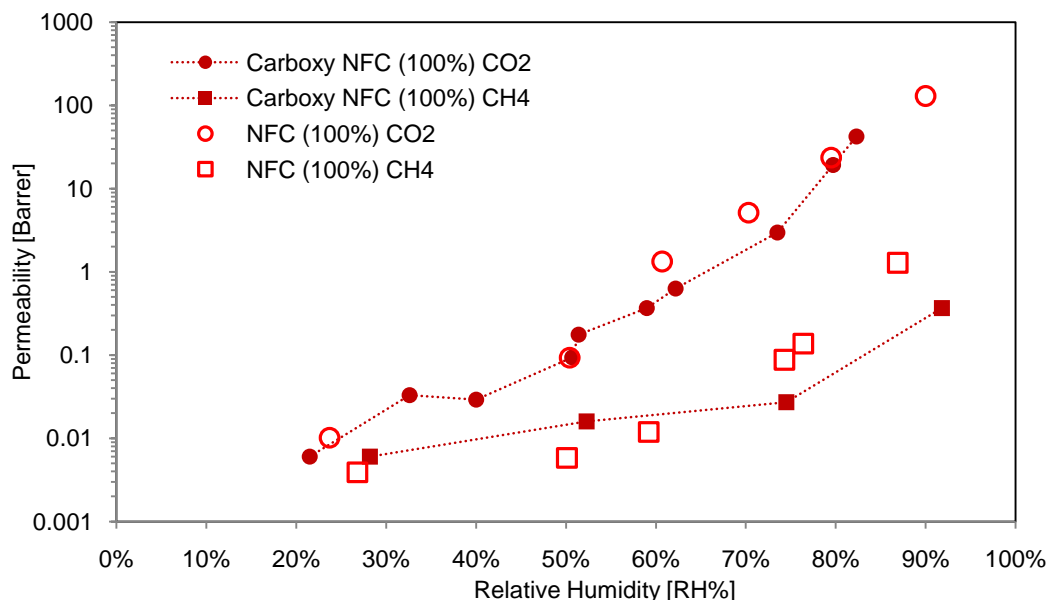

Figure 5.4: CO_2 and CH_4 permeability of the carboxymethylated NFC film as a function of relative humidity. For comparison, the results for the unsubstituted film are also reported.

Focusing on the differences in the permeability trends of the NFC/PVAm blend and pure NFC, it can be seen how the carbon dioxide curve for the blend shows the same type of change in slope at

90

swelling also observed for the untreated films. As before, this variation is not observed for the less permeating gas (here methane), which actually preserves its exponential growth even at high humidity. For pure carboxymethylated NFC, instead, the exponential trend is kept throughout the whole humidity range and it actually appears to show two different slopes for CO_2 and CH_4. In detail the increment of permeability of the first gas seems higher than the last one, with the gap between the two widening as the water activity going up. This is most likely an indication of quite different separation performances, which will be analyzed in the next paragraph.

5.1.4 Selectivity

To visualize the separation abilities of the materials prepared, Figure 5.5 shows the ideal selectivity for both the MFC/PVAm blends and the pure NFC films compared to the CO_2/CH_4 Robeson upper bound [9]. As before (§ 4.4), in order to compare results for the two different gases at the same degree of humidity, the values have been interpolated assuming a natural exponential variation respect to relative humidity.

As seen in the previous paragraphs the system appears to have similar characteristics in terms of overall trend respect to the ones previously seen, with a maximum and a subsequent drop.

Interestingly, though, the synthesized membranes are able to achieve attractive separation performances, especially in the intermediate humidity region (60-70 RH%), where the experimental data are well beyond the state-of-the-art of polymeric membranes: for example at a CO_2 permeability of 14 Barrer the cured membrane shows a selectivity up to 410 and remains above the line up to 70 RH%. Unfortunately, indeed, when the materials show a relevant increase of water uptake, which is at the highest activity inspected, the increase in permeability is accompanied by a substantial decrease in selectivity, which slowly bring the membranes below the trade-off curves of the 2008 Robeson's plot. Specifically, at a relative humidity of 70 and 85 % selectivity reaches values of 88.7 and 34.5.

Moreover, pure carboxymethylated NFC shows a particularly high selectivity too and in this case this parameter is monotonously increasing with both humidity and permeability of carbon dioxide. This is opposite to what previously observed for the unsubstituted nanocellulose, which presented a maximum value like the rest of the films. Here, from what Fig. 3.27 presents, the permeability of CO_2 grows at a constantly higher pace than the one of CH_4 and this results in a constantly increasing selectivity. At high humidity (82 RH%) this film showcases a selectivity of 462, the highest one of all films tested, paired with a permeability of 38.5 Barrer for carbon dioxide.
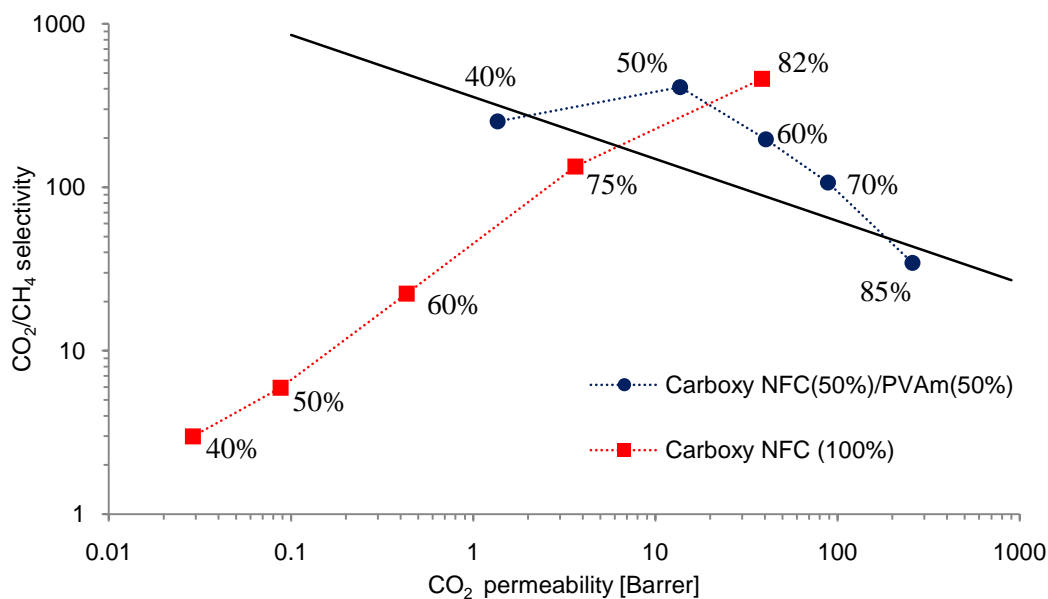
Figure 5.5: selectivity of CO_2 over CH_4 as a function of at 35 °C of CO_2 permeability for NFC/PVAm 50:50 blend (blue dots) and pure carboxymethylated NFC (red squares), compared to 2008 Robeson upper bound [9]. Next to each point is reported the relative humidity at which it was the permeability was measured.

To gain a further insight in the changes in the properties of the film with the introduction of a superficially charged nanocellulose and a curing process, Figure 5.6 compares the selectivity values of 50:50 films both with and without these characteristics (Fig. 5.6(a)) and the pure nanocellulose samples too (Fig. 5.6(b))as a function of water content. Overall, for the PVAm based blends the shape of the curves drawn by the data is fairly similar, with the main difference for the carboxymethylated and cured one to be shifted at higher selectivity values (the maximum shifts from 121 to 410). In general the cured film appears to be able to achieve better performances at lower values of water concentration.

For pure NFC, the whole trend appears to be significantly different, since the non unsubstituted material presents a quite evident maximum, after which the performances are quickly degraded, while the carboxymethylated one shows a monotonous trend, which does not appear to suffer in any way with the increment of relative humidity. This particular improvement does not appear to be related to a difference in the water uptake, since both films top at around 0.1 $g_{water}/g_{polymer}$ at the highest humidity inspected. The advantage, which the carboxymethylated nanocellulose appears to have might be related to a more compact microstructure, which acts as a better sieve for the gas species. Beyond this, the higher surface charge of the fibers might also contribute with a higher affinity towards carbon dioxide.
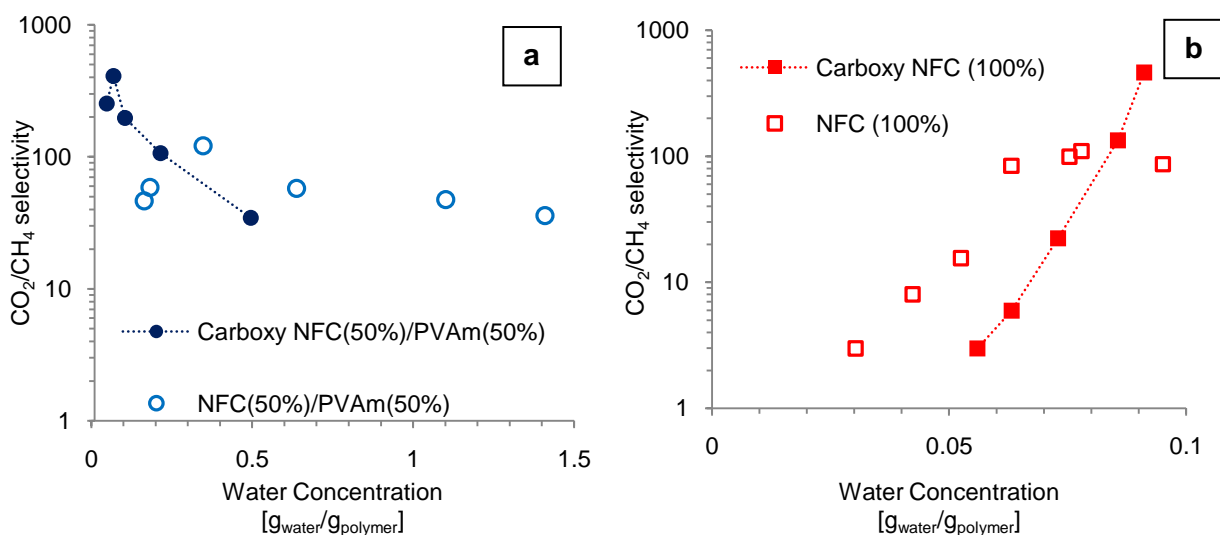
Fig. 5.6: comparison of selectivity data for the NFC/PVAm blends (thermally treated or not [48])(a), and the nanocellulose films (carboxymethylated or not)(b).

In conclusion, it can be said that a stiffer and more charged matrix can result in a significant improvement of the separation properties, since it prevent its swelling, a phenomenon, which is appears to be responsible for the loss of performances at high relative humidity. This kind of approach has been also exploited in other ways, as it will be presented in the next paragraphs.

5.2 Chemically cross-linked NFC/PVAm films

As all the data introduced up until now suggest, the separation performances of the PVAm blends are strictly connected to the amount of water, that the matrix can take in. Specifically, a matrix capable of absorbing water while minimizing swelling at high humidity appears to perform better than one, which does not.

In the previous paragraph this aim was pursued by thermally treating the material, in order to reduce the water uptake of the cellulosic fibers and possibly allowing the formation of a few cross-links in the PVAm matrix. Here, a different approach will be presented, which relies on the introduction of an external cross-linking agent in the already casted film, as a way to stabilize its structure at high humidity.

The molecule chosen for this objective was glutaraldehyde (GA), which showed itself quite performing in the case of polyvinylalcohol (§ 2.3.1). The exact cross-linking procedure has been already outlined in Par. 2.3.5 and the films have been characterized following the procedures presented before. The next paragraphs will therefore focus on the presentation and discussion of the results obtained by FTIR analyses, water sorption isotherms and permeation experiments.

5.2.1 FTIR analysis

In order to assess the chemical modifications applied to the films, FTIR in attenuated total reflection has been used as outlined in Par. 2.2.3. Figure 5.7 and 5.8 summarize the spectra resulting from the analysis of three cross-linked materials, specifically the ones treated with a solution of GA at a concentration of 1, 5 and 25 wt%. To minimize the number of parameters, only the 50/50 NFC/PVAm blend has been subjected to this modification. As a comparison, the spectra of pure nanocellulose and the 50/50 untreated NFC/PVAm blend have been also added.
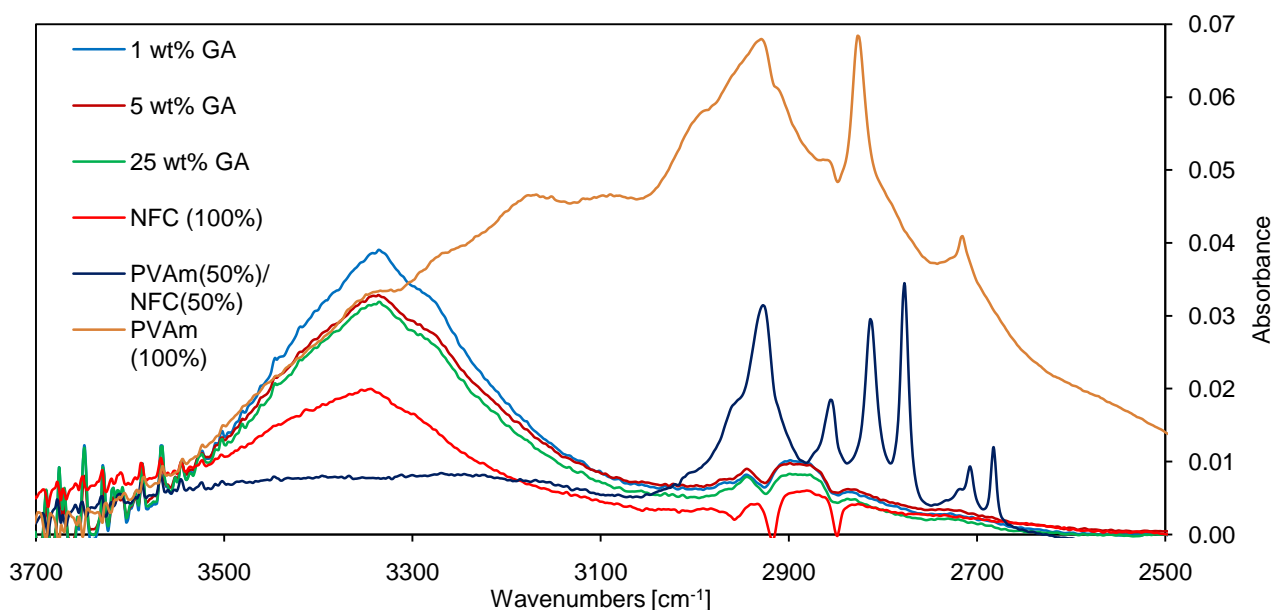

Figure 5.7: FTIR spectra of the NFC/PVAm 50/50 samples treated with different concentrations of glutaraldehyde (GA), compared with pure nanocellulose, pure Lupamin and the untreated 50/50 blend (high wavenumbers).

Figure 3.30 shows the high wavenumbers fraction of the spectra collected, from 2500 to 3700 cm^{-1}. Overall, it appears that the various cross-linked films do not differ particularly from one another and are all quite similar to pure NFC. A detailed description of the different peaks characteristics of these materials has already been done in Par.4.1, but the main ones present here will be highlighted anyway. In particular, at 3500-3200 cm^{-1} we can observe the broad peak easily relatable to the presence of the alcoholic groups on the surface of the cellulosic fibers. This peak is quite small in the non treated film and it is of course quite evident in the NFC spectrum. Interestingly, the highest values of absorbance for this peak are reached by the cross-linked samples. Moreover, the series of peaks between 2900 and 2700 cm^{-1}, which can be related to the stretching of the C-H bond for a carboxylic carbon (present in the formate ion of the Lupamin solution) are not at all present in the cross-linked polymers.

Moving forward, Figure 5.8 present the spectra in the range of 1900-650 cm^{-1} and once again the cross-linked polymers result much closer in terms of chemical structure and functionalities present to pure NFC rather than their non modified version. The peaks at 1650, 1300 and 750 cm^{-1} appear all to have almost disappeared from the original structure. The first one is the one correspondent to the stretching of the C=O bond, originating from the residual formamide groups attached to the polymeric chain as well as the formate ion. The other two peak can be correlated as well to the presence of this residual salt.
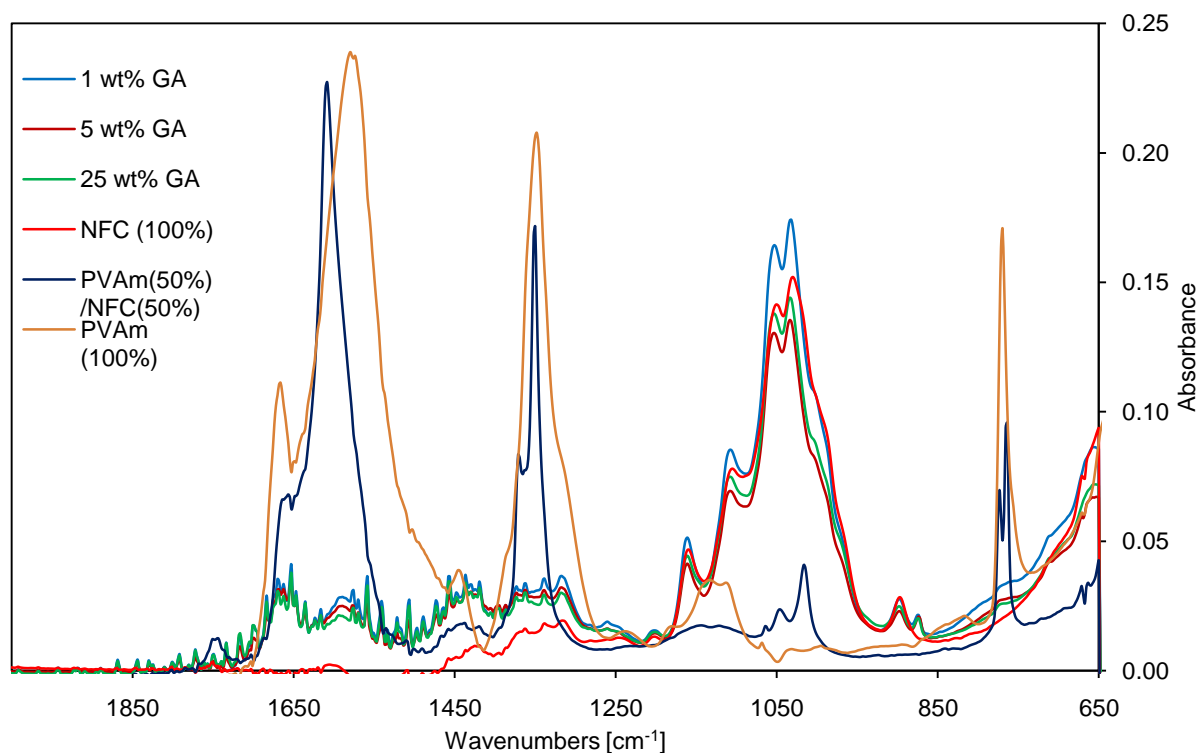
Figure 5.8: FTIR spectra of the NFC/PVAm 50/50 samples treated with different concentrations of glutaraldehyde (GA), compared with pure nanocellulose, pure Lupamin and the untreated 50/50 blend (low wavenumbers).

Beyond this, at 1050 cm^{-1}, the main peak related to the presence of nanocellulose (stretching of C-O bond) is almost identical between the cross-linked films and pure NFC, while it was almost negligible in the original blend.

All the peaks characteristics for the commercial PVAm have been drastically reduced in intensity, suggesting a strong variation in the actual concentration of Lupamin in the treated membrane. Moreover, since FTIR-ATR is a superficial analysis, the cross-linking might be concentrated in the first few microns of the films, which have been extensively reticulated respect to the bulk of the material.

5.2.2 Water absorption

As all the sorption tests showed up until this point, these too have been performed using the quartz spring apparatus outlined in Par.2.2.2.1. In order to have a way to compare the results with the ones previously obtained, all tests have been run at the usual temperature of 35 °C in a range of water activity between 0.1 and 0.75. Three samples have been tested in this way, each one treated in a solution of glutaraldehyde with a different concentration, specifically 10, 25 and 50 wt%. Like before, all samples treated had a starting weight ratio between nanocellulose and Lupamin of 50:50.

In Figure 5.9 the sorption isotherms for these materials are presented, along with pure NFC and the untreated 50/50 blend for comparison. Firstly, it appears quite hard to discern a particular difference in the behavior of the differently cross-linked films, whose points are densely packed together in a relatively linear trend. In terms of absolute values, at an activity of 0.1 the cross-linked films showed a water intake of around 0.03 $g_{water}/g_{polymer}$ and an almost linear trend is observed up to the highest water activity inspected. The highest values of water absorption measured are around 0.18 $g_{water}/g_{polymer}$ and are ever so slightly above a perfectly linear behavior. In comparison with the other two films plotted, the cross-linked ones appear to behave very similarly to pure nanocellulose, both in terms of overall trend and absolute values. Certainly, the gap between the original 50:50 blend and the treated ones is much wider than the one observable between these and pure NFC.
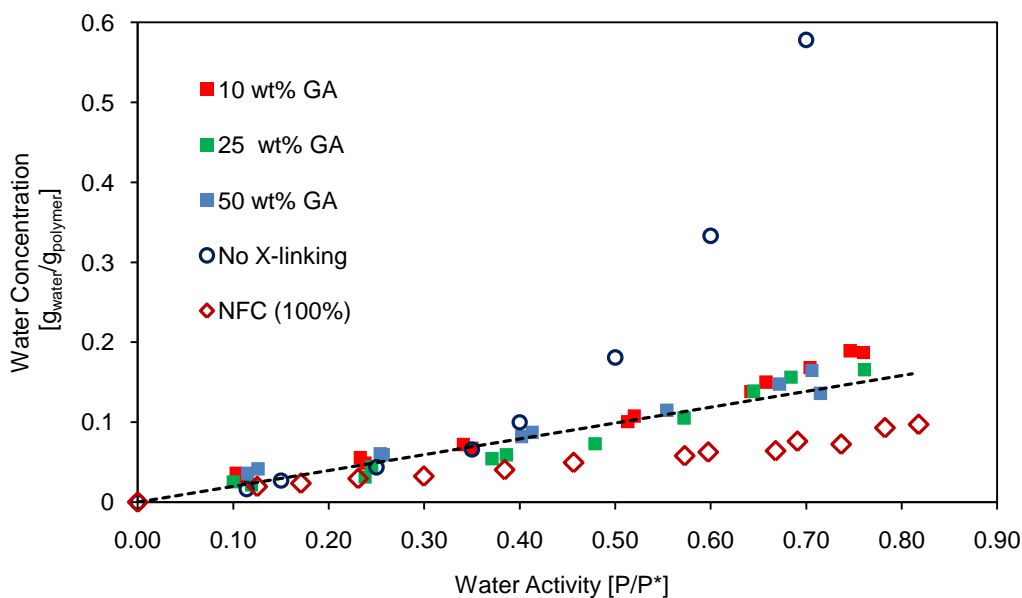
Figure 5.9: water sorption isotherms of NFC/PVAm 50/50 blends treated in a GA solution with a concentration of 10, 25 and 50 wt%. The dotted line is added to help follow the trend. For comparison the data for the untreated film and pure nanocellulose are also presented.

This gap is almost nonexistent at low humidity and prior to swelling, but quickly widens at a higher degree of hydration. In particular, at a water activity of 0.70, the untreated blend showed a water

intake of 0.58 $g_{water}/g_{polymer}$, which is reduced down to around 0.16 by the cross-linking treatment, while pure NFC has a value slightly below that at 0.07.

Both of these observations, the vicinity in behavior to pure NFC and the very small variation of results between the cross-linked samples, are quite consistent to what was observed in the FTIR analyses. Water sorption values so low can be attributable to a large extent of the chain to chain bonds created by the aldehyde, which do not allow any kind of swelling of the matrix. Since the polymeric chains are covalently bonded to each other, they do not have the possibility of separate via a large relaxation process, which is most likely at the origin of the swelling observed up until now.

In any case, the cross-linking procedure was aimed at reducing the total water intake of the films, in order to avoid swelling and this was definitely achieved, even though controlling the actual extent of the bonds formed appeared to be more difficult, than what was previously believed. In fact, the concentration of glutaraldehyde in the solution used to treat the materials did not seem to affect the characteristics tested here. This might be due to the fact that after a certain concentration, lower than the ones tested here, all the functional groups available for cross-linking have already reacted and a higher amount of GA does not have any particular effect on the system.

5.2.3 Gas permeation and selectivity

In order to put to the test the hypothesis made in the previous paragraphs, a few materials have been selected to be tested in a humid permeometer. In this case, the apparatus chosen for the testing is based on the same principle as the one described in Par. 2.2.1.1, with the only difference that the temperature is kept constant by a thermostatic bath, rather than an incubator. As before, the gas tested were CO_2, N_2 and CH_4 in a range of humidity, which went from 25 to 100 RH% at a temperature of 35 °C. In this case, it was possible to use high concentration of water in the feed, since, due to the high degree of cross-linking, there is no risk of solubilizing the film if condensation would occur.

Since the sorption results gave very similar results for all the membranes, it was assumed that their permeation results would not vary significantly having glutaraldehyde reacted with the vast majority of the functional groups. For this reason, another sample has been prepared by using a 1 wt% GA solution for the cross-linking. This was done in the hope to reduce the degree of reticulation. After the results of the permeation tests, though, this material was not deemed particularly interesting anyway and no water sorption experiment was subsequently carried on. In the end the permeation tests have been performed on the films cross-linked via a solution of 1 and

25 wt% GA, with the hope to see a significant difference in the properties due to a different extent of the cross-linking.
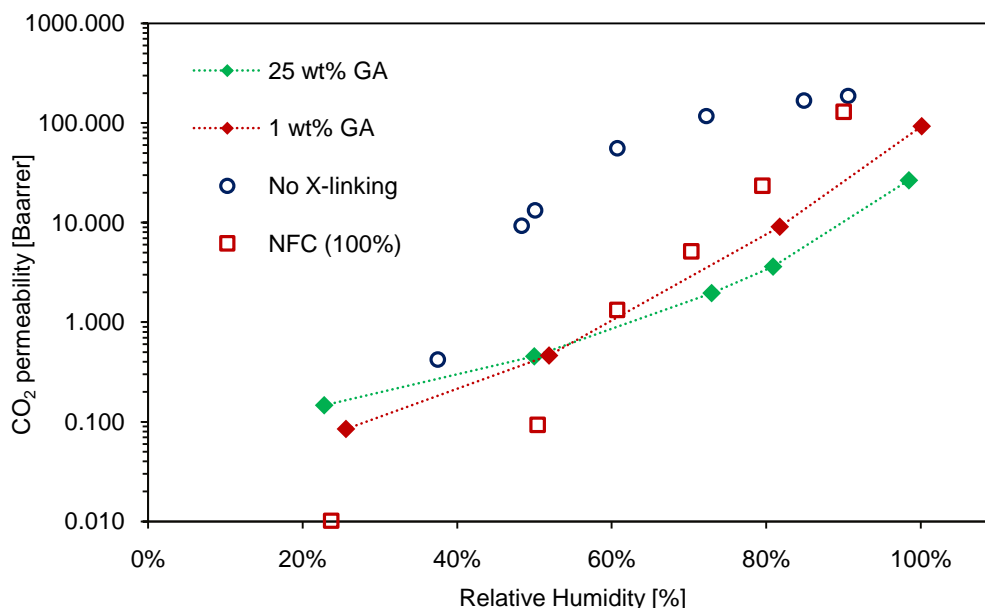

Figure 5.10: CO_2 permeability of two NFC/PVAm 50/50 film cross-linked in a solution with 1 and 25 wt% of GA. The data of the untreated blend [48] and pure NFC are also reported for comparison.

The summary of the permeability for carbon dioxide as a function of relative humidity is reported in Figure 5.10 along with the results for pure nanocellulose and the untreated 50:50 blend for comparison [48]. As it is has been seen for all the hydrophilic membranes analyzed, gas permeability increases exponentially with relative humidity. Both materials do not show any significant differences in the overall trend, with the 1 wt% GA sample starting at a slightly lower permeability at low humidity and eventually gaining the highest spot at saturation. In detail, around 25 RH% the two membranes show a CO_2 permeability of 0.09 and 0.15 Barrer, respectively for the 1 and 25 wt% GA samples. At 50 RH% the two curves overlap and present a value of about 0.5 Barrer. At the highest humidity inspected the 1 wt% GA film showed a permeability for carbon dioxide of 92.7 Barrer, while the 25 wt% GA sample stopped at 26.6 Barrer. It can be argued, then, that the possibly lower degree of cross-linking in the first sample contributed into allowing more carbon dioxide to permeate through it and that higher number of non bonded amine groups might have also contributed to this higher gas flow.

Observing the trend of the two curves in their whole, it can be noted how no significant variation of the exponential slope is present. This is quite in accord to what was evaluated in the water sorption test in the previous paragraph, which was the fact that no water swelling is present. Hence, the matrix of these films does not go through any particular variation and this is reflected by the non varying slope, which is similar to what can be observed for pure NFC. Specifically, respect to pure nanocellulose, the cross-linked films present a higher permeability from low to medium humidity,

98

but are surpassed when water activity goes beyond 0.6. At 90 RH% pure NFC shows a permeability of 130 Barrer, while at saturation the two cross-linked films settle around values of 93 and 26 Barrer for respectively the 1 and 25 wt% GA samples.

When analyzing the differences between the untreated NFC/PVAm blend, it is clear that the introduction of cross-linking determined a decrement of the permeation flow, as it would be expected. Interestingly, though, at high humidity the two types of films tend to converge back, since the untreated 50/50 film suffers from the swelling caused by the excessive water intake, which decreases its performances in this range. Even at high humidity, though, the untreated film appears to have definitely higher performances respect to the cross-linked ones.

Like done before, the gas permeability has been put in relation directly to the water content (Fig. 5.11). This has been possible only for the 25 wt% GA sample, since only for this one both the permeability and water sorption data were available. Once again the permeability appears quite closely related to the actual degree of hydration of the film. In the case of the cross-linked blend, the incapability of reaching higher permeability appears to be linked to the fact that it is not able to absorb enough water to allow carbon dioxide to dissolve and diffuse in a large enough extent. Beyond this, considering also the infrared results, it can be inferred that the cross-linking occurred extensively at the surface of the films, creating a very low permeable skin layer, which drastically reduces the permeation of all gases.

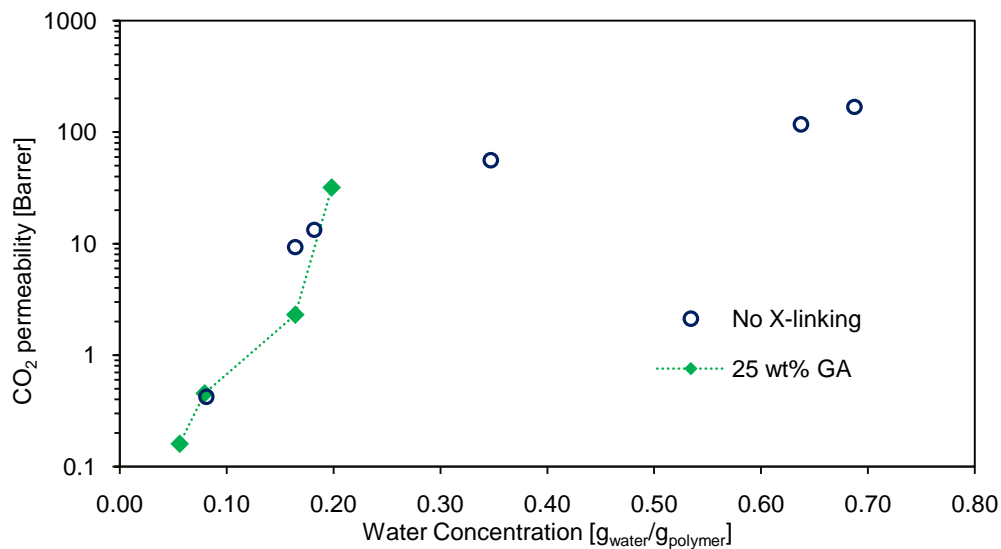
Figure 5.11: CO_2 permeability of NFC/PVAm 50/50 film cross-linked in a solution with 25 wt% of GA respect to the water content. The untreated NFC/PVAm blend has been added for comparison.

Following the interpolation procedure previously described in Par. 4.4, the ideal gas selectivity of CO_2 respect to the other two gases has been calculated for the blends treated with a solution of 1

and 25 wt% GA. Figure 5.12 place the resulting curves in comparison with the usual Robeson upper bound [53] for the gas pair CO_2 and N_2, while Figure 5.13 does the same for CO_2 and CH_4.

At a first general look it is quite evident how the selectivity values achieved by the cross-linked films are significantly lower than both the upper bound and the untreated film. Interestingly, the values do appear to show some sort of maximum in their trend, but it appears to be much less pronounced than the one showed by the untreated films.

Going into detail for each couple of gases, the selectivity towards nitrogen is fairly similar for both treated samples (Fig. 5.12), ranging from 0.7 up to 41, this last value corresponding to a permeability of CO_2 of 4.6 Barrer. At their highest permeability the curves get slightly closer to the upper bound, but eventually remain well below it, even at saturation. For this separation, the best point achieved results to belong to the 1 wt% GA film, which reaches a selectivity of 20.7 at a permeability of 98 Barrer. For comparison, at a similar permeability, the untreated film showed a selectivity of 107.

Figure 5.12: CO_2/N_2 ideal selectivity data for NFC(50%)/PVAm(50%) films cross-linked in a solution of 1 and 25 wt% GA, compared to the untreated film [48].

Moving to analyze the selectivity respect to methane (Fig. 5.13), a quite significant difference can be observed between the curves of the two materials, with the least cross-linked one (1 wt% GA) showing a higher performance than the 25 wt% GA, even though both of them still place themselves quite underneath the upper bound. Specifically, the first film showed a maximum selectivity of 94, paired with a CO_2 permeability of 4.6 Barrer, while the 25 wt% GA film reached only 8.7 at 2.3 Barrer. In comparison though, the highest selectivity point achieved by the non cross-linked film is 121 at a permeability of 50.6 Barrer.

Overall, it appears that this modification protocol does not improve any of the gas permeation properties of the films, since both permeability and selectivity appear to be significantly reduced in all cases. By analyzing the outputs of the tests presented up until now on these materials, it could be argued that the cross-linking procedure could have a negative effect on the structure of the material, especially on the PVAm based phase.
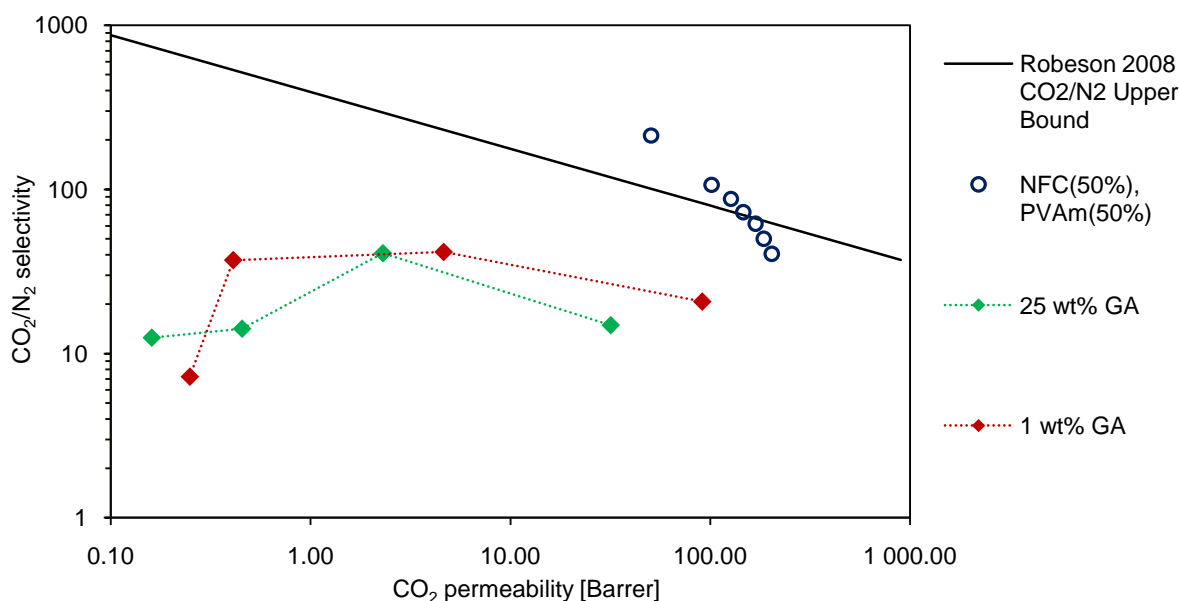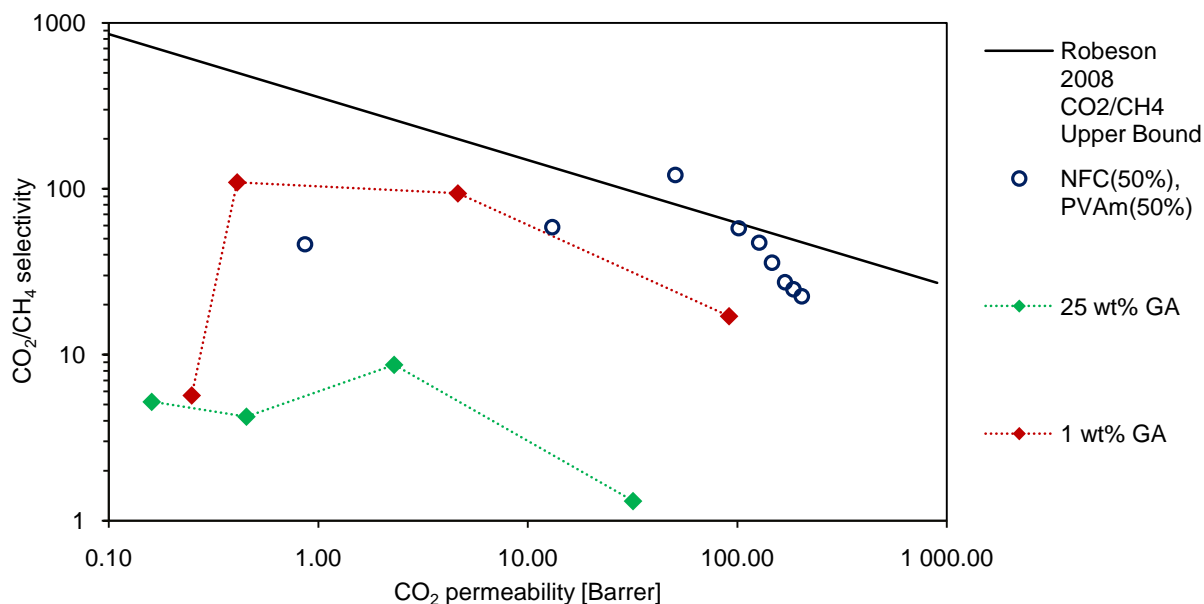

Figure 5.12: CO_2/N_2 ideal selectivity data for NFC(50%)/PVAm(50%) films cross-linked in a solution of 1 and 25 wt% GA, compared to the untreated film [48].

In fact, the dipping process in an aqueous solution could have favored an extraction of the water sensitive Lupamin . This appears to be confirmed by the FTIR analyses performed before, as well as the water sorption ones, which showed a structure and a behavior very similar to pure nanocellulose. Beyond this, since the amount of glutaraldehyde introduced in the system is probably in excess, a high number of the reactive moieties present in the matrix have already reacted forming a covalent bond. This tightly packed structure did not allow enough water to be absorbed so that the difference in solubility of the various gases could be exploited to its full potential. Moreover, even if not all groups have been cross-linked, the surface of the films appear to be the one mainly affected by the reaction, creating a fairly impermeable skin layer, which drastically compromises the permeation properties.

For these reasons, this method for the modification of the NFC/PVAm films has been deemed inefficient and it has not been investigate further.

5.3 Purified PVAm and Nanocellulose films

As mentioned in Par. 2.1, the commercial solution Lupamin® 9095, which represented the source of PVAm for the preparations presented during this work, does have beyond the polymer itself a residual salt impurity, specifically sodium formate. This component is a residual of the hydrolysis reaction, which is performed to obtain polyvinylamine from poly(N-vinylformamide). Since it was decided to use commercially available components for the film castings, in order to keep an eye on a possible scale up of the process, this salt has been left within the solution for the various preparations. From the results obtained, it appeared quite clear how the degree of impurities present is enough to significantly influence the separation properties. In particular, in Chapter 4 it has been showed how the salt can drive an excessive water uptake and create imperfections at high humidity, which significantly lower the selectivity. To reduce the impact of this issue, it has been decided to purify the solution prior to the film preparation protocol, as outlined in Par. 2.2.3, and test its properties for both water sorption and gas permeation.

5.3.1 FTIR analysis

Firstly, in order to assess a good purification, FTIR-ATR spectroscopy in single bounce mode was performed on both the commercial and the purified solution (Fig. 5.13).
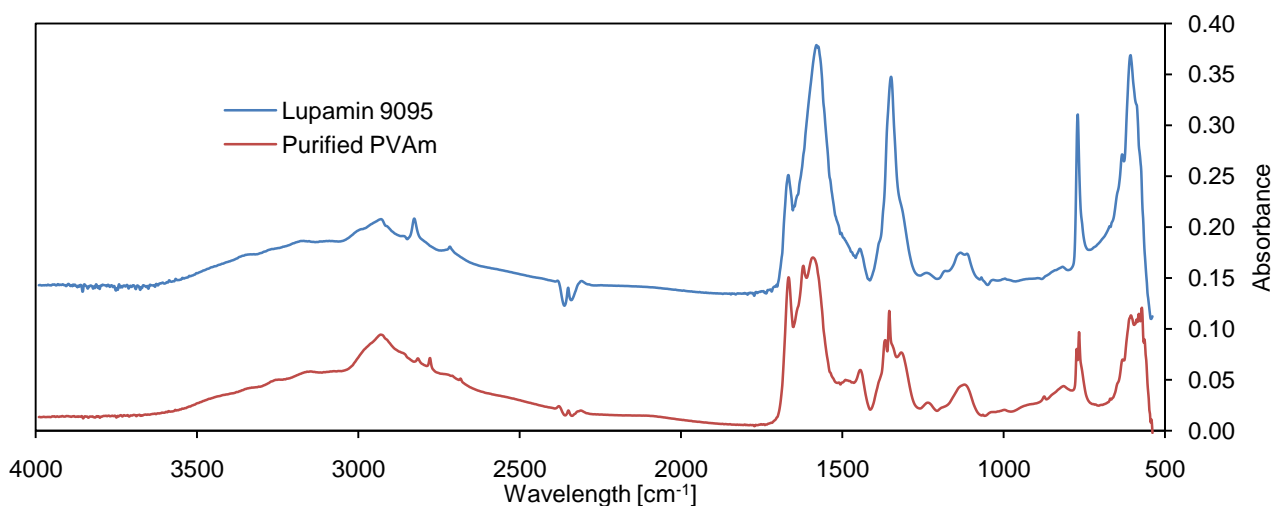
Figure 5.13: FTIR-ATR absorbance spectra of commercial Lupamin® 9095 and the purified polymer.

Analyzing the spectra obtained, it can be seen how at high wavelengths (3500-2000 cm^{-1}), the two materials do not different in any significant way and this has to be seen as a positive result. In fact, the both the broad peak between 3500 and 3000 cm^{-1} (related to the stretching of the N-H bond) and the sharp one at 2900 cm^{-1} (associated to the stretching of the C-H group) are correlated to the presence of the PVAm polymeric chains. Being these fairly similar to each other is an indication of

how the purification process did not alter the polymer in a measurable way. Moving towards lower frequencies, a few differences start to appear. As mentioned in Par. 4.1, sodium formate shows a few very sharp and characteristics peaks, the first one of them being the one correlate to the stretching of the C=O bond at 1600 cm^{-1}. This results to be significantly reduced for the purified form and the residual peak can be imputable to some residual salt, but also to the 5 mol% of formamidic groups always present in the chain structure of the polymer (§ 2.1). A similar outcome can be observed for both the peak at 1350 and 750 cm^{-1}, with the first one being probably related to the stretching of the C-O bond and the second to the bending of the C-H bond. All these peaks presented a significantly diminished height, strongly suggesting a consistent removal of, if not all, a large part of the salt present in the Lupamin solution. The obtainment of these results was deemed encouraging and a series of blends with nanocellulose was prepared with it.

5.3.2 Water absorption

Like before, the properties of the films prepared were assessed firstly via a water sorption test, using the procedure already outlined in Par. 2.2.2.1. In order to be able to compare the results obtained here the temperature of the test was kept at the usual 35 °C and the water activity inspected ranged from 0.15 up to 0.94.

Figure 5.14 reports the water sorption isotherms for both the purified PVAm polymeric film and its 50:50 blend with nanocellulose. For reference, the isotherms corresponding to the non purified polymer and blend have been also reported.
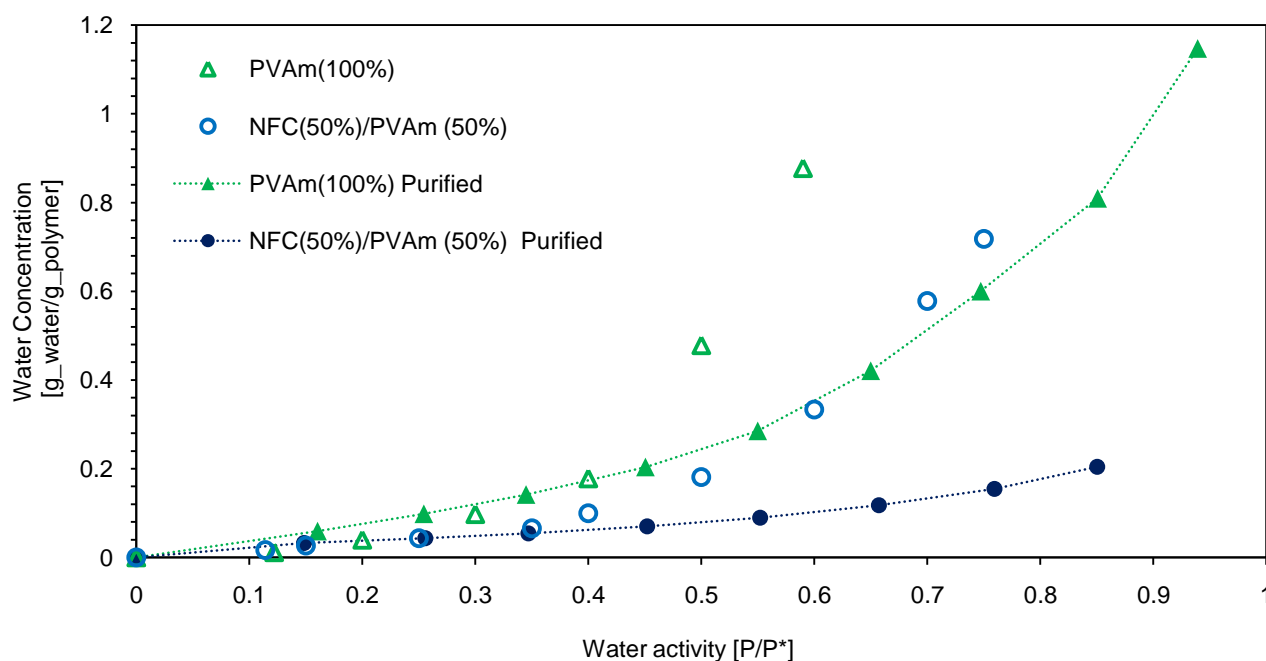

Figure 5.14: water absorption isotherms at 35 °C of the purified PVAm and its 50:50 blend with nanocellulose, compared to Lupamin® 9095 and the non purified blend with NFC.

From a first look, the curves related to the purified polymer appear to be significantly lower than their respective non purified counterparts, strengthening the hypothesis of the salt playing a significant role in the water intake process. In particular, the purified polyvinylamine shows a water concentration ranging from 0.06 up to 1.15 $g_{water}/g_{polymer}$ in the water activity interval between 0.15 and 0.94. Comparing it to the commercial polymer, it can be seen that at a water activity of 0.6 this last one reaches a water intake of almost 0.9 $g_{water}/g_{polymer}$, while the purified one equilibrated at the much lower value of 0.35 $g_{water}/g_{polymer}$. The trend of the curve is still an exponential one, suggesting the existence of a swelling process, but the extent of this one appears to be significantly diminished. In fact, when comparing it to the 50:50 NFC/PVAm blend, casted with the non purified polymer, it can be noted how at high humidity the nanocomposite actually surpasses the pure polymer, despite having been blended with a low absorbing phase such as nanocellulose. When observing the blend prepared with the newly purified PVAm, it results quite immediate how the swelling behavior seems to be extremely reduced and barely noticeable. As a reference, at an activity of 0.75 the original film reached a water concentration of almost 0.72 $g_{water}/g_{polymer}$, while the one with purified polyvinylamine stopped at 0.15 $g_{water}/g_{polymer}$ at a similar water activity. Overall, this new material topped its water uptake at 0.20 $g_{water}/g_{polymer}$ at the highest water activity inspected of 0.85.

Hence, it can be argued that these results strongly support the idea that the residual sodium formate is highly responsible for the excessive water uptake and consequent swelling observed for most of the films analyzed during the work.

5.3.3 Gas permeation and selectivity

In order to assess how the reduced water intake would affect the gas permeation and separation properties the 50/50 NFC/Purified PVAm film was tested in the usual humid permeometer, described in Par. 2.2.1.1. As before, tests were performed at a temperature of 35 °C and it was chosen to start the testing at a relative humidity higher than 50 %, since from previous experiments it was noticed that no interesting performances are usually achieved below this threshold. The permeability of CO_2, along with N_2 and CH_4 has been assessed in these conditions and the results are presented in Figure 5.15.
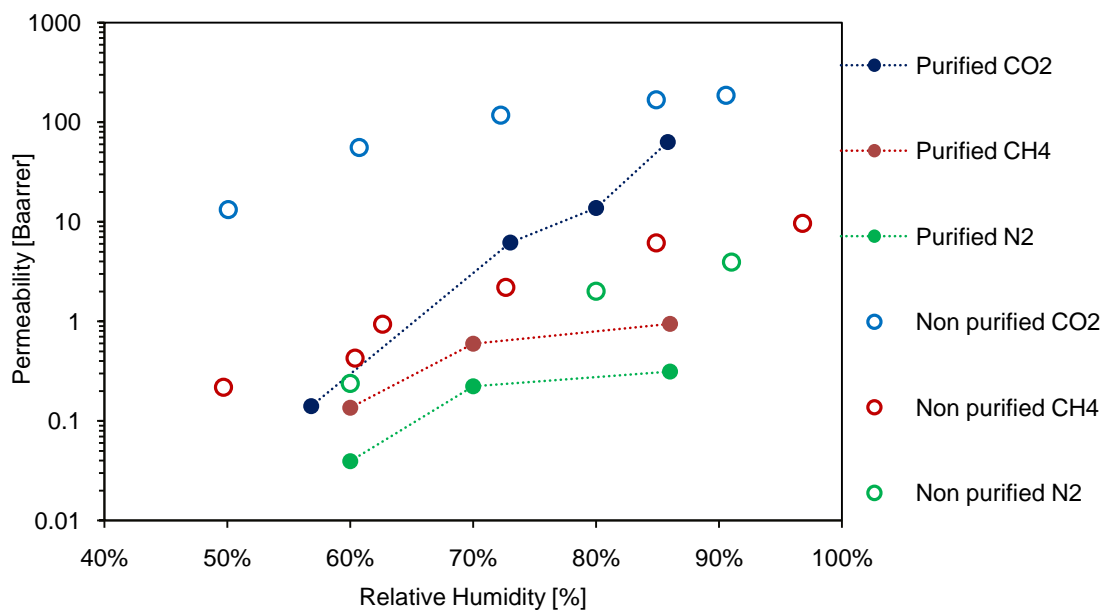
Figure 5.15: CO_2, N_2 and CH_4 permeability of NFC(50%)/purified PVAm(50%) blends as a function of relative humidity, compared to the blend with non purified Lupamin [48].

The results outlined here show the usual exponential trend for the permeability of carbon dioxide with humidity, which ranges from 0.14 Barrer at 55 RH%, up to 63 Barrer at the maximum relative humidity inspected of 86 %. Compared to the results of the original blends, these permeability are definitely lower, but the overall slope of the curve appear to be greater for the purified PVAm blend, showing a consistent exponential increment even at high humidity.

Considering the other two gases, it can be seen how these have similar trends and their growth with relative humidity appears to quite smaller respect to what observed for CO_2. As a consequence, the gap between the carbon dioxide and the nitrogen and methane permeability widens as humidity goes up, which is quite the opposite of what was observed for the non purified PVAm based composite. In terms of absolute values, N_2 permeability goes from 0.04 Barrer at 60 RH% up to 0.31 Barrer at 86 %, while CH_4 stretches from 0.14 Barrer at 60 RH% to 0.94 Barrer at 86 RH%.

If we report the same permeability results as a function of the water content (Fig. 5.16), the overall trends of the permeation curves do not appear to change significantly. Comparing these points with the ones of the non purified blend, it can be seen how, the purified film is capable of achieving the same permeability at a lower water intake. This could be due to a higher affinity of the matrix, which now has a higher concentration of amine moieties, since most of the salt has been removed.
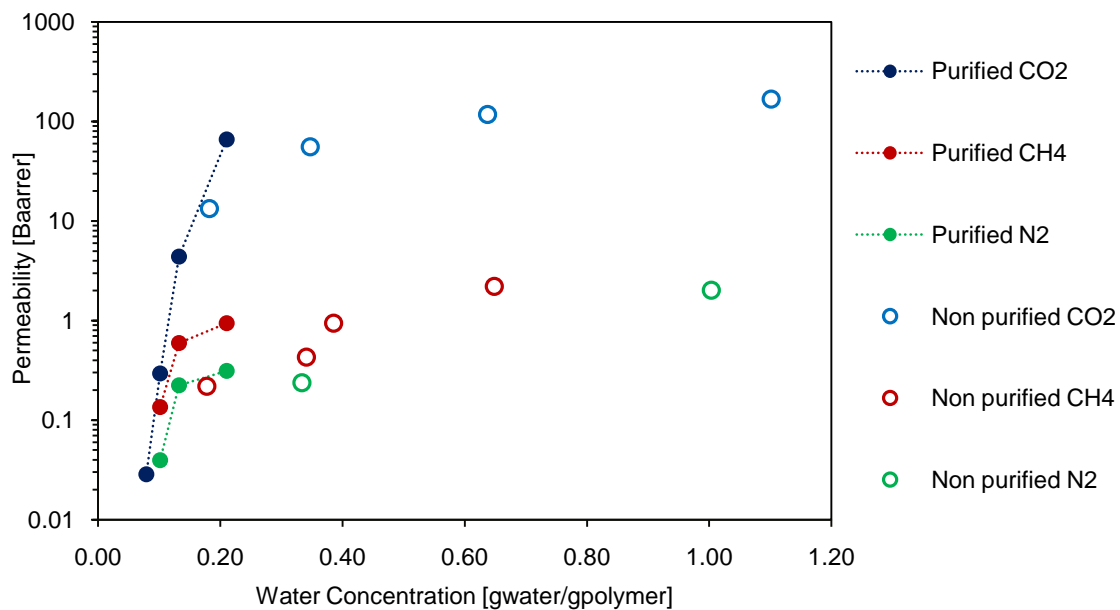
Figure 5.16: CO_2, N_2 and CH_4 permeability of NFC(50%)/purified PVAm(50%) blends as a function of water content, compared to the blend with non purified Lupamin [48].

The fact that the non purified blend still has a higher permeability is most likely due to the fact that is capable of absorbing a larger amount of water, hence better exploiting the larger solubility that carbon dioxide have in it.

As before, the permeation data have been elaborated via the interpolation method explained in Par. 4.4, in order to calculate the ideal selectivity and the results are reported in Figure 5.17 an 5.18. the first figure presents the selectivity of carbon dioxide respect to nitrogen, compared against the usual Robeson's upper bound [53]. For further reference, the curves corresponding to the non purified NFC/PVAm blend has been also added. From a first glance, it shows how the trends of the blends before and after the purification process are substantially different, since the selectivity of the non purified blend decreases significantly at high humidity, while the purified one keeps on growing. Specifically, the ideal selectivity grows from 0.12 at 0.03 Barrer up to 212 at 66 Barrer, hence reaching the highest separation factor achieved for the non purified blend, but showing an even higher CO_2 permeability. Moreover, this last point is also above the upper bound, indicating an improvement respect to the state of the art.

Figure 5.17: CO_2/N_2 ideal selectivity of NFC(50%)/purified PVAm(50%) blend as a function of CO_2 permeability, compared to the blend with non purified Lupamin [48] and pure PVAm [58] Next to each point is reported the relative humidity at which the selectivity was calculated.

A quite similar behavior can be observed for the CO_2/CH_4 separation (Fig. 5.18); also here a monotonous increasing trend of the selectivity can be observed for the purified PVAm, opposite to the decreasing behavior, that the non purified film takes after the maximum. In this case, the selectivity values range from 0.82 at 0.03 Barrer up to 100, achieved at 63 Barrer.
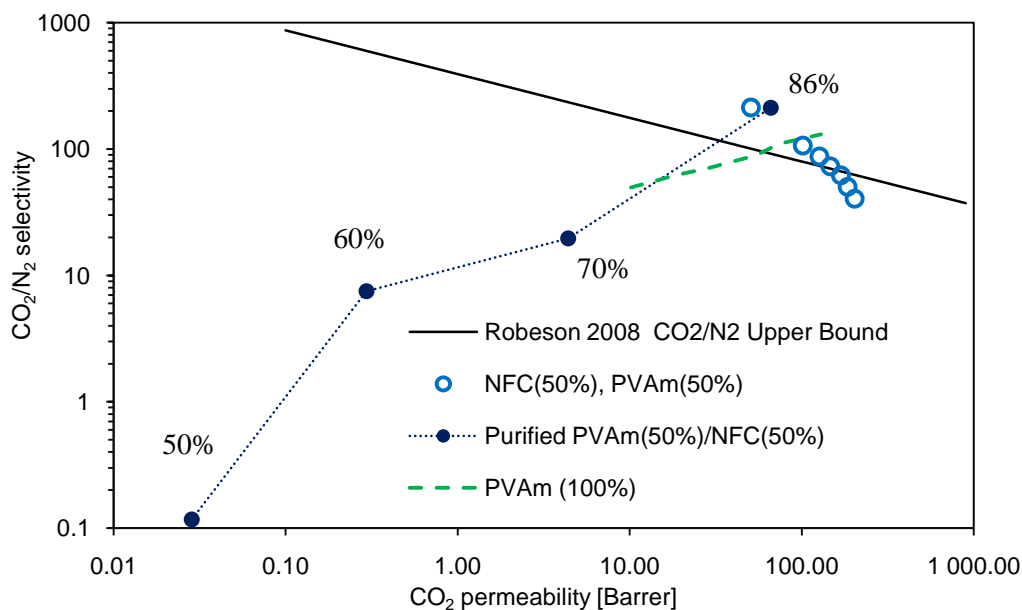

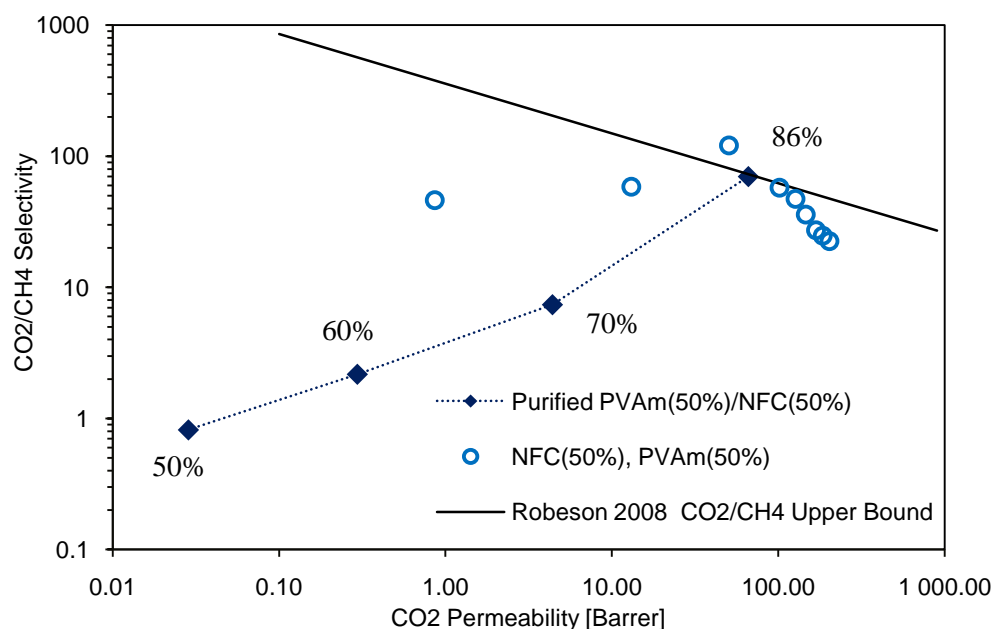*Figure 5.17: CO_2/N_2 ideal selectivity of NFC(50%)/purified PVAm(50%) blend as a function of CO_2 permeability, compared to the blend with non purified Lupamin [48]. Next to each point is reported the relative humidity at which the selectivity was calculated*

Here, the maximum selectivity measured is lower than the one of the non purified blend (121), but still quite remarkable. Comparing it to data from pure PVAm retrieved in literature [58], it can be observed that no particular loss in permeability can be found as result of the blending process with nanocellulose.

Overall, it can be confidently stated that the purification protocol is a viable method for obtaining a film with minimal swelling, proving that the impurities of salt in the starting commercial material are cause of lack of selectivity and can create instability of the structure of the film at high humidity. By removing this impurity, the membrane appeared to have enhanced stability at high humidity, a characteristic, which allowed to tests their performances at high temperature, as it will be presented in the next paragraph.

5.3.4 High temperature gas permeation

The removal of salts though purification procedure allowed to reduce material swelling and increase membrane stability but also reduced overall permeability. For this reason, in view of the higher resistance of the membrane it was deemed interesting to test the material at high temperature and in presence of large quantities of water in order to maximize the permeability by operating in optimal membranes conditions. It was indeed shown in previous studies that amine based facilitated transport membranes reach higher performances when operating at temperatures in the order of 100°C[59].The membrane chosen for this purpose is the NFC(50%)/purified PVAm(50%) blend, whose properties have been already analyzed at low temperature in the previous paragraphs.

In order to perform a permeation test at high temperature, the apparatus described in Par. 2.2.1.3 has been employed. Instead of relying on a bubbler for the humidification of the gas stream, this system directly pumps a steady flow of liquid water into the feed stream, which is then vaporized in the oven. Because of this way of functioning, the presence of some liquid water, that might come in contact with the film cannot be excluded during the test. For this reason, the film chosen was the one, which showed the least sensitivity to a high humidity environment. Preliminary test made using a film with a strong presence of salt, namely the NFC(50%)/PVAm(50%) non purified, showed that the stream was able to solubilize large portions of the material, creating discontinuities and leakages through the film. In the case of the purified films, these issues were not present and it was possible to carry on several tests at different temperature and water content.

In particular, two main temperature have been investigated: 75 and 100 °C. Since there are no hygrometers, which can directly measure the relative humidity inside the oven, this parameter has been calculated by the knowledge of the molar flow of the gas and the water sent to the upstream

side of the permeation cell. This allowed the calculation of the molar fraction of water in the feed and by also knowing the temperature (hence the saturation pressure) it was possible to evaluate the relative humidity as outline by the equations below (Eq. 5.1 and 5.2).

$$y_{H2O} = \frac{\dot{n}_{H2O}}{\sum_i \dot{n}_i}$$ (5.1)

$$RH = \frac{P \cdot y_{H2O}}{P^*(T)} \cdot 100$$ (5.2)

In general, though, most of the results will be presented directly as a function of the water fraction of the feed, since Eq. 5.2 is affected by temperature variations within the oven itself.

Even though the permeometer is capable of dealing with multiple gases at the same time, due to time restrictions during the project, it was possible to evaluate the permeability of only pure humidified CO_2. The calculation of permeability has been made via Eq. 2.3.

Each test has been performed using a dry gas flow of 500 cm^3/min, to which a variable amount of water has been added. This amount is tightly connected to the temperature, at which the film is working, due to the variability of the saturation pressure and of the specific feature of the system.

The used apparatus indeed is currently able only to humidify the feed stream while the purge enters the system in dry conditions, water initially have to humidify both feed and purge streams by permeating through the membrane. For this reason water contents higher than the saturation where considered during tests to allow the system to operate at high humidity at both side of the membranes.

In particular at 75 °C the water fed to the gas stream ranged from 3 to 5.5 g/h, in order to achieve reasonably high relative humidity. When the temperature was raised up to 100 °C, the water flow needed increased by almost one order of magnitude ranging from 10 to 35 g/h.

The purge flow of nitrogen fed on the downstream side is of 80-100 cm^3/min; an amount mainly controlled by the sensitivity of the gas cromatograph, since higher flow-rates would dilute the permeating gases to levels, which would be difficult to evaluate with enough confidence. The pressure on the upstream side was kept at 3 bar, while on the downstream side was slightly above the atmospheric pressure.

In Figure 5.18, the carbon dioxide permeation results are presented for the two different temperatures and as a function of the water concentration in the feed side expressed as a molar percentage.
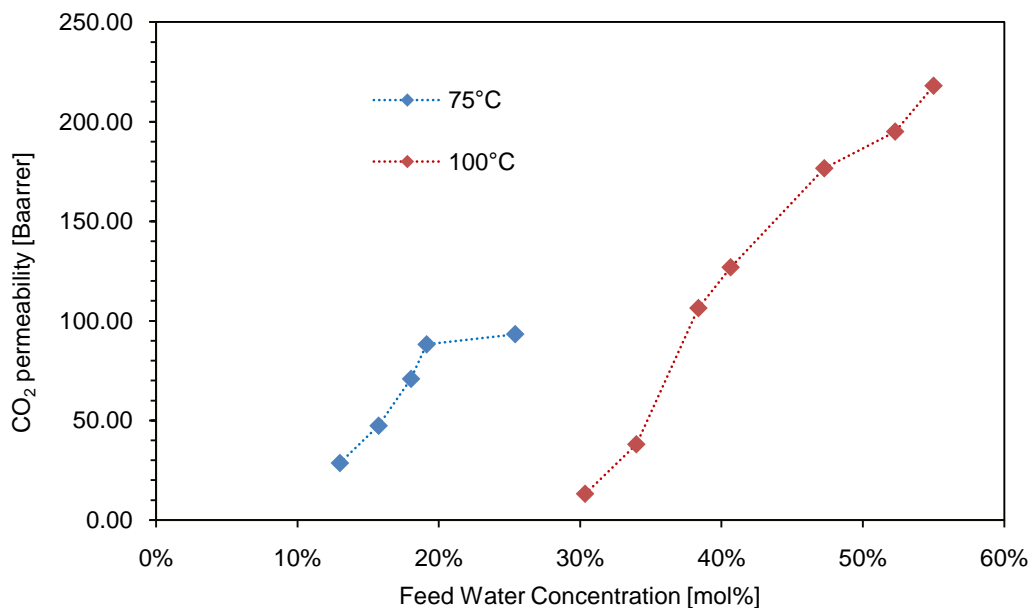
Figure 5.18: CO₂ permeability of the NFC(50%)/purified PVAm(50%) blend at 75 and 100 °C as a function of the feed water content expressed in mol%.

At a first look it appears evident the large difference in the values reached by the two curves, underlining the effect of that temperature can have on these materials. The curve acquired at 75 °C showed a fairly linear trend starting at 13 Barrer, before reaching a plateau around 90 Barrer once the water content reached 25 mol%. The curve related to the 100 °C test, instead, showed a constantly increasing quasi linear trend, which stretched the permeability values from 13 Barrer at 31 mol%, up to 218 Barrer at 55 mol% of water, making this the highest permeability measured for this specific film.

Fig. 5.19: schematization of the water concentration gradient in the polymeric film during a permeation test in the apparatus described in Par. 2.2.1.3. The water activity profile is not necessarily linear, but it has been drawn in this way for simplicity.

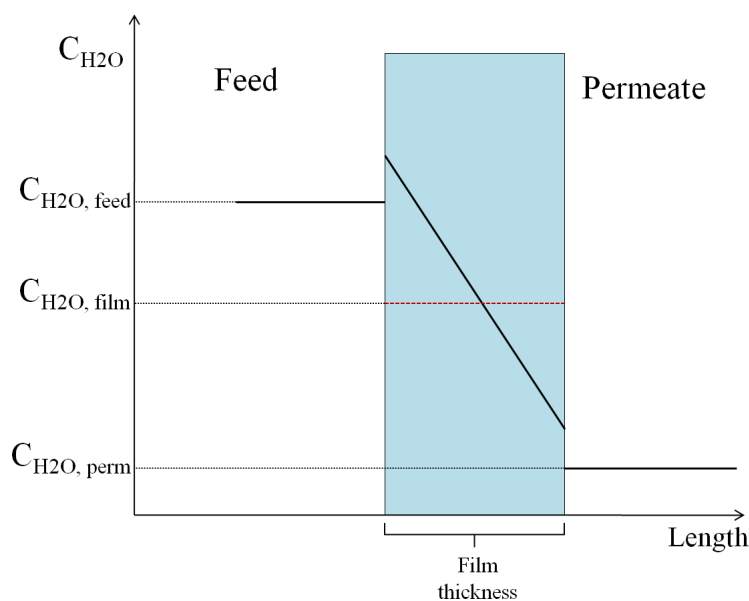In view of the above considered features of the humidification system and the consequent distribution of water in the system, exemplified by Fig. 5.19, the actual water activity at which the film will be operating at will be smaller than the one, which can be calculated via the method outlined by Eq. 5.1 and 5.2. Hence, the amount of water which can be fed to the film, can be actually higher than the saturation point for that temperature, since a significant fraction of it will actually permeate through the film itself.

The permeability limit showed by the membrane at 75 °C, is not necessarily related to the saturation of the membrane with water, but rather to the reaching of a fluid dynamic limit related to the its transport across the film. In other words, the membrane might not be able to allow enough water through it to allow the saturation of both sides.

It can be said in conclusion that the film based on purified PVAm and nanocellulose shows interesting permeation properties and more importantly a high stability at both high temperature and high humidity. As expected the permeation properties increased with temperature, reaching interesting values for a possible large scale application. Unfortunately, in the timeframe of the present PhD project it was not possible to complete the optimization of the materials properties which therefore still present high possibilities of improvements in view of it application to real industrial separation. .

Conclusions

During this project, several facilitated transport membranes for CO_2 separation were successfully synthesized via a number of techniques and their water sorption and permeation properties assessed in various conditions of temperature (35, 75, and 100 °C) and humidity (from 25 RH% to saturation). The work passed through the preparation of polyvinyl alcohol (PVA) based films, which were modified in two main different ways. Firstly via the chemical grafting of an aminated silane on a cross-linked matrix then through the addition of amine functionalized nano-particles.

The first films, prepared following protocols already available in the open literature, showed a permeability towards CO_2 up to 179 Barrer and a selectivity respect to H_2 of 21 and were considered an encouraging introduction to the field of transport facilitation, which was never treated before within the research group. the second series of PVA films has been synthesized at the Norwegian University of Science and Technology (NTNU), as part of an exchange period within the PhD program. Amine functionalized nanoparticles were dispersed in a hydrophilic matrix and casted onto a porous support. Even though it was not possible to observe a definitive improvement given by the addition of these functionalities, the films showed a permeability of up to 440 Barrer for carbon dioxide in saturation conditions and a selectivity towards nitrogen of 63.

Following these introductory works, the main project of the PhD program was tackled. This consisted in the preparation of gas separation films by blending polyvinylamine (PVAm) and

nanocellulose (NFC), in order to exploit the amine moieties of the first for the transport and the enhanced stability brought by the second as well as other synergetic effect given by the good affinity of the two compounds and the polar character of nanocellulose. Different ratios of the two materials were considered, obtaining membranes with PVAm percentage going from 30 to 70 wt%. Results performed with these unmodified polymers allowed CO_2 permeability to reach values above the state of the art, defined as the Robeson plot, for both the CO_2/N_2 separation and the CO_2/CH_4. In particular, at 35 °C membranes with 30 wt% of PVAm showed a maximum CO_2 permeability of 74 Barrer at 89 RH% and a top selectivity respect to N_2 of 135 at 60 RH%, while the films containing 70 wt% PVAm reached a permeability of 187 Barrer at 81 RH% for carbon dioxide and a top selectivity towards nitrogen of 211, also at 60 RH%. This last blend appeared to be the best performing one, amongst the non modified films, most likely due its capability of absorbing a large amount of water respect to the others. In terms of water absorption, all films containing nanocellulose showed an intake of humidity lower than what was predicted by a purely additive model, indicating that the cellulosic fibers probably contributed to limiting the matrix relaxation and an excessive swelling. Beyond better performances in mechanical terms, the addition of NFC did not appear to hinder the permeation of gases and in its pure form actually showed interesting separating capabilities. Overall, the parameter, which mostly controlled the permeselectivity, appeared to be the water concentration within the film. Membranes, which could absorbed a higher amount of water showed better permeability than others, who could not achieve the same values. Apparently, compared to water intake, transport facilitation appeared to play a minor role in the permeation of gases.

This correlation, though, came with a drawback, since during the tests a large swelling phenomenon was observed at medium high humidity, which determined the loss of most of the selectivity achieved at lower water activity. This was considered a strange behavior for facilitates transport membranes, which usually show a contemporary increase of both permeability and selectivity. For this reason, in the last part of the project a series of methodologies were tested, in order to approach and resolve this issue.

Chemically induced cross-linking was carried on by using glutraldheyde (GA) and allowed to eliminate completely the swelling behavior, but at a great cost in permeation performances. Films treated with a solution containing 1 and 25 wt% GA showed a maximum permeability at 100 RH% of respectively 93 and 27 Barrer, paired with a CO_2/N_2 selectivity of 21 and 15. In terms of permeability, this meant a drop of respectively 94 and 160 Barrer respect to the non cross-linked one in similar conditions. Thermally treating the film and at the same time employing a

nanocellulose with a modified surface (consisting in a higher surface charge related to the carboxymethylation process carried on the original cellulose fibers prior to homogenization) resulted in achieving the highest selectivity for the pair CO_2/CH_4 (410); during the same series of tests it was also noticed that non blended carboxymethylated nanocellulose proved to have itself very interesting separation capabilities, encouraging the use of the material for further applications, nonetheless it was still showing the selectivity loss at high relative humidity. These improved performances appeared to be related to a reduced water uptake respect to the no treated film, which allowed the membrane to limit the swelling process. Moreover, FTIR spectra indicated the presence of changes in the membrane composition due to the thermal treatment, concerning especially the nanocellulosic phase.

For this reason, the focus was again towards the polymer and aimed at enhancing the properties and stailbity of PVAm, by removing most of the impurities, that can be found in the commercial solution. Following this method proved to be a good choice, since swelling was greatly reduced in the pure polymer and almost cancelled in the blend. These purified blends showed a very interesting increment with humidity of both permeability and selectivity at the same time, reaching values above the state of the art (63 Barrer and a selectivity towards N_2 of 211 at 86 RH%). Thanks to the purification process, it was also possible to test these films at high humidity on the feed side and high temperature (75 and 100 °C), in order to evaluate the influence of this variable. At 100 °C, the film showed a CO_2 permeability of up to 218 Barrer, proving an enhancement of the properties in these conditions.

In conclusion, during the doctoral experience the mechanisms of facilitated transport have been explored via a series of experiments and new materials have been developed for the separation of carbon dioxide, which represent a significant improvement respect to the current state of the art.

A future work might be focused on addressing the need of a better purification strategy, since the presence of impurities proved to be a significant limiting factor for a larger employment of polyvinylamine. Hence, with a more stable polymer, it would be most likely possible to reduce the amount of NFC needed to achieve the same (if not better ones) mechanical and absorption properties achieved here. Lastly, since nanocellulose proved to be a quite performing material by itself, it is arguable that a chemical modification of its structure could result in a much higher affinity towards CO_2, thus obtaining interesting separation performances.

Acknowledgments

The author would like to thank Prof. Marco Giacinti Baschetti for his constant supervision and patience during the years of the PhD program. Along with him, the author is profoundly thankful for all the help received by the many members of the MEMLAB research group, which all collaborated in some extent to make this work possible.

For the experience spent at NTNU Trondheim, the author would like to thank Prof. May-Britt Hägg for the supervision and all the members of the MEMFO research group.

References

[1]   IPCC, Climate Change 2014 Synthesis Report Summary Chapter for Policymakers, Ipcc. (2014) 31. doi:10.1017/CBO9781107415324.

[2]   R.D. Garreaud, Earth System Research Laboratory, Curso Climas SA. (2011) 2011.

[3]   D.M. D'Alessandro, B. Smit, Carbon Dioxide Capture, 2010. doi:10.1002/anie.201000431.

[4]   D. Aaron, C. Tsouris, Separation of CO_2 from Flue Gas: A Review, Sep. Sci. Technol. 40 (2005) 321–348. doi:10.1081/SS-200042244.

[5]   P. Bernardo, E. Drioli, G. Golemme, Membrane gas separation: 1 review of state of the art, Ind. Chem. Eng. 48 (2009) 4638–63.

[6]   E. Favre, Carbon dioxide recovery from post-combustion processes: Can gas permeation membranes compete with absorption?, J. Memb. Sci. 294 (2007) 50–59. doi:10.1016/j.memsci.2007.02.007.

[7]   R.W. Baker, K. Lokhandwala, Natural Gas Processing with Membranes: An Overview, Ind. Eng. Chem. Res. 47 (2008) 2109–2121. doi:10.1021/ie071083w.

[8]   R.W. Baker, Future Directions of Membrane Gas Separation Technology, Ind. Eng. Chem. Res. 41 (2002) 1393–1411. doi:10.1021/ie0108088.

[9]   L.M. Robeson, The upper bound revisited, J. Memb. Sci. 320 (2008) 390–400. doi:10.1016/j.memsci.2008.04.030.

[10] W.J. Ward, W.L. Robb, Carbon dioxide-oxygen separation: Facilitated transport of carbon dioxide across a liquid film, Science (80-.). 156 (1967) 1481–1484. http://www.scopus.com/inward/record.url?eid=2-s2.0-0014208271&partnerID=tZOtx3y1.

[11] R.D. Noble, Generalized microscopic mechanism of facilitated transport in fixed site carrier

membranes, J. Memb. Sci. 75 (1992) 121–129. doi:10.1016/0376-7388(92)80011-8.

[12] O.H. LeBlanc Jr., W.J. Ward, S.L. Matson, S.G. Kimura, Facilitated transport in ion-exchange membranes, J. Memb. Sci. 6 (1980). doi:10.1016/S0376-7388(00)82175-4.

[13] H. Matsuyama, M. Teramoto, H. Sakakura, K. Iwai, Facilitated transport of CO2 through various ion exchange membranes prepared by plasma graft polymerization, J. Memb. Sci. 117 (1996) 251–260. doi:10.1016/0376-7388(96)00072-5.

[14] H. Matsuyama, M. Teramoto, H. Sakakura, Selective permeation of CO2 through poly 2-(N,N-dimethyl)aminoethyl methacrylate membrane prepared by plasma-graft polymerization technique, J. Memb. Sci. 114 (1996) 193–200. doi:10.1016/0376-7388(95)00318-5.

[15] T.J. Kim, L.I. Baoan, M.B. Hägg, Novel fixed-site-carrier polyvinylamine membrane for carbon dioxide capture, J. Polym. Sci. Part B Polym. Phys. 42 (2004) 4326–4336. doi:10.1002/polb.20282.

[16] J. Zou, W.S.W. Ho, CO2-selective polymeric membranes containing amines in crosslinked poly(vinyl alcohol), J. Memb. Sci. 286 (2006) 310–321. doi:10.1016/j.memsci.2006.10.013.

[17] L. Deng, T.-J. Kim, M.-B. Hägg, PVA/PVAm blend FSC membrane for CO2-capture, Desalination. 199 (2006) 523–524. doi:10.1016/j.desal.2006.03.118.

[18] D. Grainger, M.-B. Hägg, Techno-economic evaluation of a PVAm CO2-selective membrane in an IGCC power plant with CO2 capture, Fuel. 87 (2008) 14–24. doi:10.1016/j.fuel.2007.03.042.

[19] S.Y. Hu, Y. Zhang, D. Lawless, X. Feng, Composite membranes comprising of polyvinylamine-poly(vinyl alcohol) incorporated with carbon nanotubes for dehydration of ethylene glycol by pervaporation, J. Memb. Sci. 417–418 (2012) 34–44. doi:10.1016/j.memsci.2012.06.010.

[20] A. Dufresne, Nanocellulose: a new ageless bionanomaterial, Mater. Today. 16 (2013) 220–227. doi:10.1016/j.mattod.2013.06.004.

[21] W.Y. Miao, Chuanwei Hamad, Tensile and thermal properties of nanocellulose-reinforced poly(vinyl alcohol) nanocomposites, Biomacromolecules. 17 (2013) 36–40. doi:10.1016/j.jiec.2010.10.006.

[22] Cambridge University Engineering Department, Materials data book, Mater. Courses. (2003) 1–41. doi:10.1016/0261-3069(88)90026-X.

[23] G. Siqueira, J. Bras, A. Dufresne, Cellulosic Bionanocomposites: A Review of Preparation, Properties and Applications, Polymers (Basel). 2 (2010) 728–765. doi:10.3390/polym2040728.

[24] C. Miao, W.Y. Hamad, Cellulose reinforced polymer composites and nanocomposites: a critical review, Cellulose. 20 (2013) 2221–2262. doi:10.1007/s10570-013-0007-3.

[25] D. Klemm, F. Kramer, S. Moritz, T. Lindström, M. Ankerfors, D. Gray, A. Dorris, Nanocelluloses: a new family of nature-based materials., Angew. Chem. Int. Ed. Engl. 50 (2011) 5438–66. doi:10.1002/anie.201001273.

[26] C. Ruiz-Palomero, M.L. Soriano, M. Valcárcel, Nanocellulose as analyte and analytical tool: Opportunities and challenges, TrAC Trends Anal. Chem. 87 (2017) 1–18.

References

doi:10.1016/j.trac.2016.11.007.

[27]   M.I. et al. Johansson C., Bras J., Renewable fibers and Bio-based materials for packaging applications-A review of recent developements, 7 (2012) 2506–2552.

[28]   J.S. Vrentas, C.M. Vrentas, Solvent Self-DIffusion in Glassy Polymer-Solvent Systems, J. Polym. Sci. Part B Polym. Phys. 30 (1994) 1005–1011. doi:10.1002/polb.1992.090300908.

[29]   L.. Robeson, Polymer membranes for gas separation, Curr. Opin. Solid State Mater. Sci. 4 (1999) 549–552. doi:10.1016/S1359-0286(00)00014-0.

[30]   L.M. Robeson, Correlation of separation factor versus permeability for polymeric membranes, J. Memb. Sci. 62 (1991) 165–185. doi:10.1016/0376-7388(91)80060-J.

[31]   University of Michigan, The Celle Membrane, (2003). doi:http://oerpub.github.io/epubjs-demo-book/content/m46021.xhtml.

[32]   Y. Zhao, W.S. Winston Ho, Steric hindrance effect on amine demonstrated in solid polymer membranes for CO2 transport, J. Memb. Sci. 415 (2012) 132–138. doi:10.1016/j.memsci.2012.04.044.

[33]   Z. Tong, V.K. Vakharia, M. Gasda, W.S.W. Ho, Water vapor and CO2 transport through amine-containing facilitated transport membranes, React. Funct. Polym. 86 (2015) 111–116. doi:10.1016/j.reactfunctpolym.2014.09.010.

[34]   M. Caplow, Kinetics of carbamate formation and breakdown, J. Am. Chem. Soc. 90 (1968) 6795–6803. doi:10.1021/ja01026a041.

[35]   L. Deng, M.-B. Hägg, Carbon nanotube reinforced PVAm/PVA blend FSC nanocomposite membrane for CO2/CH4 separation, Int. J. Greenh. Gas Control. 26 (2014) 127–134. doi:10.1016/j.ijggc.2014.04.018.

[36]   T.-J. Kim, H. Vrålstad, M. Sandru, M.-B. Hägg, Separation performance of PVAm composite membrane for CO2 capture at various pH levels, J. Memb. Sci. 428 (2013) 218–224. doi:10.1016/j.memsci.2012.10.009.

[37]   Y. Chen, W.S.W. Ho, High-molecular-weight polyvinylamine/piperazine glycinate membranes for CO2 capture from flue gas, J. Memb. Sci. 514 (2016) 376–384. doi:10.1016/j.memsci.2016.05.005.

[38]   L. Wågberg, G. Decher, M. Norgren, T. Lindström, M. Ankerfors, K. Axnäs, The build-up of polyelectrolyte multilayers of microfibrillated cellulose and cationic polyelectrolytes, Langmuir. 24 (2008) 784–795. doi:10.1021/la702481v.

[39]   M. Minelli, M.G. Baschetti, F. Doghieri, M. Ankerfors, T. Lindström, I. Siró, D. Plackett, Investigation of mass transport properties of microfibrillated cellulose (MFC) films, J. Memb. Sci. 358 (2010) 67–75. doi:10.1016/j.memsci.2010.04.030.

[40]   J. Catalano, M. Giacinti Baschetti, G.C. Sarti, Influence of water vapor on hydrogen permeation through 2.5 μm Pd-Ag membranes, Int. J. Hydrogen Energy. 36 (2011). doi:10.1016/j.ijhydene.2011.03.139.

[41]   E. Piccinini, M. Giacinti Baschetti, G.. Sarti, Use of an automated spring balance for the simultaneous measurement of sorption and swelling in polymeric films, J. Memb. Sci. 234 (2004) 95–100. doi:10.1016/j.memsci.2003.12.024.

[42] J. Crank, The mathematics of diffusion, Oxford Univ. Press. (1975) 414. doi:10.1016/0306-4549(77)90072-X.

[43] R. Xing, W.S.W. Ho, Crosslinked polyvinylalcohol–polysiloxane/fumed silica mixed matrix membranes containing amines for CO2/H2 separation, J. Memb. Sci. 367 (2011) 91–102. doi:10.1016/j.memsci.2010.10.039.

[44] L. Deng, M.-B. Hägg, Swelling behavior and gas permeation performance of PVAm/PVA blend FSC membrane, J. Memb. Sci. 363 (2010) 295–301. doi:10.1016/j.memsci.2010.07.043.

[45] K. Yamamoto, Y. Imamura, E. Nagatomo, T. Serizawa, Y. Muraoka, M. Akashi, Synthesis and Functionalities of Poly (N -vinylalkylamide). XIV . Polyvinylamine Produced by Hydrolysis of Poly (N - vinylformamide) and Its Functionalization, (2002).

[46] L. Deng, T.-J. Kim, M.-B. Hägg, Facilitated transport of CO2 in novel PVAm/PVA blend membrane, J. Memb. Sci. 340 (2009) 154–163. doi:10.1016/j.memsci.2009.05.019.

[47] N.I. of S. and T. (NIST), Nation, (n.d.). http://webbook.nist.gov/cgi/cbook.cgi?ID=B6010183&Mask=80.

[48] L. Ansaloni, J. Salas-Gay, S. Ligi, M.G. Baschetti, Nanocellulose-based membranes for CO2 capture, J. Memb. Sci. 522 (2017) 216–225. doi:10.1016/j.memsci.2016.09.024.

[49] D. Venturi, L. Ansaloni, M.G. Baschetti, Nanocellulose based facilitated transport membranes for CO2 separation, Chem. Eng. Trans. 47 (2016) 349–354. doi:10.3303/CET1647059.

[50] E.M. Davis, Y.A. Elabd, Water Clustering in Glassy Polymers, J. Phys. Chem. B. 117 (2013) 10629–10640. doi:10.1021/jp405388d.

[51] S. Belbekhouche, J. Bras, G. Siqueira, C. Chappey, L. Lebrun, B. Khelifi, S. Marais, A. Dufresne, Water sorption behavior and gas barrier properties of cellulose whiskers and microfibrils films, Carbohydr. Polym. 83 (2011) 1740–1748. doi:10.1016/j.carbpol.2010.10.036.

[52] H.W. Thorp, Chemical Engineers' Handbook. Second edition (Perry, John H., ed.), 1942. doi:10.1021/ed019p449.2.

[53] L.M. Robeson, The upper bound revisited, J. Memb. Sci. 320 (2008) 390–400. doi:10.1016/j.memsci.2008.04.030.

[54] B.S. Jursic, Z. Zdravkovski, A Simple Preparation of Amides from Acids and Amines by Heating of Their Mixture, Synth. Commun. 23 (1993) 2761–2770. doi:10.1080/00397919308013807.

[55] U. Weise, Hornification - Mechanisms and terminology, Pap. Ja Puu/Paper Timber. 80 (1998) 110–115. http://www.scopus.com/inward/record.url?eid=2-s2.0-0031704811&partnerID=tZOtx3y1.

[56] J.L. Minor, Hornification -Its origin and meaning, Progrress Pap. Recycl. 3 (1994) 93–95. http://www.fpl.fs.fed.us/products/publications/specific_pub.php?posting_id=18820&header_id=p.

[57] A. Idström, H. Brelid, M. Nydén, L. Nordstierna, CP/MAS ^{13}C NMR study of pulp

References

hornification using nanocrystalline cellulose as a model system., Carbohydr. Polym. 92 (2013) 881–4. doi:10.1016/j.carbpol.2012.09.097.

[58] T.-J. Kim, H. Vrålstad, M. Sandru, M.-B. Hägg, The effect of pH on CO2-separation from post combustion gas by polyvinylamine based composite membrane, Energy Procedia. 37 (2013) 986–992. doi:10.1016/j.egypro.2013.05.194.

[59] L. Ansaloni, Y. Zhao, B.T. Jung, K. Ramasubramanian, M.G. Baschetti, W.S.W. Ho, Facilitated transport membranes containing amino-functionalized multi-walled carbon nanotubes for high-pressure CO2 separations, J. Memb. Sci. 490 (2015) 18–28. doi:10.1016/j.memsci.2015.03.097.